AN INTRODUCTION TO SUPERCONDUCTIVITY

P. Darriulat

CERN, May 98

Contents

1 PREAMBLE

1.1 General scope

It is somewhat ridiculous to write down lecture notes on superconductivity when so many excellent text books, often written by prestigious physicists, have been available for decades [1]. The only excuse is the need for a written record for those who actually attended the course.

The lectures are aimed at an audience of physicists having some familiarity with non-relativistic quantum mechanics but only little training in solid state physics, as is often the case for CERN physicists. The only ambition is to demystify a subject which is sometimes considered difficult to penetrate and to provide enough keys to open the doors giving access to the relevant literature.

The very short time imparted to the course precludes any pretention at completeness. Only the most important features have been reviewed, leaving major chapters uncovered. In particular high T_c superconductivity has been completely left out. The hope is simply to encourage CERN physicists, who rely so heavily on superconductivity for the successful operation of their accelerators and detectors, to get some acquaintance with one of the most fascinating fields of physics.

1.2 Some historical landmarks

Traditionally, a course on superconductivity starts with a review of the developments which took place over the half century between discovery and understanding. Lack of time prevents such an approach in the present course, the lines below try to compensate for this deficiency [2].

In 1911, three years after having achieved the liquefaction of helium, Kamerlingh Onnes [3] discovered that the resistivity of mercury, which happens to have a critical temperature just below the liquefaction temperature of helium, was becoming unmeasurably small at low temperatures (Fig. 1.1). It is traditionally considered that solid state physics was born in 1912 with the discovery of X-ray diffraction by Von Laue, Friedrich and Knipping. The discovery of the first important property of superconductivity, namely a perfect dc conductivity, was therefore a truly prehistoric event. It took twenty-two years before the other important property of superconductivity, namely a perfect diamagnetism, was discovered by Meissner and Ochsenfeld [4]. They observed that a sphere of pure tin, cooled below critical temperature in the presence of an external magnetic field, would expell the field from its interior. This was going beyond the property of perfect conductors to resist the penetration of magnetic field by the generation of eddy currents (Fig. 1.2).

Yet another twenty-four years were necessary for superconductivity to be understood and for its microscopic theory to be written down by Bardeen, Cooper and Schrieffer [5]. Meanwhile the various pieces of the jigsaw puzzle had been patiently collected and assembled by the London brothers [6], by Gorter and Casimir [7], by Pippard [8], by Ginzburg and Landau [9] and by many other experimenters and theorists whose contributions have been essential to the 1957 BCS success. From then on superconductivity has been understood as the effect of the attractive one-phonon-exchange interaction between conducting electrons, the presence of an energy gap — commensurate with the critical temperature — between the ground state and the first excited states being the source of the rigidity of the wave function at low temperatures and the cause for both perfect conductivity and perfect diamagnetism.

The years which followed have been the golden years of superconductivity with particularly remarkable contributions from Russian prestigious scientists such as Bogolioubov, Gorkov, Abrikosov and Eliashberg who refined the BCS theory and expressed it in a very elegant form which found applications in many other fields of physics.

At the same time new superconducting alloys were discovered, the properties of the mixed phase of type II superconductors were studied, the tunneling effects predicted by Josephson [10] were experimentally confirmed.

By 1963 it could seem that it was all over and Pippard could say [11] in his concluding talk at the Colgate Conference 'The success is so remarkable that I almost believe you would forgive me if I were to say there now remain no problems in superconductivity' ... and, later in his talk, 'we are in the process of handing over to engineers the problem of superconductivity'.

He was nearly right, except for the discovery of high T_c superconductors which took place in 1986 [12]. Despite the interest triggered by this discovery and the paramount effort dedicated to the field by the community of solid state physicists, the detailed nature of the interaction responsible for high T_c superconductivity is not yet fully understood.

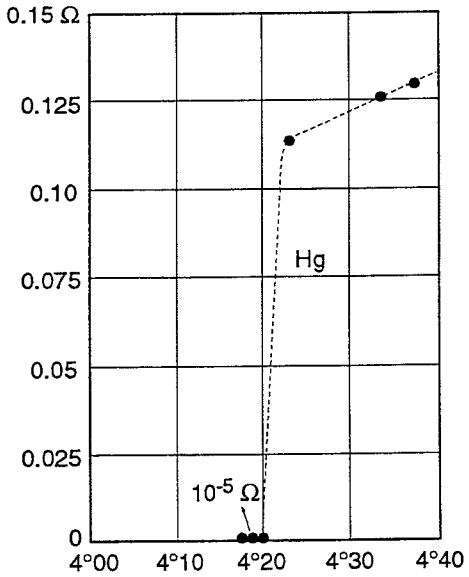

Figure 1.1: Perfect conductivity.

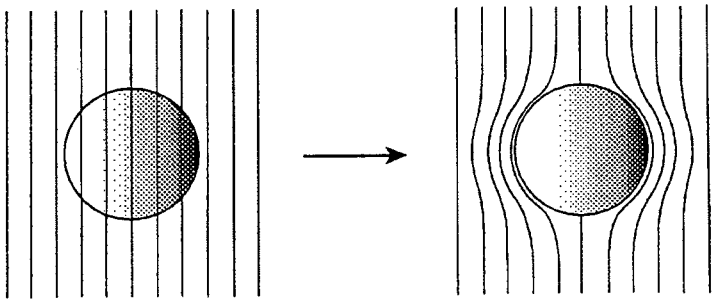

Figure 1.2: Perfect diamagnetism.

2 METALS, NORMAL CONDUCTIVITY

The present chapter introduces some basic notions which are essential for the following. It aims at refreshing the memory of the reader who was once introduced to such notions, or at making the essential points as simply as possible for the reader who was not, or does not remember having been. Hence its somewhat handwaving and untidy nature.

2.1 Lattice periodicity, Bloch functions

As many other solid bodies, metals are made of small crystals (grains) closely packed together. As many others of their properties normal- and super-conductivities can be understood at the crystal level. In the solid metallic state each atom is in practice split into an ion and one (or more) conduction electron(s). The conduction electrons have wave functions extending over the whole crystal and the ions occupy the sites of the lattice. The large mass ratio, $m(\text{ion})/m(\text{electron}) \gtrsim 10^4$, makes it usually possible to ignore the ions movements and to consider the lattice as rigid. Whether atomic crystals are mono- or poly-atomic, whether there is a single conduction electron per atom or more, whether the crystal lattice has one or the other of fourteen possible structures, these are details which are largely irrelevant to most of the considerations of interest here. The study of normal- and super-conductivity deals mostly with the conduction electrons and the states in which they are, making abstraction, as much as possible, of the presence of the ion lattice. As much of the Coulomb interactions within the set of electrons and ions is in practice absorbed in the average potential responsible for the global cohesion of the crystal, the conduction electrons behave as nearly free electrons, having only to obey the constraints imposed by the crystal symmetries. This is best expressed in terms of Bloch functions as sketched below.

The reader is familiar with Fourier series expansions of periodic functions of a single variable. Generalization to three dimensions, as required for crystals, is straightforward.

	One dimension	Three dimensions
Periodicity	n integer $\forall n\ f(x + A_n) = f(x)$ $A_n = na$	$\tilde{n} = (n_1, n_2, n_3)$ integers $\forall \tilde{n}\ f(r + A_{\tilde{n}}) = f(r)$ $A_{\tilde{n}} = \sum_i n_i\ a_i$
Fourier Series	$f(x) = \sum_m c_m \exp(i\ A^*_m x)$ $A^*_m = m\ a^*$ $a^* a = 2\pi$	$f(r) = \sum_{\tilde{m}} c_{\tilde{m}} \exp(i\ A^*_{\tilde{m}} \cdot r)$ $A^*_{\tilde{m}} = \sum_i m_i\ a^*_i$ $a^*_i \cdot a^*_j = 2\pi\delta ij$

A lattice periodic function, with the elementary cell spanned by a_1, a_2, a_3, can be analysed in terms of a Fourier series of the form

$$f(r) = \sum_{A^*} C_{A^*} \exp\ (i\ A^* \cdot r) \tag{2.1}$$

where A^* are vectors of the reciprocal lattice having as a basis a^*_1, a^*_2, a^*_3

$$a^*_3 = 2\pi \frac{a_1 \wedge a_2}{a_1 \cdot a_2 \wedge a_3} \quad , \text{ and circ. perm.}$$

The elementary cell of the reciprocal lattice is called the first Brillouin zone (Fig. 2.1).

The mean lattice periodic potential governing the motion of a single conduction electron can accordingly be written

$$U(r) = \sum_{A^*} U_{A^*} \exp\ (i\ A^* \cdot r) \tag{2.2}$$

Developing the electron state $|\psi\rangle$ on plane waves

$$|\psi\rangle\ = \sum_{k} C_k\ |k\rangle \tag{2.3}$$

the Schrödinger equation reads

$$0 = (H - E)|\psi\rangle\ = \sum_{k} C_k (H - E)|k\rangle \tag{2.4}$$

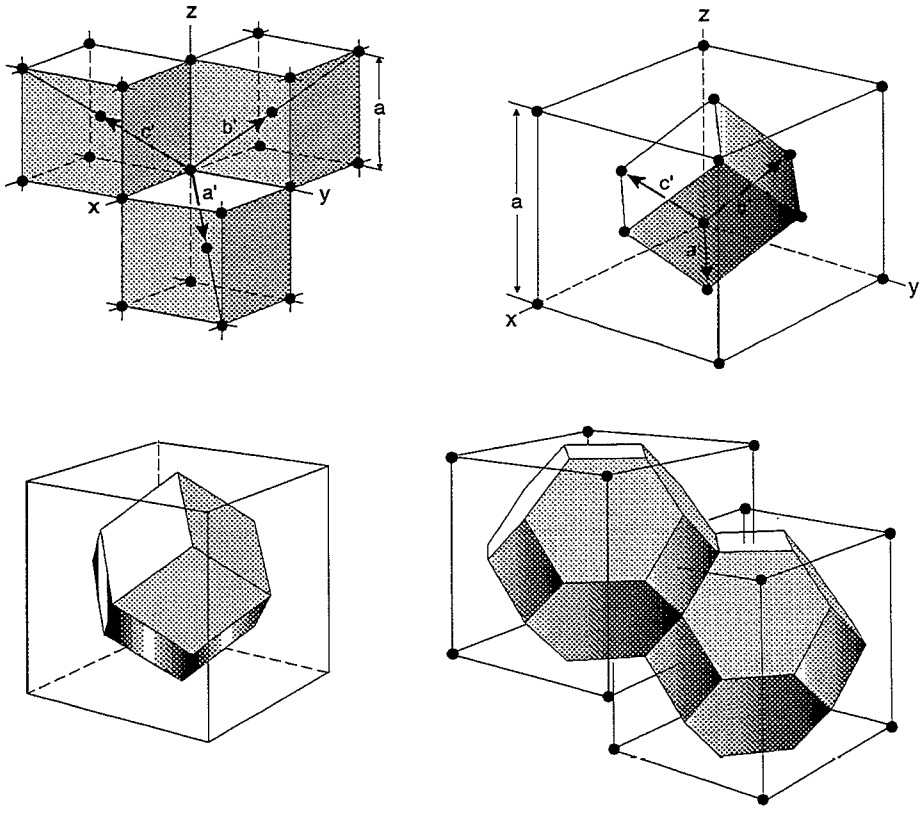

Figure 2.1: Elementary cells of two usual lattices (top) and of their reciprocal lattices (bottom).

but

$$(H - E)|k\rangle\ = \left(\frac{\hbar^2 k^2}{2\ m}\ - E\right)|k\rangle + \sum_{A^*} U_{A^*}\ |k + A^*\rangle \tag{2.5}$$

reducing the Schrödinger equation to a system of equations in C_k (an infinity!)

$$\left(\frac{\hbar^2 k^2}{2\ m} - E\right)\ C_k + \sum_{A^*} U_{A^*}\ C_{k-A^*} = 0 \tag{2.6}$$

The sum on k in (2.3) reduces to a sum on A^*.
For a given wave vector k the electron is therefore in a state (Bloch theorem)

$$\begin{cases} \psi_k(r) = u_k(r) \ \exp \ (ik.r) \\ \text{with } u_k(r) = \sum_{A^*} \ C_{k-A^*} \ \exp \ (-i \ A^* \cdot r) \\ \text{being lattice periodic} \end{cases} \tag{2.7}$$

The functions $\psi_k(r)$ are called Bloch functions. The lattice periodic function $u_k(r)$ is obtained by solving the system of equations (2.6). There may be values of E for which this system has no solution, giving rise to forbidden bands. This is best illustrated by a one-dimensional toy model with U having the form of a square wave (Kronig-Penney). It is left as an exercise to the reader (see Fig. 2.2). While the band structure is central to the study of insulators and semi-conductors, it is of peripheral importance for metals, where the conduction band is far from being full or empty.

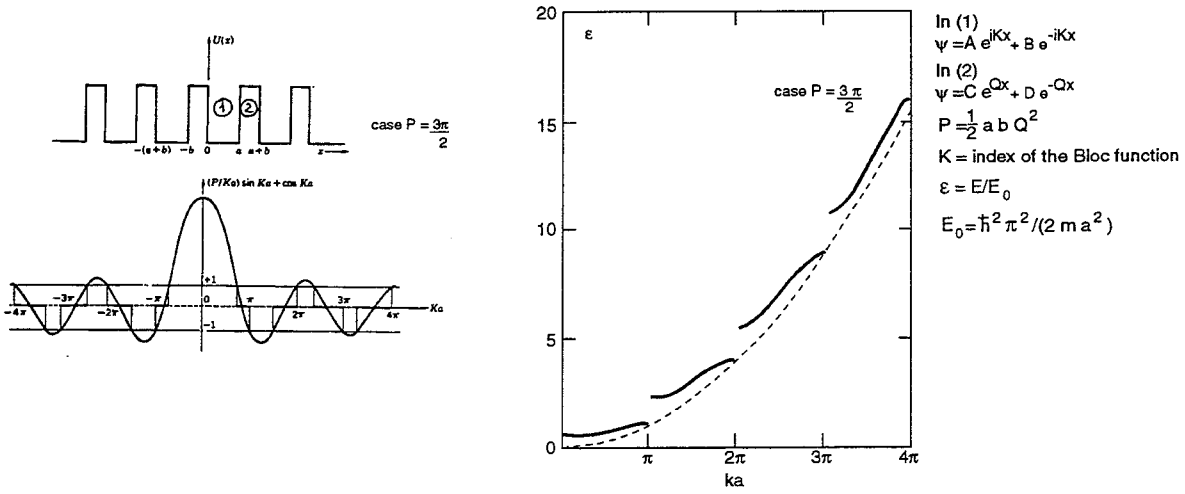

Figure 2.2: The Kronig-Penney toy model.

The deviation between a Bloch function and its supporting plane wave causes the dispersion relation $E = f(k)$ to differ from the free electron expression $E = \hbar^2 k^2 / 2 \ m$. Similarly it implies that the effective mass $m^* = dp/dv$ differs from the free electron mass (p = momentum, v = velocity).

2.2 Lattice vibrations, phonons

Lattice vibrations can be reduced to fundamental modes for which the displacement $\delta_{\tilde{n}}$ of an ion around its equilibrium position at site $A_{\tilde{n}}$ takes the form

$$\delta_{\tilde{n}} = \delta_0 \ \exp \ (i[k \cdot A_{\tilde{n}} - \omega t]) \tag{2.8}$$

Once k is given (limited to the first Brillouin zone) $\delta_{\tilde{n}}$ can be calculated.

The restoring force exerted on an ion at the origin by another ion at site $A_{\tilde{m}}$ and displaced by $\delta_{\tilde{m}}$ can be written, to first order, $-\overline{\overline{C}}_{\tilde{m}} \ \delta_{\tilde{m}}$ where $\overline{\overline{C}}_{\tilde{m}}$ is a third rank tensor and $\overline{\overline{C}}_{\tilde{m}} = \overline{\overline{C}}_{-\tilde{m}}$. M being the ion mass, the equation of motion is

$$M \frac{d^2}{dt^2} \ \delta_{\tilde{n}} = -\sum_{\tilde{m}} \overline{\overline{C}}_{\tilde{m}} \ \delta_{\tilde{n}+\tilde{m}} \tag{2.9}$$

$$-M\omega^2\ \delta_{\tilde{n}} = -\sum_{\tilde{m}} \overline{\overline{C}}_{\tilde{m}}\ e^{i(k\cdot A_{\tilde{m}})}\ \delta_{\tilde{n}} \tag{2.10}$$

or writing

$$\overline{\Gamma} = \frac{1}{M}\ \sum_{\tilde{m}}\ \overline{\overline{C}}_{\tilde{m}}\ \exp\ (i[k\cdot A_{\tilde{m}}]) \tag{2.11}$$

$$(\omega^2 - \overline{\Gamma})\ \delta_{\tilde{n}} = 0 \tag{2.12}$$

Writing the eigenvalues of (2.12) ω_α, the three eigenvectors have the form ($\alpha = x,\ y,\ z$)

$$\delta^\alpha_{\tilde{n}}(k) = \delta^\alpha_0(k)\ \exp\ (i[k\cdot A_{\tilde{n}} - \omega_\alpha(k)t]) \tag{2.13}$$

where the dependence on k is made explicit.

The group velocity

$$v_g = \nabla_k \omega \tag{2.14}$$

vanishes at the edges of the Brillouin zone (standing wave). Once quantized the energy of a mode is

$$\epsilon = \left(n + \frac{1}{2}\right)\hbar\omega = \frac{1}{2}\rho V\omega^2\delta_0^2 \tag{2.15}$$

where ρ and V are the density and volume of the sample. A quantum of vibration, $\hbar\omega$, is called a phonon. It has no momentum but behaves in interactions as if it had a momentum $\hbar k$, called the crystal momentum (i.e. $\hbar k$ must be included in the balance equation of the total momentum).

The dispersion relation $\omega = f(k)$ (see Fig. 2.3) is related to the density of states $\mathcal{D}(\omega)$. As it is $(2\pi)^{-3}$ in k-space for a unit volume of the crystal (see next section)

$$d\omega\mathcal{D}(\omega) = \frac{V}{(2\pi)^3}\ \int_\omega^{\omega+d\omega}\ d^3k \tag{2.16}$$

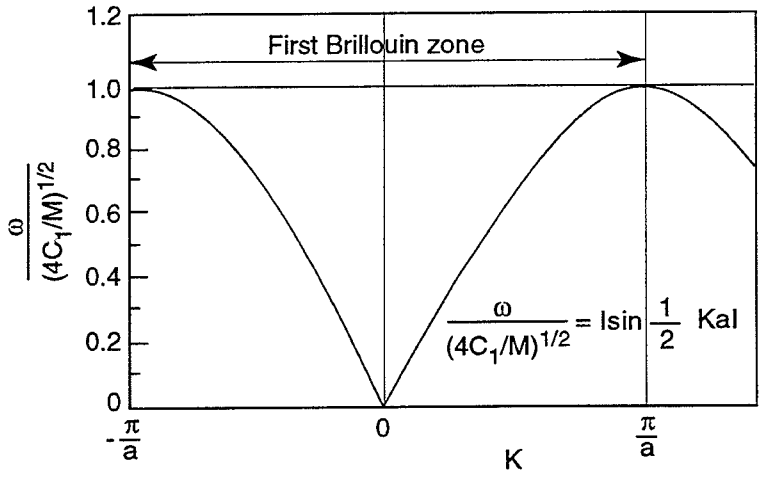

Figure 2.3: Dispersion relation in one dimension ($\overline{\overline{C}} = C_1$).

and, introducing the sound velocity, $v_g = \nabla_k(\omega)$

$$\mathcal{D}(\omega) = \frac{V}{(2\pi)^3}\ \int_{S_\omega}\ \frac{d\ S_\omega}{v_g} \tag{2.17}$$

where dS_ω is a surface element on the surface S_ω of constant ω in k-space.

For constant v_g (Debye approximation) the dispersion relation is simply $\omega = v_g\, k$ and

$$\mathcal{D}(\omega) = \frac{V}{(2\pi)^3}\,\frac{4\pi\omega^2}{v_g^3} = \frac{V\omega^2}{2\pi^2 v_g^3} \tag{2.18}$$

until ω reaches the cut-off frequency ω_D which exhausts the total number of atoms in the crystal, N

$$\omega_D = v_g\left(\frac{6\pi^2 N}{V}\right)^{1/3} \quad \text{for} \quad \int_0^{\omega_D} \mathcal{D}(\omega)\, d\omega = \frac{V\omega_D^3}{6\pi^2 v_g^3} \tag{2.19}$$

ω_D is called the Debye frequency (Fig. 2.4).

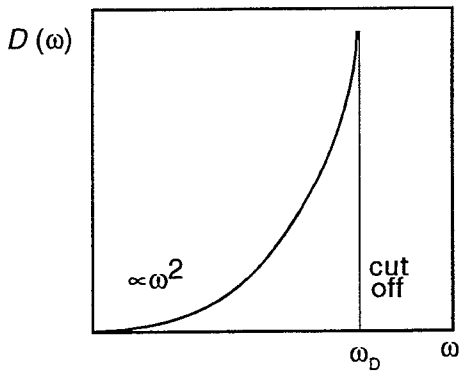

Figure 2.4: $\mathcal{D}(\omega)$ in the Debye approximation.

Experimentally the density of states $\mathcal{D}(\omega)$ is deduced from neutron diffraction and tunneling experiments and is observed to retain the two above features of an ω^2 dependence at low values of ω and a cut-off at the Debye frequency. However, inbetween these limits, it exhibits a complex structure (Van Hove singularities). Figure 2.5 shows examples of $\alpha^2\,\mathcal{D}(\omega)$ where α is the electron-phonon coupling constant with little ω dependence.

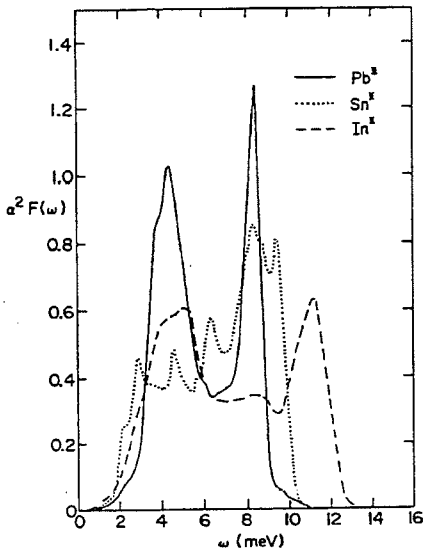

Figure 2.5: Examples of $\alpha^2\,\mathcal{D}(\omega)$ vs ω.

2.3 Free electron gas, response to an electromagnetic field

Many properties of a metal can be qualitatively understood by considering the limiting case of a free electron gas with n non-interacting electrons per unit volume. The reason for such a crude picture to be a sensible approximation to reality is twofold:

i) the dominant rôle played by the Pauli principle which imposes that a state be occupied by at most two electrons, one with spin up and the other with spin down;

ii) the fact that Bloch functions are relatively modest distortions of their supporting plane waves.

The hamiltonian decouples in a sum of n individual hamiltonians $H_i = (\hbar^2/2\,m)\,k_i^2$ and its eigenstates are simply the product of n single electron plane waves of the form $\Psi_k = \exp\,(ik\cdot r)\mid\alpha\rangle$ where $\mid\alpha\rangle = \mid\uparrow\rangle$ or $\mid\downarrow\rangle$ for the spin part. By convention we write Ψ_k as above rather than with $(2\pi)^{-3/2}$ factors in front, so its Fourier transform is $\frac{1}{(2\pi)^3}\,\delta(k'-k)$. Remember that plane waves are not normalizable, a plane wave describing a density of one particle per unit volume in r-space corresponds to a volume of $(2\pi)^3$ in k-space.

The ground-state corresponds therefore to all low energy states being occupied by a pair $(\uparrow\downarrow)$ up to an energy E_F, called the Fermi energy and such that $n = 2\,(4/3)(\pi k_F^3)/(2\pi)^3$

$$E_F = \frac{\hbar^2\,k_F^2}{2\,m} \tag{2.20}$$

$$n = \frac{k_F^3}{3\pi^2} \tag{2.21}$$

Excited states are simply obtained by lifting an electron from the 'Fermi sea', $E < E_F$ to $E' > E_F$, which is most easily achieved when both E and E' are close to the Fermi surface (see Fig. 2.6).

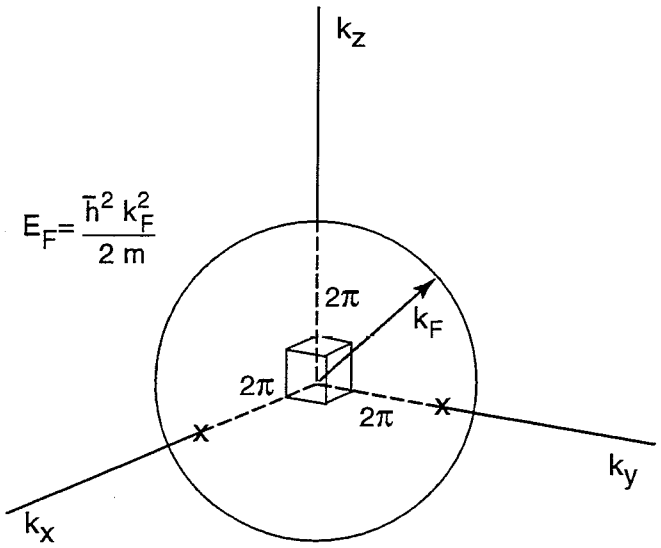

Figure 2.6: The Fermi sphere.

Introducing the Fermi velocity v_F and the Fermi density of states per unit energy N_F we have (see Figs. 2.7 and 2.8)

$$\begin{cases} k_F &= (3\pi^2 n)^{1/3} \\ E_F &= (\hbar^2/2\ m)\ (3\pi^2 n)^{2/3} \\ v_F &= (\hbar/m)\ (3\pi^2 n)^{1/3} \\ N_F &= \frac{dn}{dE}|_F = 3n/(2E_F) \end{cases} \tag{2.22}$$

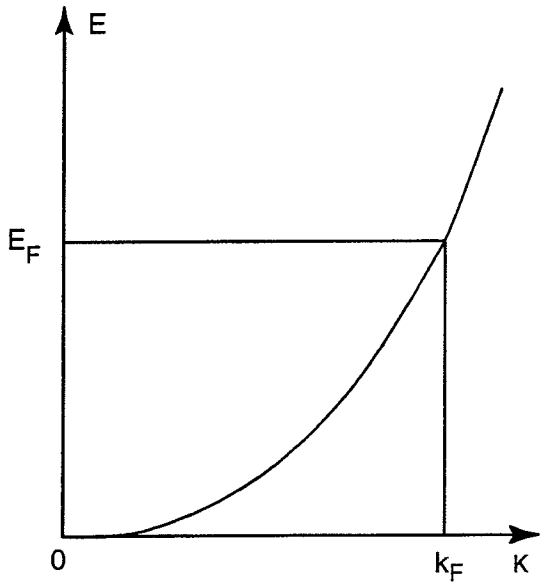

Figure 2.7: E vs k.

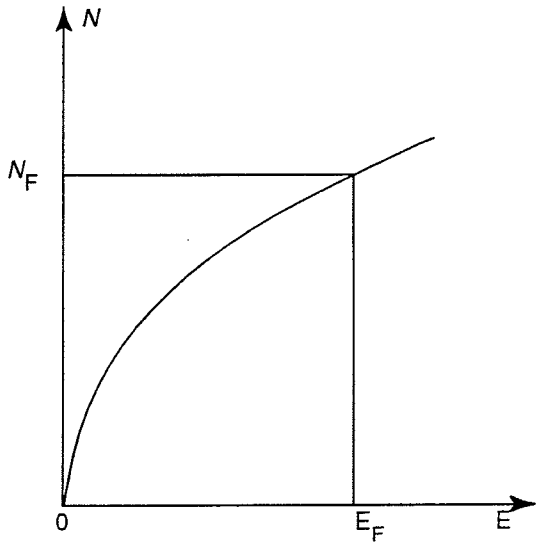

Figure 2.8: N vs E.

Note that for $n = 1$ electron per 10 Å^3

$$\beta_F = \frac{v_F}{c} = \frac{197\ \text{MeV fm}}{0.511\ \text{MeV}} \left(\frac{3\pi^2}{10 \times 10^{15}\ \text{fm}^3} \right)^{1/3} = 5.5 \times 10^{-3}$$

which justifics thc usc of non-relativistic quantum mechanics.

In real life the Fermi surface, which contains the occupied states of the normal ground state and on which $E = \text{cte} = E_F$ may significantly differ from a sphere (see Fig. 2.9).

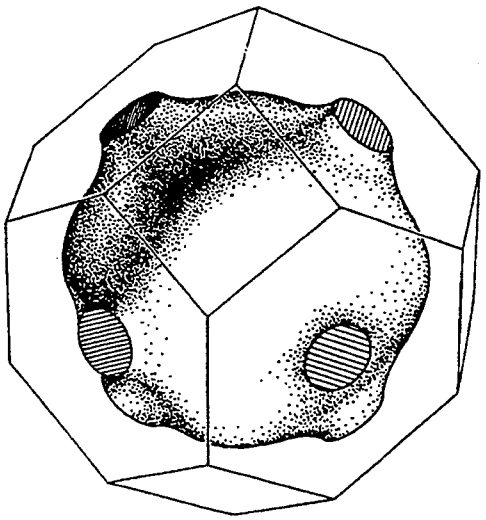

Figure 2.9: The Fermi surface of copper.

Response to a constant electric field

In a constant electric field E each electron feels a force

$$\frac{dp}{dt} = e\,E \;(e < 0) \tag{2.23}$$

resulting in a translation of the whole Fermi sphere at uniform velocity in k-space, $e\,\frac{E}{\hbar}$. A current (more properly a current density) $j = (ne/m)\,p$ is generated with

$$\frac{dj}{dt} = \frac{ne^2}{m}\,E \tag{2.24}$$

(see Fig. 2.10).

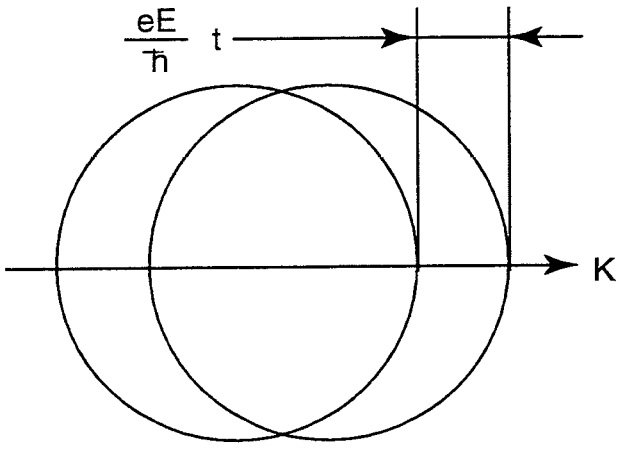

Figure 2.10: Translation of the Fermi sphere in the presence of a constant electric field E.

In a perfect conductor each electron would be uniformly accelerated but in a real conductor collisions with impurities and defects limit this progression. Such collisions can

be characterized by a relaxation time τ such that a state of non-zero current in zero field ($E = 0$) would return to equilibrium ($j = 0$) according to a law

$$\frac{dj}{dt} = -\frac{1}{\tau}\, j \tag{2.25}$$

(see Fig. 2.11).

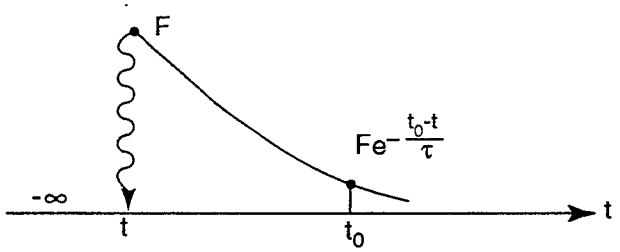

Figure 2.11: See text.

Combining both effects

$$\frac{dj}{dt} = \frac{\sigma E - j}{\tau} \tag{2.26}$$

with $\sigma = \frac{ne^2\tau}{m}$ being the conductivity.

At equilibrium $dj/dt = 0$

$$J = \sigma E \qquad \text{(Ohm's law)} \tag{2.27}$$

Response to a constant magnetic field

In a constant magnetic field H each electron feels an acceleration

$$\frac{dv}{dt} = +\frac{e}{mc}\, v_\wedge\, H \tag{2.28}$$

corresponding to a uniform rotation with frequency ω_c (cyclotron frequency)

$$\omega_c = \frac{eH}{mc} = 17.6 \text{ MHz/G} \tag{2.29}$$

resulting in a zero net current. However in the simultaneous presence of an electric field the current is affected. In a crossed field configuration ($H \cdot E = 0$)

$$j = \sigma E \ \cos\theta \text{ with } \tan\theta = \omega_c\, \tau \tag{2.30}$$

and j making an angle θ with respect to E in the plane normal to H (Fig. 2.12). This is the Hall effect.

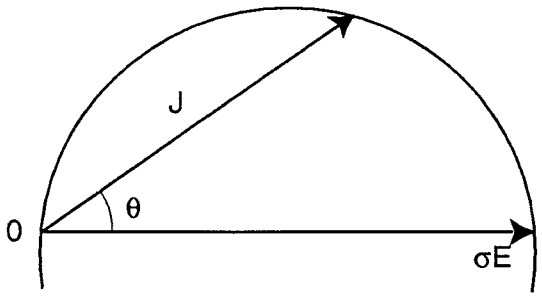

Figure 2.12: Hall effect.

Returning to the $H = 0$ case, the hamiltonian is $\frac{1}{2\,m}\,(p - \frac{e}{c}\,A)^2$ where A is the vector potential, $H = \nabla_\wedge\, A$.

Indeed, writing

$$p = mv + \frac{e}{c}\,A \tag{2.31}$$

and

$$\mathcal{H} = \frac{1}{2\,m}\,v^2 = \frac{1}{2\,m}\,(p - \frac{e}{c}\,A)^2 \tag{2.32}$$

one can verify that the Hamilton equations hold, i.e.

$$\begin{cases} \frac{\partial \mathcal{H}}{\partial p_i} &= \frac{dx_i}{dt} \\ \frac{\partial \mathcal{H}}{\partial x_i} &= -(F_i + \frac{e}{c}\,v \cdot \nabla A_i) = -\frac{dp_i}{dt} \end{cases} \tag{2.33}$$

For a constant magnetic field one can choose

$$A = H_\wedge r = H_\wedge r_\perp$$

and

$$(p - \frac{e}{c}\,A)^2 = p_\parallel^2 + (p_\perp^2 + \frac{e^2}{c^2}\,H^2\,r_\perp^2) - \frac{eH}{mc}\,L_\parallel \tag{2.34}$$

The first term decouples the longitudinal motion (parallel to H) and the last term does not change the energy. However the second term is an harmonic oscillator hamiltonian in the plane normal to H, with discrete eigenstates equally spaced by $\hbar\omega_c$. The energy spectrum condenses in a set of equally spaced states (Fig. 2.13) and the Fermi sphere in a set of coaxial cylinders having their axis parallel to H.

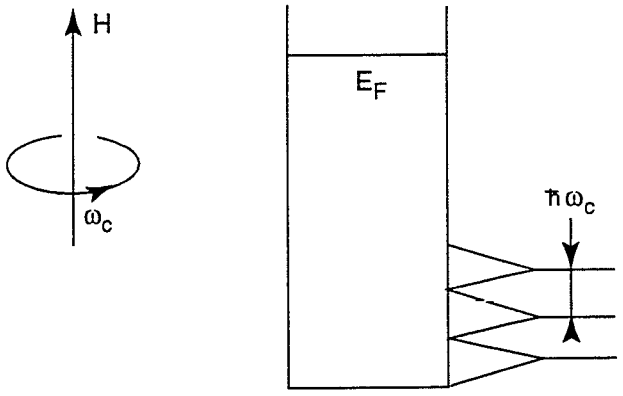

Figure 2.13: See text.

As this is important in the understanding of the Meissner effect, consider it in more detail.

Taking

$$A = x\,H\,\hat{y} \qquad \nabla_\wedge\, A = H\hat{z} \qquad p = \frac{\hbar}{i}\,\nabla$$

$$-\frac{\hbar^2}{2\,m}\,\nabla^2\,\Psi - \frac{e}{mc}\,\frac{\hbar}{i}\,x\,H\frac{\partial \Psi}{\partial y} + \frac{e^2x^2H^2}{2\,mc^2}\,\Psi = E\Psi$$

Writing

$$\Psi = \varphi(x)\ \exp\ (i[k_y\ y + k_z\ z])$$

$$\begin{aligned}
\frac{\partial \Psi}{\partial y} &= i k_y\ \Psi \qquad & \frac{\partial^2 \Psi}{\partial y^2} &= -k_y^2\ \Psi \\
\frac{\partial^2 \Psi}{\partial x^2} &= \varphi''(x)\frac{\Psi}{\varphi} \qquad & \frac{\partial^2 \Psi}{\partial z^2} &= -k_z^2\ \Psi \\
\frac{\hbar^2}{2\,m}\,\varphi'' &= \left\{\frac{1}{2\,m}\left(\hbar k_y - \frac{e}{c}\,Hx\right)^2 - \left(E - \frac{\hbar^2\ k_Z^2}{2\,m}\right)\right\}\ \varphi \\
\omega_c &= \frac{eH}{mc} \qquad & x_0 &= \frac{\hbar c\ k_y}{eH} \\
E &= \frac{\hbar^2\ k_z^2}{2\,m} + (n + \frac{1}{2})\ \hbar\omega_c
\end{aligned}$$

$$\frac{\hbar^2}{2\,m}\,\varphi'' - \left(\frac{1}{2}\,m\omega_c^2[x - x_0]^2 - [E - \frac{\hbar^2 k_Z^2}{2\,m}]\right)\ \varphi = 0$$

From which

$$e\langle A\rangle\ =\ e\langle x\rangle\ H_{\hat{y}} = e\,\frac{\hbar c}{eH}\ \langle k_y\rangle\ H_{\hat{y}} = \hbar c\langle k_y\rangle\hat{y}$$

and

$$\langle p\rangle = \hbar\langle k_y\rangle\hat{y} = \frac{e}{c}\ \langle A\rangle\ .$$

The current J reads

$$J = \frac{e}{m}\langle p - \frac{e}{c}A\rangle\ =\ 0\ . \tag{2.35}$$

The current vanishes as the paramagnetic term $J_p = (e/m)\ p$ exactly cancels the diamagnetic term $J_D = (e^2/mc)\ A$.

Finally note that the mismatch near E_F between the last $\hbar\omega_c$ band and the Fermi level results in small effects (weak Landau diamagnetism and de Haas-van Alphen effect).

Response to a spatially varying electric field

In a spatially varying electric field Ohm's law starts failing. Consider electrons around the phase-space point (r, k) at time t_0. From the remote past its energy has been shifted by a quantity ΔE due to collisions. To evaluate ΔE it is useful to note that the action of a force $F(r,t)$ which acted at time $t < t_0$ (see Fig. 2.11) has been attenuated at time t_0 by a factor $\exp\,[-(t_0 - t)/\tau]$ due to the restoring effect of successive collisions. Namely

$$\begin{aligned}
\Delta E\ &=\ \int_{-\infty}^{t_0}\ v\cdot F(r,t)\ e^{(t-t_0)/\tau}\ dt \qquad (2.36)\\
&=\ \int_{-\infty}^{r_0}\ F_{\|}(r,t)\ e^{-|r-r_0|/\ell}\ dr
\end{aligned}$$

with $F_{\|} = F\cdot v/v$ and $\ell = v\tau$ (mean free path).

Rewriting

$$\Delta E = \int_0^{\infty}\ e\,\frac{\tilde{E}\cdot R}{R}\ e^{-R/\ell}\ dR$$

with $R \parallel v$ and $\tilde{E} = E(r - R,\ t - \frac{R}{v})$ and noting that the equilibrium current is

$$J = \oint \frac{\Delta s \Delta k}{4\pi^3}\, ev$$

with $\Delta s = k_F^2 \Delta\Omega$ on the Fermi sphere and $\Delta k = \frac{m\Delta v}{\hbar} = \frac{\Delta E}{\hbar v}$

$$J = \frac{e^2}{4\pi^3\hbar}\, k_F^2 \int \frac{R(\tilde{E}\cdot R)}{R^4}\, e^{-R/\ell}\, d^3R \tag{2.37}$$

This is known as Chambers' equation and replaces Ohm's law when the electric field varies significantly over a mean free path [13]. Such a case is realized with high frequency electromagnetic waves. Consider a wave (E_x, H_y) incident on the plane (x, y) surface of a conductor. Inside the conductor Maxwell's equations imply

$$\frac{\partial E_x}{\partial z} = -i\omega H_y \qquad \frac{\partial H_y}{\partial z} = \frac{4\pi}{c}\, J_x$$

$$i.e.\ \frac{\partial^2 E_x}{\partial z^2} = -\frac{4\pi}{c}\, i\omega J_x$$

Writing $J_x = \sigma E_x$ (Ohm's law) results in

$$E_x(z) = E_x(0)\ e^{-\gamma z} \qquad \text{with} \qquad \gamma = \frac{1+i}{\lambda}\,, \qquad \lambda = \left(\frac{2\pi}{c}\,\omega\sigma\right)^{-1/2} \tag{2.38}$$

Here λ is the skin depth through which the field penetrates. The surface impedance reads

$$Z_s = \frac{E_x(0)}{\int_0^\infty J_x(z)dz} = \frac{1}{\sigma}\,\frac{1+i}{\lambda} = R_s + i\, X_s \tag{2.39}$$

where R_s is the surface resistance and X_s the surface reactance. Here

$$R_s = \left(\frac{2\pi\omega}{\sigma}\right)^{1/2} = X_s\ . \tag{2.40}$$

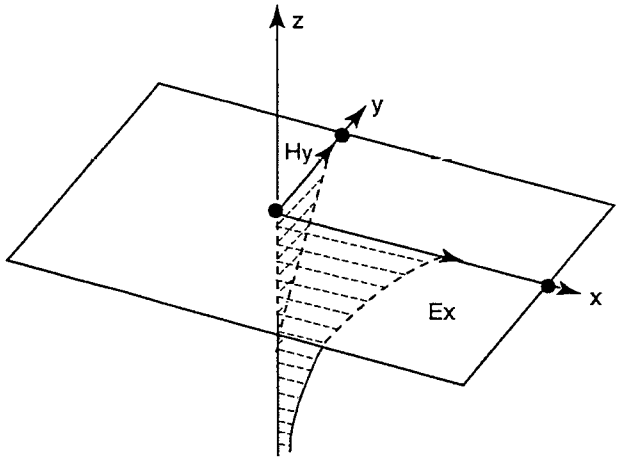

Figure 2.14: See text.

For $\lambda \approx \ell$ or smaller the above calculation is no longer valid. Ohm's law must be replaced by Chambers' equation, resulting in the 'anomalous skin effect'.

2.4 Fermion creation and annihilation operators

The use of creation and annihilation operators when dealing with multifermion states is extremely convenient. For the purpose of the present lectures an elementary introduction is sufficient.

A n-fermion state where the n fermions occupy single particle states $|\Psi_i\rangle$, $i = 1, 2 \ldots n$ must be antisymmetric in the exchange of any two particles. It reads therefore

$$|\Psi_1 \Psi_2 \ldots \Psi_n\rangle = \sum_P (-)^P \frac{I}{\sqrt{n!}} |\Psi_{i1}\rangle |\Psi_{i2}\rangle \ldots |\Psi_{in}\rangle \tag{2.41}$$

where the sum is over all permutations P changing $(1, 2 \ldots n)$ to $(i_1, i_2 \ldots i_n)$. This can also be written as

$$\langle \varphi_1 \varphi_2 \ldots \varphi_n | \Psi_1 \Psi_2 \ldots \Psi_n \rangle = \text{Det} \left(\langle \varphi_i | \Psi_j \rangle \right) \tag{2.42}$$

Such a determinant is called a Slater determinant.

One defines the creation operator for a particle in state $|\xi\rangle$ as $a^+(\xi)$ such that

$$\begin{cases} a^+(\xi) |\Psi_1 \Psi_2 \ldots \Psi_n\rangle = |\xi, \Psi_1 \Psi_2 \ldots \Psi_n\rangle \\ a^+(\xi)|0\rangle = |\xi\rangle \end{cases} \tag{2.43}$$

What is $a(\xi)$?

$$\begin{aligned} &\langle \varphi_1 \varphi_2 \ldots \varphi_n | a(\xi) | \Psi_1 \Psi_2 \ldots \Psi_n \rangle = \langle \Psi_1 \Psi_2 \ldots \varphi_n | \xi \varphi_1 \varphi_2 \ldots \varphi_n \rangle^* \qquad (2.44) \\ = &\sum_{k=1}^{n} \left\{ (-)^{k-1} \langle \Psi_k | \xi \rangle \text{Det}_{i \neq k} \langle \Psi_i | \varphi_j \rangle \right\}^* \\ = &\sum_{k=1}^{n} (-)^{k-1} \langle \xi | \Psi_k \rangle \langle \varphi_1 \varphi_2 \ldots \varphi_{n-1} | \Psi_1 \Psi_2 \Psi_k \ldots \Psi_n \rangle \end{aligned}$$

As this is true for any $|\varphi_1 \varphi_2 \ldots \varphi_n\rangle$, $a(\xi)$ is the annihilation operator for state $|\xi\rangle$.

The anticommutation relations

$$[a(\varphi_1),\ a(\varphi_2)]_+ = [a^+(\varphi_1),\ a^+(\varphi_2)]_+ = 0 \tag{2.45}$$

are trivially verified. Moreover

$$\begin{aligned} a(\varphi_1) a^+(\varphi_2) |\Psi_1 \Psi_2 \ldots \Psi_n\rangle &= \langle \varphi_1 | \varphi_2 \rangle |\Psi_1 \Psi_2 \ldots \Psi_n\rangle \\ &+ \sum_k (-)^k \langle \varphi_1 | \Psi_k \rangle |\varphi_2 \Psi_1 \Psi_2 \ldots \not{\Psi}_k \ldots \Psi_n\rangle \\ a^+(\varphi_2)\ a(\varphi_1) |\Psi_1 \Psi_2 \ldots \Psi_n\rangle &= \sum_k (-)^{k-1} \langle \varphi_1 | \Psi_k \rangle |\varphi_2 \Psi_1 \ldots \not{\Psi}_k \ldots \Psi_n\rangle \\ \text{i.e } [a(\varphi_1),\ a^+(\varphi_2)]_+ &= \langle \varphi_1 | \varphi_2 \rangle \end{aligned} \tag{2.46}$$

For an orthonormal $|\varphi\rangle$ basis

$$\begin{cases} [a_\alpha,\ a_\beta]_+ - \left[a_\alpha^+,\ a_\beta^+\right]_+ - 0 \\ \left[a_\alpha,\ a_\beta^+\right]_+ = \delta_{\alpha\beta} \end{cases} \tag{2.47}$$

A similar calculation for multiboson states would show that their annihilation and creation operators obey instead commutation relations of the same form.

The relations below illustrate the use of creation and annihilation operators in simple examples.

$$|x_1 x_2 \ldots x_n\rangle = a^+(x_1)\ a^+(x_2) \ldots a^+(x_n)|0\rangle \tag{2.48}$$

$$|k_1\ k_2 \ldots k_n\rangle = a^+(k_1)\ a^+(k_2) \ldots a^+(k_n)|0\rangle \tag{2.49}$$

$$[a(x),\ a^+(x')]_+ = \delta^3(x - x') \tag{2.50}$$

$$[a(k),\ a^+(k')]_+ = (2\pi)^3\ \delta^3\ (k - k') \tag{2.51}$$

$$|k\rangle = \int d^3x\ |x\rangle\langle x|k\rangle = \int d^3x\ e^{ik\cdot x}|x\rangle \tag{2.52}$$

$$a^+(k) = \int d^3x\ a^+(x)\ e^{ik\cdot x} \tag{2.53}$$

$$a^+(x) = \int \frac{d^3k}{(2\pi)^3}\ a^+(k)\ e^{-ik\cdot x} \tag{2.54}$$

The particle number operator is

$$\mathcal{N} = \sum\ a_\alpha^+\ a_\alpha = \int\ d^3x\ a^+(x)a(x) = \int\ \frac{d^3k}{(2\pi)^3}\ a^+(k)\ a(k) \tag{2.55}$$

The total momentum operator is

$$P = \int\ \frac{d^3k}{(2\pi)^3}\ \hbar k\ a^+(k)\ a(k) = \int\ d^3x\ a^+(x)\ \frac{\hbar}{i}\ \bigtriangledown\ a(x) \tag{2.56}$$

In a potential $V(x)$ the single particle hamiltonian is

$$H^1 = \frac{p^2}{2\ m} + V(x) \qquad \langle x|H^1|x'\rangle = (-\frac{\hbar^2}{2\ m}\ \bigtriangledown^2 + V)\delta^3(x - x') \tag{2.57}$$

and the total hamiltonian is then simply

$$H\ =\ \int\ d^3\ x\ a^+(x)\Big\{-\frac{\hbar^2\bigtriangledown^2}{2\ m} + V(x)\Big\}\ a(x) \tag{2.58}$$

$$\begin{aligned}\langle k|H^1|k'\rangle\ &=\ \frac{\hbar^2k^2}{2\ m}\ (2\pi)^3\delta^3(k - k') + \int d^3x\ e^{-ik\cdot x}\ V(x)\ e^{ik'\cdot x} \\ &=\ \frac{\hbar^2\ k^2}{2\ m}\ (2\pi)^3\ \delta^3(k - k') + \tilde{V}\ (k - k')\end{aligned} \tag{2.59}$$

with

$$\tilde{V}(q) = \int\ d^3x\ V(x)\ e^{-iq\cdot x} \tag{2.60}$$

Then

$$H\ =\ \int \frac{d^3k}{(2\pi)^3}\ \frac{\hbar^2k^2}{2\ m}\ a^+(k)\ a(k) + \int \frac{d^3k}{(2\pi)^3}\ \int \frac{d^3q}{(2\pi)^3}\ \tilde{V}(q)\ a^+(p+q)\ a(p) \tag{2.61}$$

Here the last term is a sum over terms which annihilate a particle of momentum p and recreate it with momentum $p + q$

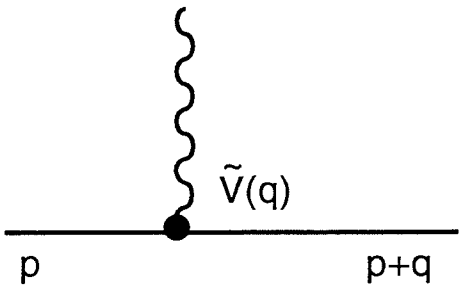

Figure 2.15: See text.

Note that writing

$$\rho(x) = a^+(x)\ a(x) \tag{2.62}$$

one obtains

$$\mathcal{N} = \int\ d^3x\ \rho(x) \tag{2.63}$$

$$V = \int\ d^3x\ V(x)\ \rho(x) \tag{2.64}$$

Consider now a two-body potential

$$V^{(2)}\ (x_i,\ x_j) = V^{(2)}(x_j,\ x_i) = V(|x_j - x_i|) \tag{2.65}$$

$$V^{(2)} = \frac{1}{2}\ \int d^3x \int d^3y\ |x,y\rangle\ V^{(2)}\ (x,y)\ \langle x,y| \tag{2.66}$$

$$\begin{aligned} V^{(1)} &= \frac{1}{2}\int d^3x \int d^3y\ V^{(2)}\ (x,y)\ \rho(x)\ \rho(y) \\ &= V + \frac{1}{2}\int d^3x\ V^{(2)}\ (x,y)\ \rho(x) \end{aligned} \tag{2.67}$$

$$V = \frac{1}{2}\int \frac{d^3q}{(2\pi)^3} \int \frac{d^3p}{(2\pi)^3} \int \frac{d^3p'}{(2\pi)^3}\ \tilde{V}(q)\ a^+(p+q)\ a^+(p'-q)\ a(p')a(p) \tag{2.68}$$

$$V|p_1p_2\rangle = \int \frac{d^3q}{(2\pi)^3}\ \tilde{V}(q)|p_1+q,\ p_2-q\rangle \tag{2.69}$$

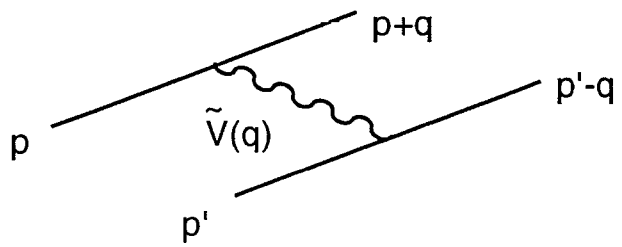

Figure 2.16: See text.

In order to get more familiarity with the algebra of the operators a and a^+, consider the following wave function which will be useful in BCS theory:

$$|\Psi\rangle = \Pi_k\ (\cos\theta_k + \sin\theta_k\ a_k^+)|0\rangle \tag{2.70}$$

Unless all θ_k are 0 modulo $\frac{\pi}{2}$, $|\Psi\rangle$ is not an eigenstate of $\mathcal{N}$. Let us evaluate the root mean square deviation of $\mathcal{N}$ with respect to its mean

$$\mathcal{N}_i|\Psi\rangle = \Pi_k \ldots a_i^+ \, a_i \, (\cos\theta_i + \sin\theta_i \, a_i^+) \ldots |0\rangle$$

$$= \Pi_k \ldots \sin\theta_i \, a_i^+ \ldots |0\rangle = \sin\theta_i \, |\Psi, i\rangle$$

but $|\Psi\rangle = \cos\theta_i|\Psi, \bar{i}\rangle + \sin\theta_i|\Psi, i\rangle$

$$\langle\mathcal{N}\rangle = \sum_i \langle\Psi|\mathcal{N}_i|\Psi\rangle = \sum_i \sin^2\theta_i \tag{2.71}$$

Similarly

$$|\Psi, i\rangle = \cos\theta_j \, |\Psi, i\bar{j}\rangle + \sin\theta_j \, |\Psi, ij\rangle$$

$$\langle\Psi, i|\Psi, j\rangle = \sin\theta_i \, \sin\theta_j \; (i \neq j)$$

$$\begin{aligned} \langle\mathcal{N}^2\rangle &= |\sum_i \mathcal{N}_i|\Psi\rangle|^2 = \sum_{ij} \sin\theta_i \, \sin\theta_j \langle\Psi, i|\Psi, j\rangle \\ &= \sum_i \sin^2\theta_i + \sum_{i\neq j} (\sin\theta_i \, \sin\theta_j)^2 \end{aligned} \tag{2.72}$$

$$\langle\mathcal{N}^2\rangle - \langle\mathcal{N}\rangle^2 = \sum_i \sin^2\theta_i \, \cos^2\theta_i \leq \sum_i \sin^2\theta_i$$

from which follows that

$$Rms \; (\mathcal{N}) \leq \sqrt{\langle\mathcal{N}\rangle} \tag{2.73}$$

If $\mathcal{N}$ is very large its distribution is very narrow and the state $|\Psi\rangle$ is nearly an eigenstate of $\mathcal{N}$.

2.5 Thermal equilibrium. Free energy and entropy

Consider a system S with energy levels E_n in thermal equilibrium with a bath S'. The bath is supposed to be very large, to have continuous energy levels with a density of states $\eta(E')$, and to interact with S in such a way that it only affects the probabilities $P(E_n)$ for S to be in state E_n but does not modify the energy spectrum. Moreover $E_{\text{tot}} = E_n + E'$ is $\gg E_n$ and at thermal equilibrium

$$P(E_n) \; \propto \; \eta \; (E_{\text{tot}} - E_n) \; .$$

The above asumptions are equivalent to the scale invariance statement

$$\frac{\eta(E' + dE')}{\eta(E')} = \text{cte} \; \forall \; E', \; \text{i.e.} \; \frac{d\,\eta}{\eta \, dE'} = \text{cte}$$

$$\eta(E') \; \propto \; \exp \; (-\beta E') \; , \; \beta = \text{cte}$$

from which

$$P(E_n) \; \propto \; \exp \; (\beta[E_{\text{tot}} - E_n]) \; \propto \; e^{-\beta E_n}$$

$$\begin{cases} P(E_n) = \frac{1}{Q} \; \exp \; (-\beta \; E_n) \\ Q = \sum_n \; \exp \; (-\beta \; E_n) \end{cases} \tag{2.74}$$

β^{-1} measures the spread of S over its excited states, it is the temperature

$$\beta = \frac{1}{k_B T} \qquad 1 \text{ meV} = 11.6\ K \tag{2.75}$$

In practice one will have to solve the Schrödinger equation of a system at temperature T. At $T = 0$ the solution minimizes the energy $U = \langle E_n \rangle$. At $T \neq 0$ it minimizes a different quantity, F, called the free energy.

$$\ln\ (P_n) = -\beta\ E_n - \ln\ Q \tag{2.76}$$

$$U \equiv \langle E_n \rangle\ = -k_B T\ \ln\ Q + T(-k_B \langle \ln\ P_n \rangle) \tag{2.77}$$

The first term $F = -k_B T\ \ln\ Q$ is the free energy and $S = -k_B \langle \ln\ P_n \rangle$ is the entropy.

$$\begin{cases} F = U - TS \\ Q = \exp\ \left(-\frac{F}{k_B T}\right) = \sum_n\ \exp\ \left(-\frac{E_n}{k_B T}\right) \end{cases} \tag{2.78}$$

To see that the P_n minimize F, write

$$U = \sum_n\ P_n\ E_n \qquad S = -k_B \langle \ln\ P_n \rangle \tag{2.79}$$

$$= -k_B \sum_n\ P_n\ \ln\ P_n$$

$$\frac{\partial F}{\partial P_n} = \frac{\partial U}{\partial P_n} - T\frac{\partial S}{\partial P_n} = E_n + k_B T\ (1 + \ln\ P_n) \tag{2.80}$$

$$E_n + k_B T\ \ln\ P_n = -k_B T\ \ln\ Q \tag{2.81}$$

$$\frac{\partial F}{\partial P_n} = k_B\ T\ (1 - \ln\ Q) \tag{2.82}$$

As $\sum\ P_n = 1,\ \sum\ \delta\ P_n = 0$

$$\delta F = \sum_n\ \frac{\partial F}{\partial P_n}\ \delta\ P_n = k_B T (1 - \ln\ Q)\ \sum_n\ \delta\ P_n = 0 \tag{2.83}$$

Note that the heat W obeys $dW = TdS$ and the heat capacity

$$C = \frac{dW}{dT} = T\frac{dS}{dT}\ . \tag{2.84}$$

One can now evaluate the population of the states of a free electron gas at temperature T. There are n_j^i electrons in state ε_j, $n_j^i = 0$ or 1, where i labels a particular set of $\{n_j^i\}$. The problem needs to be solved with the additional constraint

$$N_i = \sum_j\ n_j^i = N\ , \tag{2.85}$$

the total number of particles. This constraint is most easily taken care of by working in a shifted energy scale, $\varepsilon_j - \mu$, where μ is called the chemical potential. Writing

$$Q_\mu \equiv e^{-\beta F_\mu} = \sum_i\ \exp\ \left\{-\beta\ \sum_j\ n_j^i [\varepsilon_j - \mu]\right\} \tag{2.86}$$

$$-\beta\, Q_\mu \frac{\partial F_\mu}{\partial \mu} = \sum_i \beta n_j^i \exp\left\{-\beta \sum_j n_j^i\, [\varepsilon_j - \mu]\right\} \tag{2.87}$$
$$= \beta\, Q_\mu \langle N_i \rangle$$

The constraint $\langle N_i \rangle = N$ is replaced by

$$-\frac{\partial F}{\partial \mu} = N\,. \tag{2.88}$$

Note that

$$\langle n_j^i \rangle = \frac{\partial F_\mu}{\partial \varepsilon_j} \tag{2.89}$$

Now

$$e^{-\beta F_\mu} = \Pi_j\, (1 + \exp\, \{-\beta[\varepsilon_j - \mu]\}) \tag{2.90}$$

as $n_j^i = 0$ or 1.

$$F_\mu = -\frac{1}{\beta} \sum_i \ln\, \{1 + \exp\, (-\beta[\varepsilon_i - \mu])\} \tag{2.91}$$

$$\langle n_j^i \rangle = \frac{\partial F_\mu}{\partial \varepsilon_j} = \frac{\exp\, (-\beta[\varepsilon_j - \mu])}{1 + \exp\, (-\beta[\varepsilon_j - \mu])} \tag{2.92}$$

$$\langle n_j \rangle = \frac{1}{1 + \exp\, (\beta[\varepsilon_j - \mu])} \tag{2.93}$$

At $T = 0$, $\mu = E_F$ and μ differs very little from E_F when T increases

$$\mu(T) \approx E_F \left(1 - \frac{\pi^2}{12} \frac{k_B^2 T^2}{E_F^2}\right). \tag{2.94}$$

Figures 2.17 and 2.18 illustrate this result.

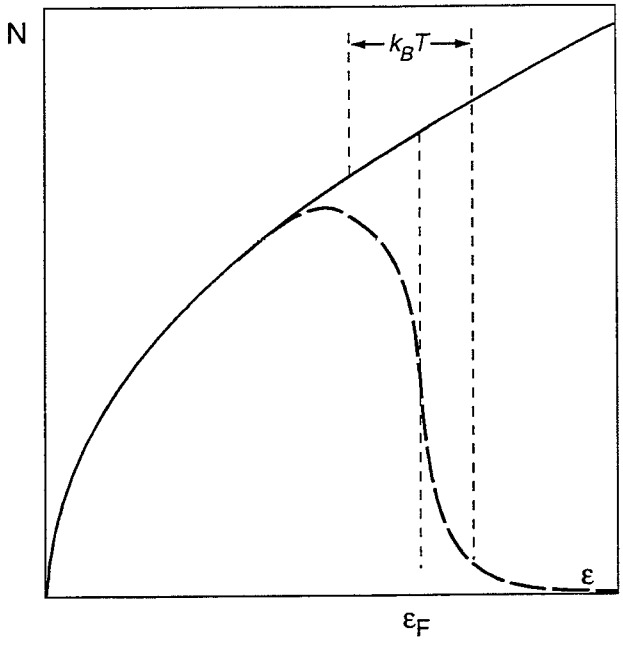

Figure 2.17: See text.

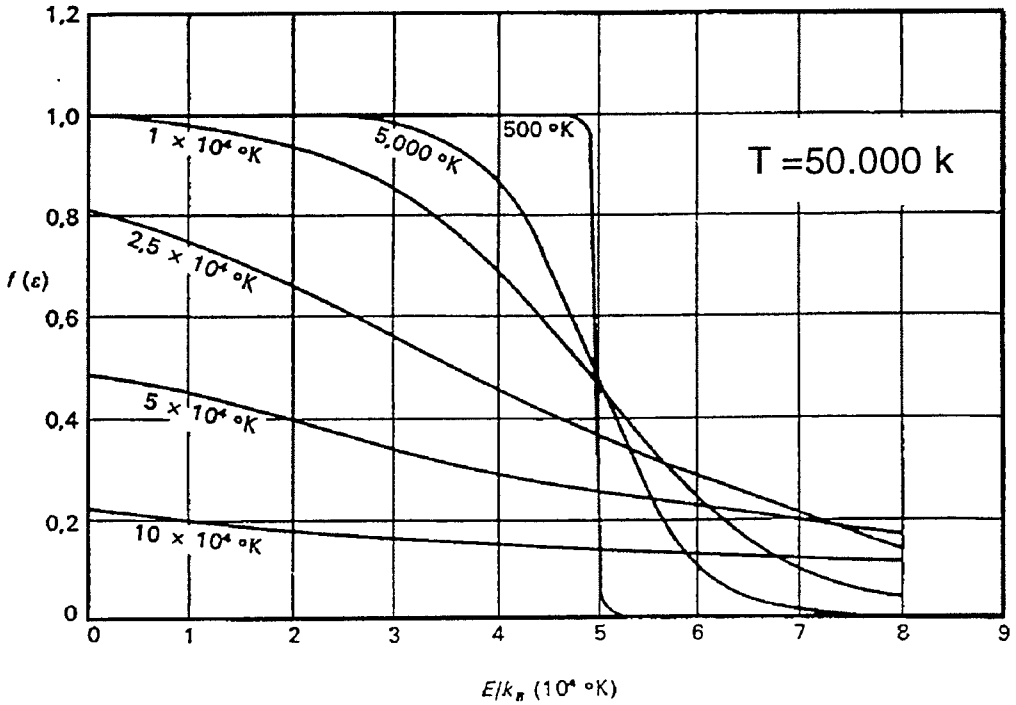

Figure 2.18: See text.

To count the amount of excitation it is convenient to introduce the concept of quasi particles.

Writing the ground state as

$$|G\rangle = a_1^+ \, a_2^+ \ldots a_F^+ \, |0\rangle \tag{2.95}$$

and introducing

$$\begin{aligned} b_k &= a_k \text{ for } k > k_F \\ &= a_k^+ \text{ for } k \leq k_F \end{aligned} \tag{2.96}$$

$$[b_k, \, b_{k'}]_+ = [b_k^+, \, b_{k'}^+]_+ = 0 \quad [b_k, \, b_{k'}^+]_+ = \delta_{kk'}$$

The excited states are $|\phi\rangle = \Pi_i \, b_i^+ |G\rangle$

$$b_i|G\rangle = 0 \qquad N = N_0 + \sum_i sgn(\xi_i) \, b_i^+ \, b_i \tag{2.97}$$

$$E = E_0 + \sum_i sgn(\xi_i) \, \xi_i \, b_i^+ \, b_i$$

with

$$\xi_i = \varepsilon_i - E_F \, .$$

3 SUPERCONDUCTIVITY IN THE ABSENCE OF AN EXTERNAL FIELD

3.1 Cooper pairs [14]

A free electron gas has a ground state such that most electrons are kind of frozen inside the Fermi sphere. What happens if one adds to it a pair of electrons having an attractive interaction between them? To give a chance to the pair to be in as low energy as possible a state, say the pair is at rest and one electron has spin up, the other spin down. Moreover mimic the presence of the Fermi sphere by imposing (Fig. 3.1) $|k| > k_F$ for each of the electrons in the pair (this is of course perfectly illegitimate, there is no reason *a priori* to treat differently the electrons in the sphere and those of the pair). The pair state can be written as

$$\begin{cases} |\Psi\rangle = \sum_k g_k |k\rangle \text{ where } |k\rangle \text{ means} \\ |k\rangle = |k\uparrow, \ -k\downarrow\rangle \end{cases} \tag{3.1}$$

$$\langle r_1 r_2 | \Psi \rangle = \sum_k g_k \, e^{ik.(r_1 - r_2)} \tag{3.2}$$

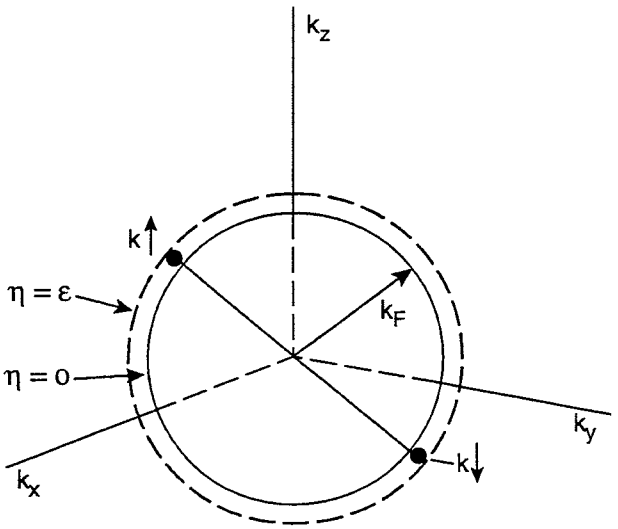

Figure 3.1: A Cooper pair.

Note that the wave function is antisymmetric, as it should, and depends only on $R = r_1 - r_2$ as the pair is at rest. Define 2η as the pair kinetic energy in excess of the Fermi level

$$\frac{\hbar^2 k^2}{2\,m} = E_F + \eta, \quad \frac{d\eta}{dk} = k\,\frac{\hbar^2}{m} = \hbar\, v, \quad \eta > 0 \tag{3.3}$$

Now switch on a small attractive potential $-V$ between the electrons in the pair.

If it were not for the condition $|k| > k_F$ there would be no bound state until V reaches some threshold $\approx \hbar^2/2m\rho^2$, ρ being the range of V. This is no longer the case with the boundary condition $|k| > k_F$.

Indeed, writing the pair energy as

$$E_{\text{pair}} = 2E_F - 2\Delta \text{ (i.e.}\Delta > 0 \text{ means a bound state)} \tag{3.4}$$

$$(H - E_{\text{pair}})|k\rangle = (2[\eta + \Delta] - V)\ |k\rangle \tag{3.5}$$

$$0 = \langle k|H - E_{\text{pair}}|\Psi\rangle = 2(\eta + \Delta)\ g_k - \sum_{k'}\ g_{k'}\langle k|V|k'\rangle \tag{3.6}$$

Modelling V by

$$\begin{cases} \langle k'|V|k\rangle = 0 \quad \text{for } \frac{\hbar^2 k^2}{2\ m} < E_F \text{ or } > E_F + \varepsilon \\ \langle k'|V|k\rangle = cte = \tilde{V} \quad \text{for } E_F < \frac{\hbar^2 k^2}{2\ m} < E_F + \varepsilon \\ \varepsilon \ll E_F \end{cases} \tag{3.7}$$

and renaming g_k as $g(\eta)$

$$g(\eta) = \frac{1}{2(\eta + \Delta)}\ \tilde{V}\ \int_0^{\varepsilon}\ g(\eta')\ \mathcal{N}(\eta')\ d\eta' \tag{3.8}$$

where $\mathcal{N}(\eta')$ is the density of states

$$\int_0^{\varepsilon}\ g(\eta)\ \mathcal{N}(\eta)\ d\eta = \int_0^{\varepsilon}\ g(\eta')\ \mathcal{N}(\eta')\ d\eta'\ \int_0^{\varepsilon}\ \frac{\tilde{V}\ \mathcal{N}(\eta)d\eta}{2(\eta + \Delta)} \tag{3.9}$$

$$1 = \tilde{V}\ \int_0^{\varepsilon}\ \frac{\mathcal{N}(\eta)d\eta}{2(\eta + \Delta)} \tag{3.10}$$

As $\varepsilon \ll E_F$, $\mathcal{N}(\eta) \simeq \mathcal{N}_F$ and

$$1 = \tilde{V}\ \mathcal{N}_F\ \frac{1}{2}\ \ln\ \frac{\Delta + \varepsilon}{\Delta} \tag{3.11}$$

$$\Delta = \frac{\varepsilon}{\exp(2/\tilde{V}\mathcal{N}_F) - 1} \quad > 0 \qquad \forall\ \tilde{V} > 0 \tag{3.12}$$

However small is $\tilde{V}$, there is always a bound state. If it had not been for the cut at E_F, it would not have been possible to take $\mathcal{N}(\eta)$ out of the integral and $\mathcal{N}(\eta)$ would have been of the form $\eta^{1/2}$, i.e. even for $\Delta = 0$ the integral would have remained finite instead of having the log infinity it has here. For $\tilde{V}\ \mathcal{N}_F \ll 1$, the so called weak-coupling approximation,

$$\Delta = \varepsilon\ \exp\ (-2/[\tilde{V}\ \mathcal{N}_F]) \tag{3.13}$$

Note that it cannot be expanded in powers of $\tilde{V}$.

The wave function $g(\eta) \propto 1/(\eta + \Delta)$ for $\eta > 0$ vanishes for $\eta < 0$ (see Fig. 3.2)

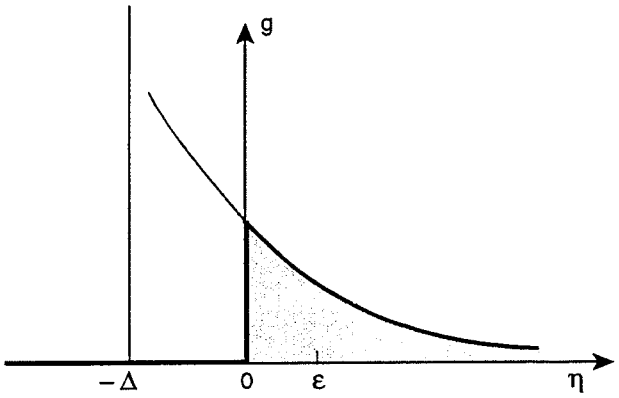

Figure 3.2: See text.

Writing $R = r_1 - r_2$

$$\Psi(R) \propto \int_{k_F}^{\infty} \frac{k^2\, dk}{\eta + \Delta} \int_{-1}^{+1} e^{ikR\cos\theta}\, d(\cos\theta) \tag{3.14}$$

$$\Psi(R) \propto \int_{k_F}^{\infty} \frac{\sin\, kR}{kR} \frac{k^2\, dk}{k^2 - k_F^2 + 2\, m\Delta/\hbar^2} \tag{3.15}$$

The second factor in the integral varies from E_F/Δ to 1 when k goes from k_F to ∞. One can expect important contributions over a range such that $k_F\, R \simeq E_F/\Delta$, i.e.

$$R \simeq \frac{1}{2} \frac{\hbar v_F}{\Delta} \tag{3.16}$$

which may be large (Fig. 3.3).

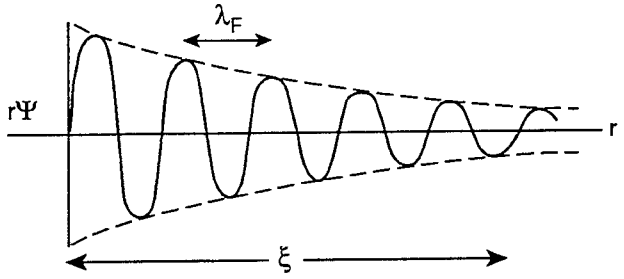

Figure 3.3: See text.

More precisely, one can calculate $\xi = \langle R^2 \rangle^{1/2}$

$$\langle R^2 \rangle = \frac{\sum (dg/dk)^2}{\sum\, g^2} = \frac{\int \mathcal{N}\, (d\eta/dk)^2 (\Delta + \eta)^{-4}\, d\eta}{\int \mathcal{N} (\Delta + \eta)^{-2} d\eta} \tag{3.17}$$

$$\approx \left(\frac{d\eta}{dk}\right)_F^2 \frac{1/3\Delta^3}{1/\Delta} = \frac{1}{3}\left(\frac{\hbar v_F}{\Delta}\right)^2,$$

giving

$$\xi = \frac{\hbar v_F}{\sqrt{3}\Delta} \qquad \frac{\hbar}{\xi} = \frac{\sqrt{3}}{2} \frac{\Delta}{E_F} p_F \tag{3.18}$$

$$\frac{\xi}{v_F} \Delta = \frac{\hbar}{\sqrt{3}} \tag{3.19}$$

The latter equation is a Heisenberg uncertainty relation between the 'energy gap' Δ and the 'coherence time' ξ/v_F. The meaning of these words will become clearer in the next sections. The existence of a bound state for any small $\tilde{V}$ suggests that the ground state of a free electron gas becomes unstable in the presence of the tiniest attractive interaction. The Fermi sphere is indeed full of $[k\uparrow,\ -k\downarrow]$ pairs which can be expected to 'bind' and to release an energy Δ, the free electrons state condensing to a lower energy state of bound pairs. This is indeed qualitatively what happens in the transition to the superconducting state.

3.2 The Fröhlich interaction [15]

Fröhlich was first, in 1950, to propose the one-phonon exchange interaction as the attractive force which would be large enough to overcompensate the repulsive Coulomb interaction and be responsible for superconductivity. It is sufficient to evaluate it on the Fermi sphere, i.e. $|k| = |k'| = |k_F|$. Let q be the exchange momentum, $q = k' - k$, corresponding to a phonon energy

$$\hbar\omega_q = \hbar v_g q, \; 0 < \hbar\omega_q < \hbar\omega_D \tag{3.20}$$

in the Debye approximation (see 2.2).

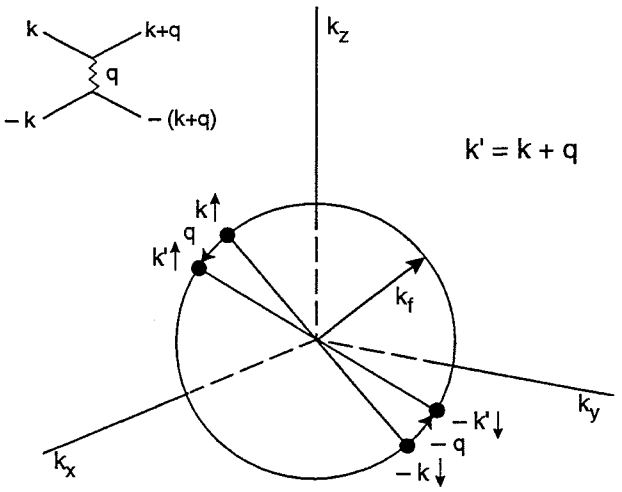

Figure 3.4: Fröhlich interaction.

The matrix element calculated between $|k\rangle$ and $|k'\rangle$ is simply

$$-2\,\frac{|W_q|^2}{\hbar\omega_q} \qquad \text{(see Fig. 3.5)} \tag{3.21}$$

where W_q is the transition amplitude at each of the electron-phonon vertices.

The Coulomb matrix element between the same states is

$$\frac{4\pi\, e^2}{q^2 + \sigma^2} \tag{3.22}$$

where σ is a phenomenological constant adjusted to simulate the screening effect from the other electrons as well as from the lattice ions. Fröhlich argued that the global interaction,

$$\frac{4\pi\, e^2}{q^2 + \sigma^2} - \frac{2|W_q|^2}{\hbar\omega_q} \qquad (\omega_q \simeq v_g\, q) \tag{3.23}$$

is likely to be negative for most superconductors[1)].

[1)] Note that the phonon exchange diagram, while formally similar to a photon exchange diagram, is in fact very different: the exchanged boson has a Debye spectrum in the former case and a bremsstrahlung spectrum in the latter

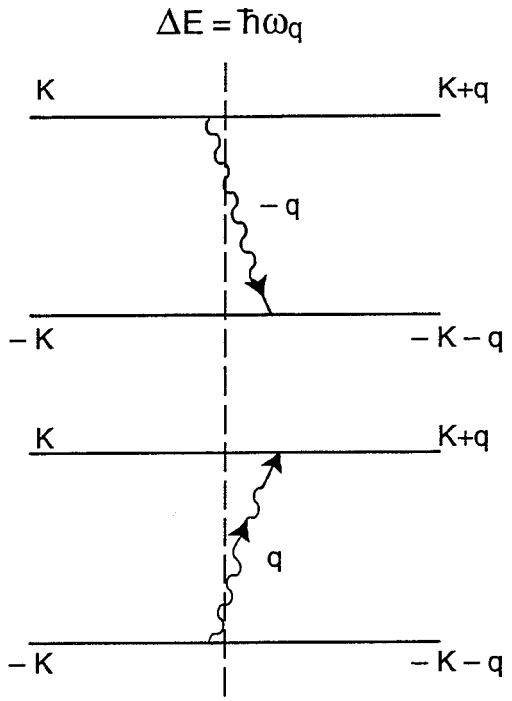

Figure 3.5: Phonon exchange in the Fröhlich interaction.

At the same time, E. Maxwell and C.A. Reynolds *et al.* [16], (Fig. 3.6) could show that the critical temperature was indeed a function of the isotopic mass of the lattice ions,

$$(v_g \propto M^{-1/2}) \tag{3.24}$$

which was recognized as a crucial proof of the implication of the lattice in superconductivity.

It is sometimes said that the attractive interaction has its origin in the slow movement of the ions toward the electron trajectory in its wake, enhancing the presence of the other electron in the increased Coulomb field. However such a picture (in r-space rather than k-space) has its limits [17].

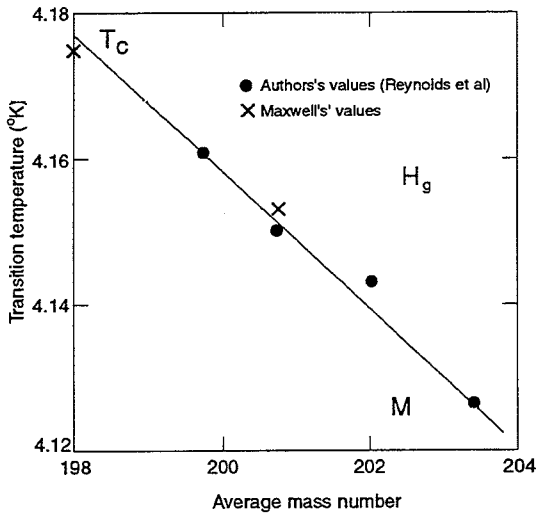

Figure 3.6: Isotopic effect of Mercury.

3.3 The BCS ground state

We now treat the problem of an electron gas perturbed by a small interaction of the type described in the preceding section. We use an ansatz of the form considered at the end of Section 2.4, but written for pairs $|k\uparrow,\ -k\downarrow\rangle$

$$|\Psi\rangle = \Pi_k\ (\cos\theta_k + \sin\theta_k\ b_k^+)|0\rangle \tag{3.25}$$

with $b_k^+ = a_{k\uparrow}^+\ a_{-k\downarrow}^+$, $b_k = a_{-k\downarrow}\ a_{k\uparrow}$. Note that all factors in (3.25) commute. We refer energies to the Fermi level

$$\xi_k = \frac{\hbar^2 k^2}{2\ m} - E_F \tag{3.26}$$

$$\langle\Psi|H|\Psi\rangle = \langle\Psi|2\sum_k \xi_k\ b_k^+\ b_k + \sum_{k\ell} V_{k\ell}\ b_\ell^+\ b_k|\Psi\rangle \qquad k \neq \ell \tag{3.27}$$

$$\begin{aligned} |\Psi\rangle &= \cos\theta_k|\Psi\not{k}\rangle + \sin\theta_k|\Psi k\rangle \\ &= \cos\theta_k\cos\theta_\ell|\Psi\not{k}\not{\ell}\rangle + \cos\theta_k\sin\theta_\ell|\Psi\not{k}\ell\rangle \\ &\quad + \sin\theta_k\cos\theta_\ell|\Psi k\not{\ell}\rangle + \sin\theta_k\sin\theta_\ell|\Psi k\ell\rangle \end{aligned} \tag{3.28}$$

$$\begin{aligned} \langle\Psi|H|\Psi\rangle &= 2\sum_k \xi_k\ \sin\theta_k\langle\Psi|\Psi\not{k}\rangle \\ &\quad + \sum_{k\ell} V_{k\ell}\ \sin\theta_k\ \cos\theta_\ell\langle\Psi|\Psi\not{k}\ell\rangle \end{aligned} \tag{3.29}$$

$$= 2\sum_k \xi_k \sin^2\theta_k + \sum_{k\ell} V_{k\ell}\ \sin\theta_k\cos\theta_k\ \sin\theta_\ell\ \cos\theta_\ell$$

$$= \sum_k \xi_k\ (1 - \cos 2\theta_k) + \frac{1}{4}\sum_{k\ell} V_{k\ell}\ \sin 2\theta_k \sin 2\theta_\ell \tag{3.30}$$

Minimizing, $\partial/\partial\theta_k\langle\Psi|H|\Psi\rangle = 0$, one obtains:

$$2\ \xi_k\ \sin\ 2\theta_k + \sum_\ell V_{k\ell}\ \cos\ 2\theta_k\ \sin\ 2\theta_\ell = 0 \qquad (V_{k\ell} = V_{\ell k}) \tag{3.31}$$

$$\tan\ 2\theta_k = -\frac{\sum_\ell V_{k\ell}\ \sin\ 2\theta_\ell}{2\ \xi_k} \tag{3.32}$$

Defining

$$\begin{cases} \Delta_k = -\sum_\ell V_{k\ell}\ \sin\theta_\ell\cos\theta_\ell \\ \varepsilon_k = (\Delta_k^2 + \xi_k^2)^{1/2} \end{cases} \tag{3.33}$$

$$\begin{cases} \sin 2\theta_k = \Delta_k/\varepsilon_k \\ \cos\ 2\theta_k = \xi_k/\varepsilon_k \end{cases} \tag{3.34}$$

(see Fig. 3.7)

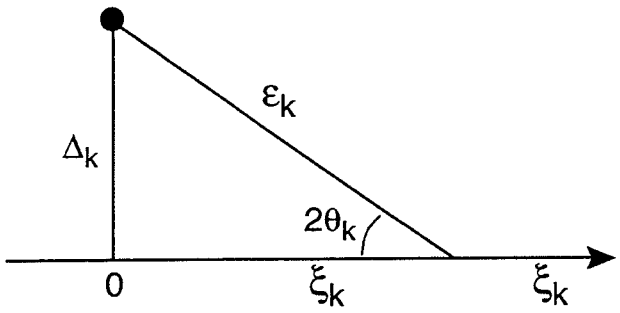

Figure 3.7: BCS ground state.

For $\Delta_k = 0$

$$\begin{cases} \cos\ 2\theta_k = 1 \quad \cos^2\theta_k = 1 \quad \xi_k > 0 \\ \cos\ 2\theta_k = -1 \quad \cos^2\theta_k = 0 \quad \xi_k < 0 \end{cases} \tag{3.35}$$

which is the free electron gas ground state.

BCS use the simplified interaction

$$\begin{cases} V_{k\ell} = -V \qquad \text{for} \qquad |\xi_k|,\ |\xi_\ell| < \hbar\omega_D \\ \quad = 0 \qquad \text{otherwise} \end{cases} \tag{3.36}$$

Then

$$\begin{cases} \Delta_k = 0 \qquad |\xi_k| > \hbar\omega_D \\ \quad = V \sum_\ell \ \sin\theta_\ell\ \cos\theta_\ell \qquad |\xi_k|,\ |\xi_\ell| < \hbar\omega_D \end{cases} \tag{3.37}$$

For $|\xi_k| < \hbar\omega_D$, Δ_k is independent of k, it takes a constant value Δ

$$\Delta = V \sum_k \frac{\Delta_k}{2\ \varepsilon_k} \qquad |\xi_k| < \hbar\omega_D \tag{3.38}$$

$$\Delta = V\Delta \int_{-\hbar\omega_D}^{+\hbar\omega_D} \frac{\mathcal{N}(\xi)d\xi}{2\ \sqrt{\Delta^2 + \xi^2}} \tag{3.39}$$

giving

$$1 = V\ \mathcal{N}_F\ \text{Argsh}\ (\hbar\omega_D/\Delta) \tag{3.40}$$

and

$$\Delta = \frac{\hbar\omega_D}{\text{sh}(1/V\mathcal{N}_F)} \simeq 2\ \hbar\omega_D\ \exp\ (-1/V\mathcal{N}_F) \tag{3.41}$$

where the second expression is written in the weak coupling limit, $V\mathcal{N}_F \ll 1$.

In the region $\hbar\omega_D < |\xi_k|$ the free electron gas solution is not affected. But for $|\xi_k| < \hbar\omega_D$

$$\begin{cases} \cos\theta_k = \{\frac{1}{2}(1 + \xi_k/\sqrt{\Delta^2 + \xi_k^2})\}^{1/2} \\ \sin\theta_k = \{\frac{1}{2}(1 - \xi_k/\sqrt{\Delta^2 + \xi_k^2})\}^{1/2} \end{cases} \tag{3.42}$$

The width of the transition is $\approx \Delta \ll \hbar\omega_D$.

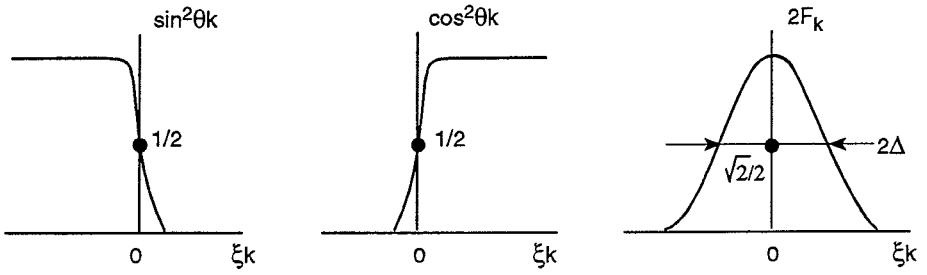

Figure 3.8: See text.

The difference between the BCS and normal state ground state energies is

$$E_{\rm cond} = \sum_k \xi_k\left(1-\frac{\xi_k}{|\xi_k|}\right)-\sum_k \xi_k\left(1-\frac{\xi_k}{\varepsilon_k}\right)-\frac{1}{4}\sum_{k\ell} V_{k\ell}\,\frac{\Delta_k}{\varepsilon_k}\,\frac{\Delta_\ell}{\varepsilon_\ell} \tag{3.43}$$
$$= 2\int_0^{\hbar\omega_D} \mathcal{N}_F\,\xi_k^2\left(\frac{1}{\varepsilon_k}-\frac{1}{\xi_k}\right)\,d\xi_k + \mathcal{N}_F^2\Delta^2 V\left\{\int_0^{\hbar\omega_D}\frac{d\xi_k}{\varepsilon_k}\right\}^2$$

Writing $\varepsilon_k = \Delta$ chu, $\xi_k = \Delta$ shu and noting that Argsh $\hbar\omega_D/\Delta = 1/V\mathcal{N}_F$ and $\int_0^{\hbar\omega_D} d\xi/\varepsilon = 1/V\mathcal{N}_F$, one gets

$$E_{\rm cond} = 2\int_0^{1/V\mathcal{N}_F} \Delta^2\mathcal{N}_F\ \text{shu}\ (\text{shu}-\text{chu})\ \text{du} + \frac{\Delta^2}{V} \tag{3.44}$$
$$= \frac{1}{2}\Delta^2\mathcal{N}_F\{\text{sh2u}-2\text{u}-\text{ch2u}\}_0^{1/V\mathcal{N}_F}+\frac{\Delta^2}{V}$$
$$= -\frac{\Delta^2}{V}-\frac{1}{2}\Delta^2\mathcal{N}_F\ [\exp\ (-\frac{2}{V\mathcal{N}_F})-1]+\frac{\Delta^2}{V}\ .$$

In the weak coupling limit the second term vanishes and

$$E_{\rm cond} = \frac{1}{2}\Delta^2\mathcal{N}_F(1-\exp\ [-\frac{2}{V\mathcal{N}_F}]) \approx \frac{1}{2}\Delta^2\mathcal{N}_F \tag{3.45}$$

As $\mathcal{N}_F/n = 3/(2\ E_F)$ the energy gain per particle is therefore

$$E_{\rm cond}/n \sim \frac{3}{4}\Delta^2/E_F\ , \tag{3.46}$$

a very small quantity.

The energy gain Δ^2/V due to the pair attraction energy is partly, but only partly, compensated by the energy loss due to the smearing of the ground state near the Fermi level,

$$\Delta^2/V - \frac{1}{2}\Delta^2\mathcal{N}_F\ . \tag{3.47}$$

The reason for this smearing is the need to 'unfreeze' the Fermi sphere in order to make room for taking advantage of the pair interaction. Indeed, in the free electron gas ground state the interaction energy vanishes. The quantity

$$F_k = \langle\Psi|b_k^+|\Psi\rangle = \sin\theta_k\ \cos\theta_k \tag{3.48}$$

(see Fig. 3.8) is called the condensation amplitude, it vanishes in the regions where the pairs do not interact.

What was suspected from the Cooper pair argument of Section 3.1 is now confirmed: a small Fröhlich-type one-phonon-exchange attractive interaction induces condensation into a lower energy BCS state. One can guess that at temperatures in excess of $\sim \Delta/k_B$ condensation will be prevented by the too large intrinsic smearing of the free electron gas ground state. This will be verified in Section 3.5. The reason for the BCS ground state to be superconducting is the existence of a gap which separates it from its excited states and makes it rigid against small perturbations. This is the subject of the next section.

3.4 Quasi-particle excitations

In deriving (3.34) one might as well have chosen

$$\begin{cases} \sin 2\theta_k = -\Delta_k/\varepsilon_k \\ \cos\ 2\theta_k = -\xi_k/\varepsilon_k \end{cases} \tag{3.49}$$

but such a solution would have been far from the free electron ground state. Consider an excited state obtained from the BCS ground state by changing one of the θ_k into

$$\theta_k^* = \theta_k \pm \frac{\pi}{2} \ . \tag{3.50}$$

The excitation energy (Fig. 3.9) is

$$\begin{aligned} & - \langle\Psi|H|\Psi\rangle + \langle\Psi^*|H|\Psi^*\rangle \\ & = 2\,\xi_k\ \cos\ 2\theta_k + V\ \sin\ 2\theta_k \sum_\ell \sin\ 2\theta_\ell \\ & = 2\,\frac{\xi_k^2}{\varepsilon_k} + 2\,\frac{\Delta_k^2}{\varepsilon_k} = 2\,\varepsilon_k > 2\,\Delta_k \ . \end{aligned} \tag{3.51}$$

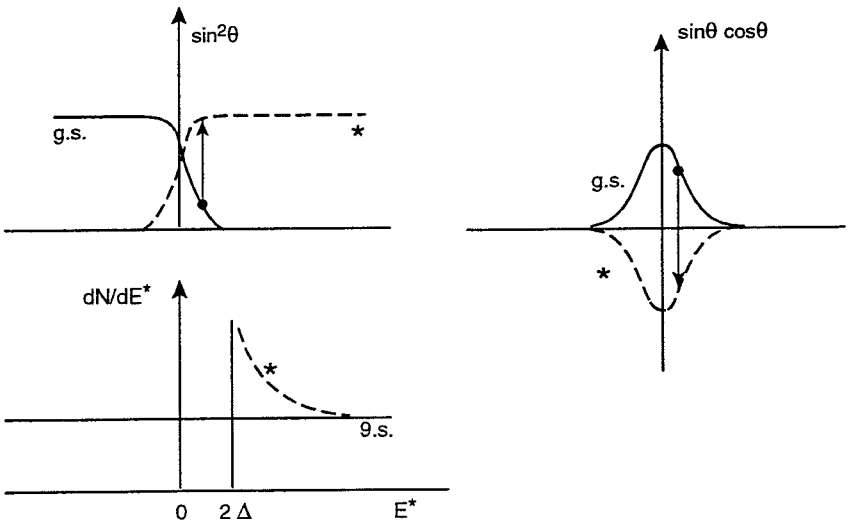

Figure 3.9: Pair excitations.

The BCS excited states obtained by exciting pair k to the state $\theta_k \pm \frac{\pi}{2}$ are separated from the BCS ground state by at least 2 Δ. The density of excited states is

$$\mathcal{N}^* = \mathcal{N}_F\,\frac{d\xi_k}{d\varepsilon_k} = \mathcal{N}_F\,\frac{\varepsilon_k}{\xi_k} = \mathcal{N}_F\,\frac{E^*}{\sqrt{E^{*2} - 4\Delta^2}} \tag{3.52}$$

But other excited states can be constructed. By adding to or removing from the BCS ground state a single particle one does not disturb the pairs in their mutual interactions and therefore obtains a possible stationary state. Noting that, for $|\Psi\rangle$ = BCS ground state

$$\begin{cases} a^+_{m\uparrow}|\Psi\rangle = \cos\theta_m|\Psi,\ m\uparrow\rangle \\ a_{-m\downarrow}|\Psi\rangle = -\sin\theta_m\ |\Psi,\ m\uparrow\rangle \end{cases} \tag{3.53}$$

we define

$$\gamma^+_{m\uparrow} = \lambda_m\ a^+_{m\uparrow} + \mu_m\ a_{-m\downarrow} \tag{3.54}$$

the quasi particle creation operator for state $m\uparrow$

$$\gamma_{m\uparrow}|\Psi\rangle = (\lambda_m\ \sin\theta_m + \mu_m\ \cos\ \theta_m)a^+_{-m\downarrow}|\Psi\rangle \tag{3.55}$$

must be zero, imposing $\lambda_m\ \sin\theta_m + \mu_m\ \cos\theta_m = 0$. We take $\lambda_m = \cos\theta_m,\ \mu_m = -\sin\theta_m$, and

$$\begin{cases} \gamma^+_{m\uparrow} = \cos\theta_m\ a^+_{m\uparrow} - \sin\theta_m\ a_{-m\downarrow} \\ \gamma^+_{m\downarrow} = \cos\theta_m\ a^+_{m\downarrow} + \sin\theta_m\ a_{-m\uparrow} \end{cases} \tag{3.56}$$

The γ and γ^+ obey fermion commutation rules and $\gamma|\Psi\rangle = 0$ as it should, i.e. the BCS ground state is their vacuum [18]

$$\begin{cases} \gamma^+_{m\uparrow}|\Psi\rangle = |\Psi_{m\uparrow}\rangle \\ \gamma^+_{m\downarrow}|\Psi\rangle = |\Psi_{m\downarrow}\rangle \end{cases} \tag{3.57}$$

The excitation energy receives a contribution $\xi_m(1-2\ \sin^2\theta_m)$ from the kinetic term and $\frac{1}{2}\ V\ \sin 2\theta_m\ \sum_\ell \sin 2\theta_\ell$ from the potential term (Fig. 3.10)

$$\begin{aligned} E^* &= \xi_m\ \cos 2\theta_m + \Delta\ \sin 2\theta_m \\ &= \xi^2_m/\varepsilon_m + \Delta^2/\varepsilon_m = \varepsilon_m \end{aligned} \tag{3.58}$$

and

$$E^* = \varepsilon_m > \Delta$$

Here again the excitation energy for a quasi particle m is ε_m and the energy gap is Δ, the density of excited states being

$$\mathcal{N}_F\ E^*/\sqrt{E^{*2} - \Delta^2}\ . \tag{3.59}$$

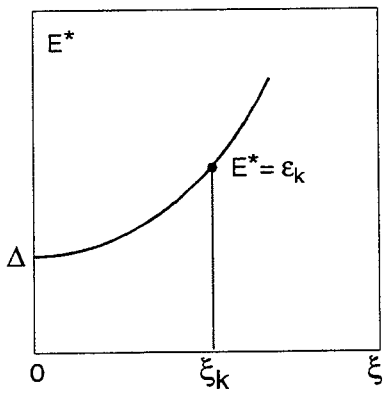

Figure 3.10: Quasi particle excitation energy.

In practice, when working at constant total number of particles, the lowest excitations imply two quasi-particles (Fig. 3.11) and the corresponding gap is 2 Δ as found earlier for pair excitations. In fact it is easy to check that $\gamma^+_{m\uparrow}\ \gamma^+_{-m\downarrow}$ changes θ_m to $\theta_m \pm \frac{\pi}{2}$, i.e. it corresponds to the excitation of a pair from the BCS ground state with excitation energy $E^* = 2\ \varepsilon_m$.

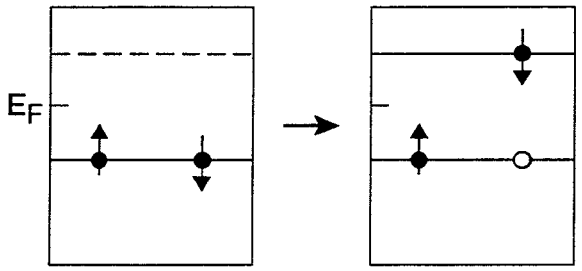

Figure 3.11: Creation of a particle-hole excitation.

3.5 Excited states, $T \neq 0$

Away from $T = 0$ quasi-particle excitations take place with a probability f_k

$$f_k = \langle \gamma^+_k \gamma_k \rangle = 1 - \langle \gamma_k \gamma^+_k \rangle \tag{3.60}$$

where spin indices have been omitted ($f_{k\uparrow} = f_{k\downarrow}$).

The free energy $F = \langle \Psi | H | \Psi \rangle - TS$, with

$$S = -2k_B \sum_k \{f_k\ \ln\ f_k + (1 - f_k)\ \ln(1 - f_k)\} \tag{3.61}$$

must be minimized to define θ_k and f_k. For $f_k = 1$ the effect of the excitation is to change θ_k into $\theta_k \pm \frac{\pi}{2}$, i.e. to change the signs of cos $2\theta_k$ and sin $2\theta_k$. For $f_k = 0$

$$\langle \Psi | H | \Psi \rangle = \sum_k\ \xi_k\ (1 - \cos\ 2\theta_k) + \frac{1}{4} \sum_{k\ell}\ V_{k\ell}\ \sin 2\theta_k\ \sin\ 2\theta_\ell \tag{3.62}$$

As the $\gamma's$ are linear in the $a's$, cos $2\theta_k$ and sin $2\theta_k$ must simply be multiplied by

$$(1 - f_k) \times (1) + f_k \times (-1) = 1 - 2f_k$$

and for any f_k

$$\begin{aligned} \langle \Psi | H | \Psi \rangle\ \ &= \sum_k\ \xi_k\ (1 - \cos\ 2\theta_k[1 - 2f_k]) \\ &+ \frac{1}{4} \sum_{k\ell}\ V_{k\ell}\ \sin\ 2\theta_k\ \sin\ 2\theta_\ell\ (1 - 2\ f_k)(1 - 2\ f_\ell) \end{aligned} \tag{3.63}$$

$$\frac{\partial F}{\partial \theta_k} = 0 = \frac{\partial}{\partial \theta_k}\ \langle \Psi | H | \Psi \rangle$$

reads

$$2\ \xi_k\ \sin\ 2\theta_k + \cos\ 2\theta_k \sum_\ell\ V_{k\ell}\ \sin\ 2\theta_\ell\ (1 - 2\ f_\ell) = 0 \tag{3.64}$$

Redefining

$$\begin{cases} \Delta_k = -\sum_\ell\ V_{k\ell}\ \sin\theta_\ell\ \cos\theta_\ell (1 - 2\ f_\ell) \\ \varepsilon_k = (\Delta_k^2 + \xi_k^2)^{1/2} \end{cases} \tag{3.65}$$

gives, as before,

$$\sin\ 2\theta_k = \Delta_k/\varepsilon_k \qquad \cos 2\theta_k = \xi_k/\varepsilon_k \tag{3.66}$$

i.e. the only change in the wave function is a modulation of the gap by a factor $(1-2f_k)$.

Writing $\partial F/\partial f_k = 0$ one gets

$$\frac{\partial}{\partial f_k}\ \langle\Psi|H|\Psi\rangle = 2\ \xi_k\ \cos\ 2\theta_k + 2\Delta_k\ \sin\ 2\theta_k \tag{3.67}$$

$$\frac{\partial}{\partial f_k}\ S = -2\ k_B\ \ln\ \frac{f_k}{1-f_k} \tag{3.68}$$

and finally

$$\xi_k\ \cos\ 2\theta_k + \Delta_k\ \sin\ 2\theta_k + k_B\ T\ \ln\ \frac{f_k}{1-f_k} = 0 \tag{3.69}$$

i.e.

$$f_k = \frac{1}{1+\exp\ (\varepsilon_k/k_BT)}\ . \tag{3.70}$$

This is the usual fermion distribution for energy ε_k, however ε_k depends on Δ_k which in turn depends on f_k, namely on T.

The expression (3.65) for Δ_k simplifies in the BCS approximation

$$\frac{\Delta}{V} = \mathcal{N}_F\ \int_{-\hbar\omega_D}^{\hbar\omega_D}\ \Delta\ \frac{1-2f(\varepsilon)}{2\varepsilon}\ d\xi \tag{3.71}$$

$$\frac{1}{\mathcal{N}_F V} = \int_0^{\hbar\omega_D}\ \frac{d\xi}{\sqrt{\Delta^2+\xi^2}}\ (1-2\ f) \tag{3.72}$$

with f given by (3.70) and $\varepsilon = \sqrt{\Delta^2+\xi^2}$. For $\Delta = 0$

$$\begin{aligned}\frac{1}{\mathcal{N}_F V}\ &= \int_0^{\hbar\omega_D}\ \frac{d\xi}{\xi}\ (1-\frac{2}{1+\exp\ (\xi/k_BT)}) \\ &= \int_0^{\hbar\omega_D}\ \text{th}\ \frac{\xi}{2\ k_BT}\ \frac{d\xi}{\xi}\end{aligned} \tag{3.73}$$

giving finally (Fig. 3.12)

$$\begin{cases}\Delta(T=0) = 1.76\ k_B\ T_c \\ k_B\ T_c \simeq 1.14\ \hbar\ \omega_D\ \exp\ (-1/\mathcal{N}_F\ V)\end{cases} \tag{3.74}$$

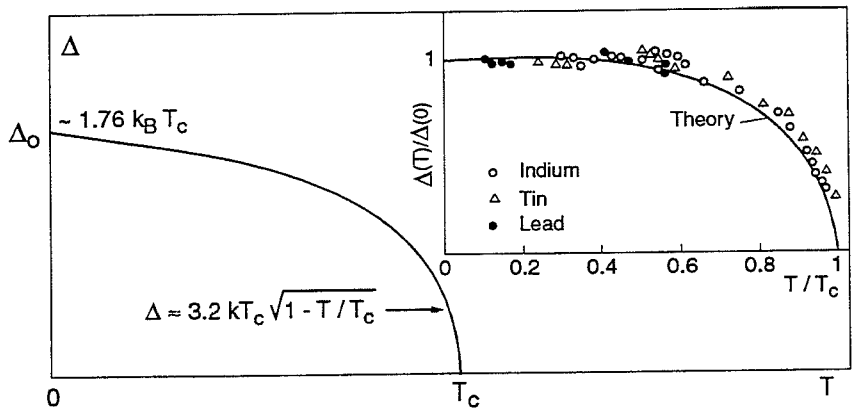

Figure 3.12: Temperature dependence of the gap.

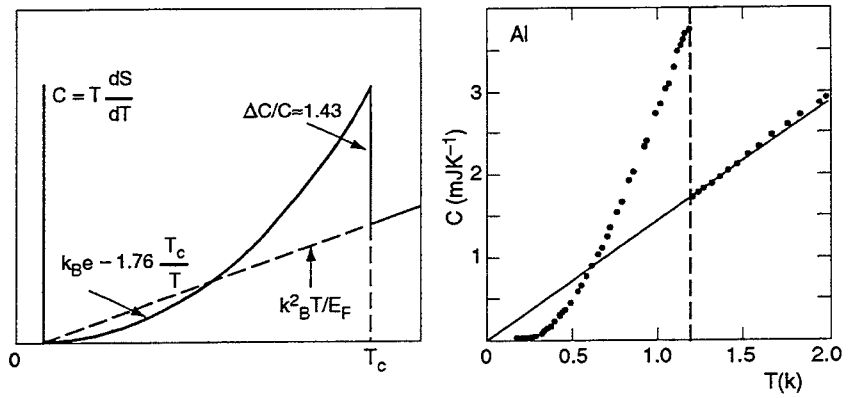

Figure 3.13: Temperature dependence of the electronic specific heat.

Similarly, near T_c

$$\Delta(T) \simeq 3.2\ k_B\ T_c\ \sqrt{1 - T/T_c} \tag{3.75}$$

Replacing (3.66) into (3.63)

$$\langle \Psi | H | \Psi \rangle = \sum_K \frac{(\varepsilon_k + \xi_k)^2}{2\ \varepsilon_k}\ f_k - \frac{(\varepsilon_k - \xi_k)^2}{2\varepsilon_k}\ (1 - f_k) \tag{3.76}$$

and replacing (3.70) into (3.61)

$$S = -2k_B \sum_k \ln\ f_k + f_k\ \exp\ (\varepsilon_k / k_B T)\quad \varepsilon_k / k_B T \tag{3.77}$$

One is now ready to calculate any thermodynamical quantity, e.g. the specific heat (electronic of course)

$$C = T\ \frac{dS}{dT} \tag{3.78}$$

$$C = -2\ k_B T \sum_k\ f_k(1 - f_k)\ \frac{\varepsilon_k}{k_B T}\ \frac{1}{k_B}\ \frac{d}{dT}\left(\frac{\varepsilon_k}{T}\right) \tag{3.79}$$

But

$$\varepsilon_k d\varepsilon_k = \Delta_k\ d\Delta_k = \Delta d\Delta \tag{3.80}$$

in the BCS approximation and

$$C = \frac{2}{k_B T^2} \sum_k\ f_k(1 - f_k)\{\varepsilon_k^2 - T\Delta\ \frac{d\Delta}{dT}\}$$

$$C = \frac{2\mathcal{N}_F}{k_B T^2} \int_0^\infty\ f(\varepsilon)\ (1 - f(\varepsilon))\ (\varepsilon^2 - T\Delta \frac{d\Delta}{dT})\ d\xi$$

In the last bracket ε^2 corresponds to the normal state and $T\Delta\ d\Delta/dT$ is the superconducting contribution. The specific heat varies (Fig. 3.13) like k_B exp $(-1.76\ T_c/T)$ at low temperature and displays a discontinuity, $\Delta C/C = 1.43$, at $T = T_c$ with respect to the normal state specific heat $C_n \propto k_B^2\ T/E_F$.

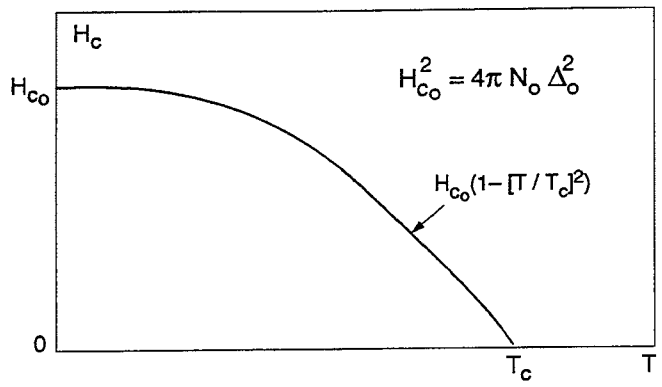

Figure 3.14: Temperature dependence of the thermodynamical critical field.

Finally, anticipating on the fact that a superconductor expels the magnetic field from its interior, by equating the magnetic field energy density $H^2/8\pi$ and the condensation energy at $T = 0$, $E_{\text{cond}} = 1/2\ \mathcal{N}_F\ \Delta^2$, one sees that when H reaches H_c thus obtained superconductivity can no longer be maintained. H_c is called the thermodynamical critical field

$$H_c^2 = 4\pi\ \Delta_0^2\ \mathcal{N}_F \tag{3.81}$$

Repeating the calculation at $T \neq 0$ gives the T dependence of H_c, which is close to the approximate form

$$H_c(T) \simeq H_c\ (0)\{1 - (T/Tc)^2\} \tag{3.82}$$

(see Fig. 3.14).

In practice, however, it may happen that between a lower critical field $H_{c1} < H_c$ and an upper critical field $H_{c2} > H_c$ the field be only partially expelled from the interior of the superconductor. This will be discussed in Chapter 4.

Figures 3.15 and 3.16 below illustrate respectively

- the deviation of $(H_c(T)/H_c(0))^2$ from its approximate form $1 - (T/Tc)^2$
- the deviation of $C/\gamma Tc$, where γ is the coefficient of T for C in the normal state, from the empirical law 3 $(T/Tc)^3$

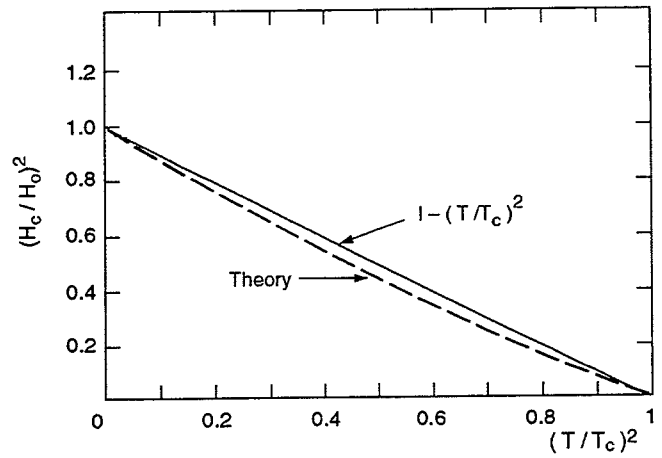

Figure 3.15: See text.

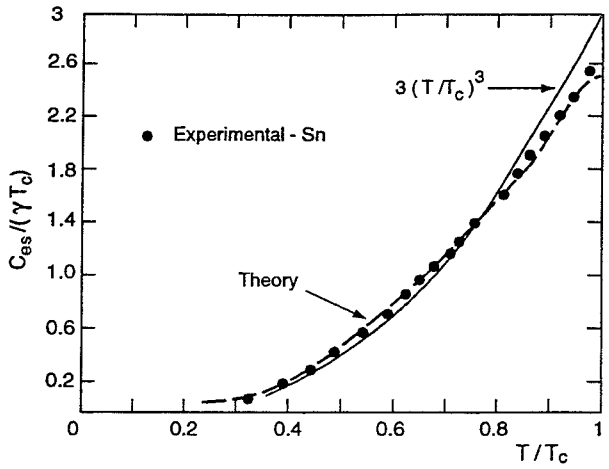

Figure 3.16: See text.

3.6 Dirty superconductors [19]

Superconductivity is observed to be surprizingly insensitive to the presence of impurities and defects. The reason is time reversal invariance in the scattering process which imposes that both electrons of a pair be scattered the same way and which preserves the coherence of the Cooper pair (Fig. 3.17).

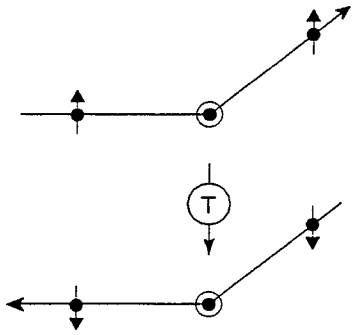

Figure 3.17: See text.

Such will not be the case for magnetic scattering centres which have a non-zero spin-flip component. Magnetic impurities are indeed observed to quickly destroy superconductivity.

Time reversal invariance implies that the eigenstates of an electron gas containing impurities will be constructed from single electron states of the form

$$\begin{aligned} |n\sigma\rangle &= \sum_k \langle n|k\rangle \; |k\sigma\rangle \\ |n\sigma\rangle_T &= \sum_k \langle k|n\rangle \; |-k-\sigma\rangle \end{aligned} \tag{3.83}$$

where the matrix elements $\langle n|k\rangle$ are those which solve the scattering problem. Of course one does not know how to calculate them but they must exist. The $|n\sigma\rangle$ and $|n\sigma\rangle_T$ are energy eigenstates with $E_n = E_{nT}$. Moreover $\sum_k \langle k|n\rangle\langle n|k\rangle = 1$.

The BCS calculation can be repeated with $|n\ n_T\rangle$ pairs replacing $|k\uparrow -k\downarrow\rangle$ pairs and all results are preserved as long as the pair interaction remains attractive. The

Fröhlich matrix element

$$V_{k\ell} = -2\frac{|W_q|^2}{\hbar\omega_q} \qquad q = \ell - k \qquad (E_k = E_\ell = E_F) \tag{3.84}$$

is now replaced by

$$V_{nn'} = -2 \sum_{k\ell} \frac{|\langle n|k\rangle|^2 |\langle n'|\ell\rangle|^2 \quad |W_q|^2}{\hbar\omega_q} \quad (E_n = E_{n'} = E_F) \tag{3.85}$$

namely the effective interaction is now averaged over some broad region of the Fermi sphere. In the BCS approximation of a constant V this does not matter and the interaction is unchanged. In real life, however, the plane waves $|k\sigma\rangle$ must be replaced by Bloch functions and the Fermi surface is no longer a sphere. Averaging the interaction over the Fermi sphere will in fact make it more plausible that the BCS approximation be valid. But it will result in a slightly lower effective interaction, therefore in slightly lower values of Δ and T_c.

3.7 Eliashberg equations, strong coupling

Giving up the simplicity of the BCS approximation is at high cost in terms of arithmetic complication and often results in relatively modest modifications of the final result. It does however provide a deeper insight in the underlying physics and a spectacular confirmation of its detailed understanding. The most elaborate generalization of the BCS theory is expressed in terms of the Eliashberg equations [20]

$$\begin{cases} \Delta(i\omega n)Z(i\omega n) &= \pi T \sum_m (\lambda_{m-n} - \mu^*)\Delta(i\omega_m)/\bar{\Delta}(i\omega_m) \\ Z(i\omega n) &= 1 + (\pi T/\omega_n) \sum_m \lambda_{m-n}\, \omega_m/\bar{\Delta}(i\omega_m) \\ \bar{\Delta}(i\omega_n) &= (\omega_n^2 + \Delta^2(i\omega_n))^{1/2} \end{cases} \tag{3.86}$$

These are coupled non-linear equations defining a gap function Δ and a renormalization function Z which are the basic components of the Green's function from which they are derived. Before expanding on the meaning of Δ and Z it is necessary to define λ and μ^*.

λ is related to the phonon mediated attraction between two electrons near the Fermi surface

$$\lambda_{m-n} = 2\int_0^\infty \frac{\alpha^2(\omega)\ F(\omega)\ \omega d\omega}{\omega^2 + (\omega_n - \omega_m)^2} \tag{3.87}$$

where ω is the frequency of the exchanged phonon, $\alpha(\omega)$ measures the electron-phonon coupling at the electron-phonon vertex and $F(\omega)$ is the phonon density of states. μ^* is the Coulomb pseudo-potential opposing superconductivity (it is cut-off at some frequency ω_c).

Solving the Eliashberg equations for the simple interaction

$$\begin{cases} \lambda_{m-n} = \lambda & \text{for} \quad |\omega_n|,\ |\omega_m| < \omega_c \\ \qquad = 0 & \text{otherwise} \end{cases} \tag{3.88}$$

yields

$$\begin{cases} Z(i\omega_n) = 1 + \lambda \\ \Delta(i\omega_n) = \Delta_{BCS}(T) \quad \text{for } |\omega_n| < \omega_c \\ \qquad\quad = 0 \qquad\qquad \text{otherwise} \end{cases} \tag{3.89}$$

where $\Delta_{BCS}\ (T)$ is the temperature-dependent BCS gap calculated for

$$\mathcal{N}_F V = \frac{\lambda - \mu^*}{1 + \lambda} \tag{3.90}$$

Other than taking explicit account of the Coulomb repulsion, via μ^*, and of the spectral dependence of the phonon-exchange interaction, via $\alpha^2\ F(\omega)$, the Eliashberg equations take also proper account of the retarded nature of the interaction and of the mass renormalization terms which are present in both the normal and superconducting states and which were neglected in the BCS approximation (where only terms of the form $V_{k\ell}\ b_\ell^+\ b_k$ had been retained).

Tunneling data are efficient in measuring $\alpha^2\ F(\omega)$ and μ^* from the current-voltage characteristics of S-N tunnel junctions (superconductor and normal metal separated by a thin oxide layer). The result can be compared with direct calculations or with experiments, such as neutron scattering, which produce information on the phonon spectral density.

Excellent agreement is usually observed. See Figs. 3.18 to 3.26 and Ref. [21].

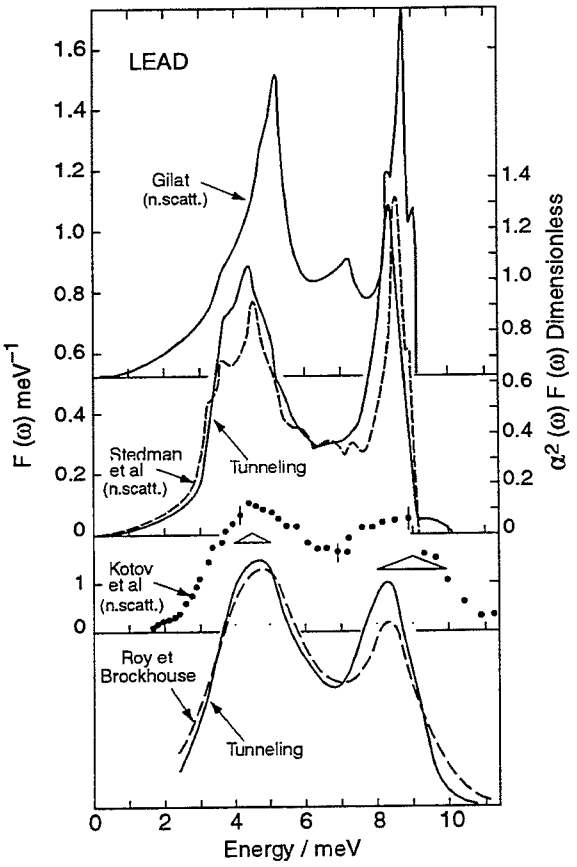

Figure 3.18: Phonon density of states for Pb.

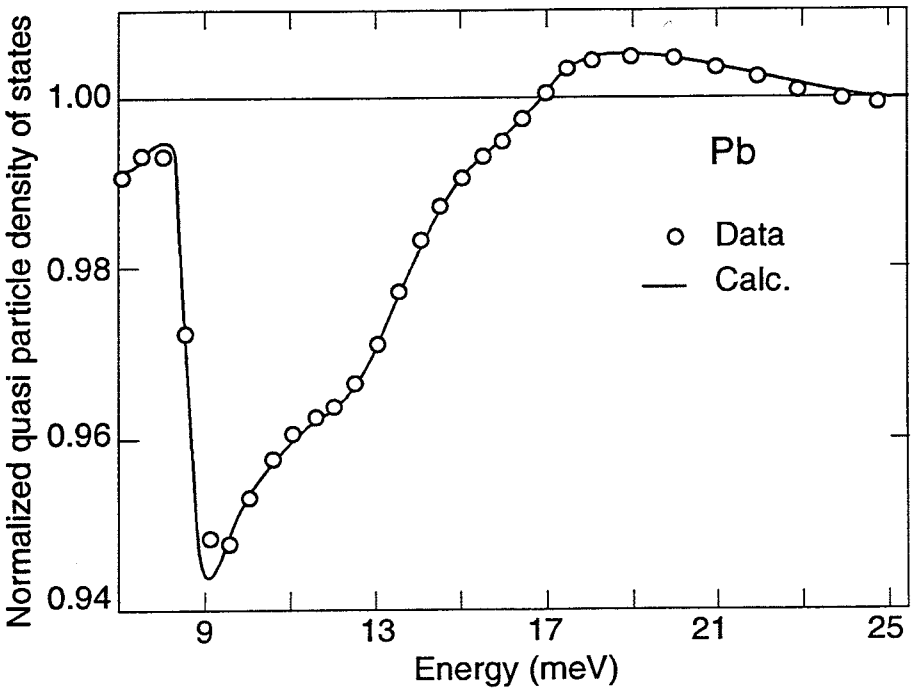

Figure 3.19: See text.

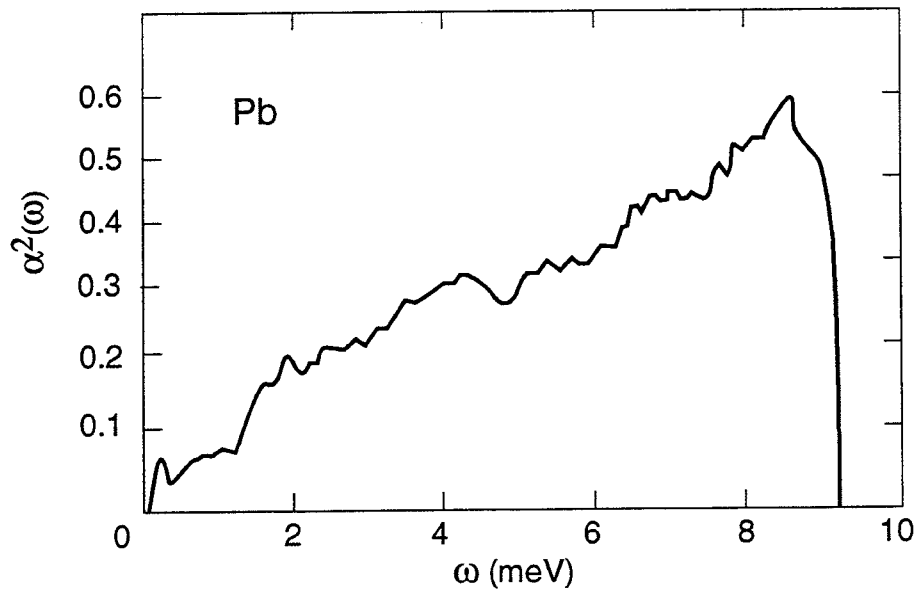

Figure 3.20: See text.

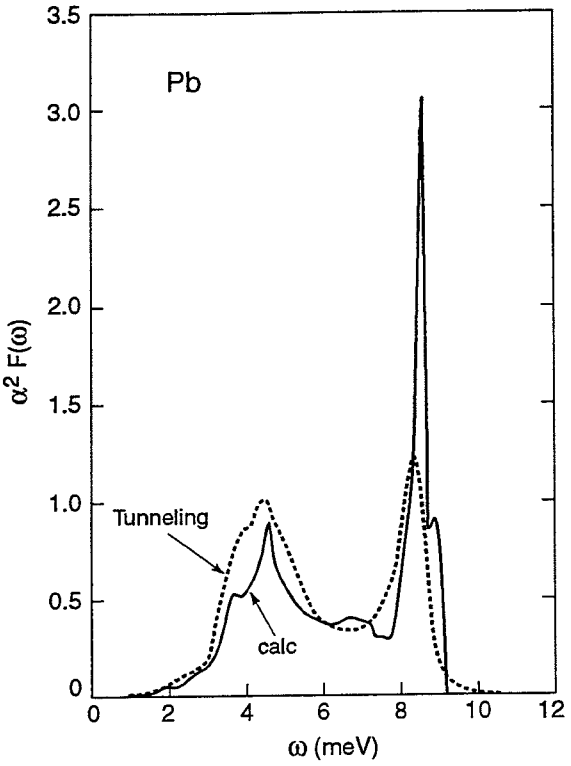

Figure 3.21: Phonon spectral density in lead.

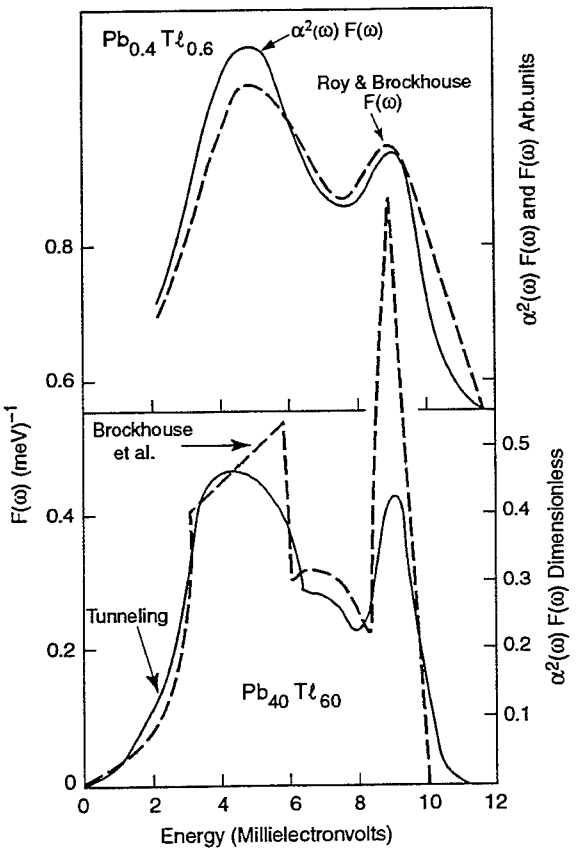

Figure 3.22: PSD in PbTa.

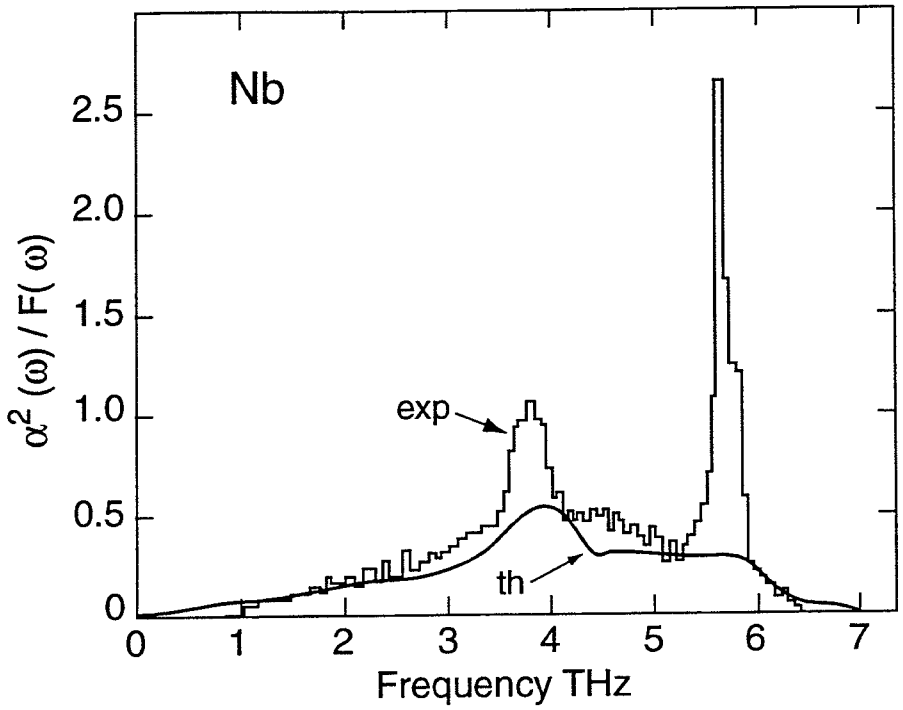

Figure 3.23: PSD in Nb.

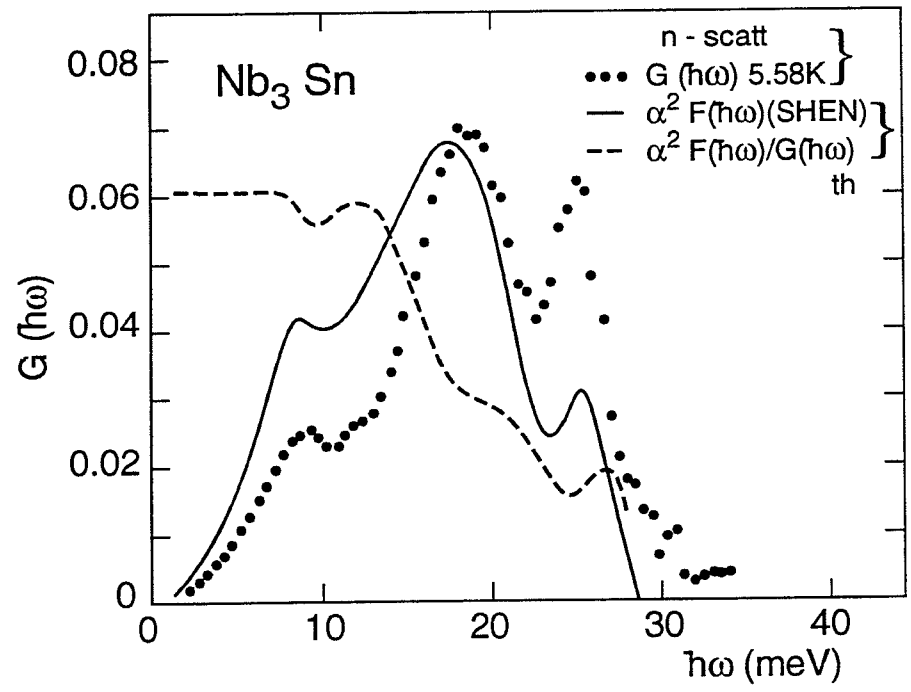

Figure 3.24: PSD in Nb_3 Sn.

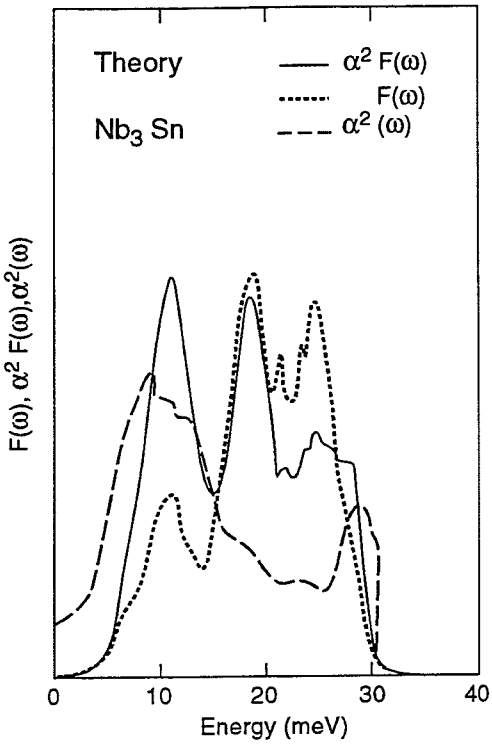

Figure 3.25: PSD in Nb_3 Sn.

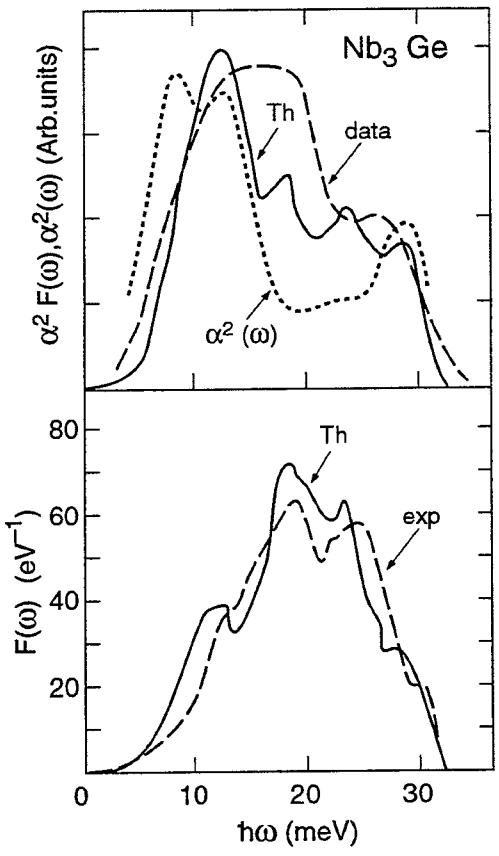

Figure 3.26: PSD in Nb_3 Ge.

Solving the Eliashberg equations is often done iteratively. An important concept in the game is that of functional derivatives which measure the sensitivity of a given quantity to a localized change (i.e. at some value of ω) of $\alpha^2\ F(\omega)$.

Eliashberg equations have been used [21] to get some global feeling of the changes they imply with respect to the BCS approximation. Examples are reviewed below.

Critical temperature (see Fig. 3.27)

The Allen and Dynes relation reads

$$k_B T_c = \frac{\hbar\omega_{\ln}}{1.2}\ \exp\left(-\frac{1.04\ (1+\lambda)}{\lambda - \mu^*(1+0.62\lambda)}\right) \tag{3.91}$$

where $\omega_{\ln}$ is a parameter which enters many expressions obtained from (simplified) Eliashberg equations,

$$\omega_{\ln} = \exp\ \left\{\frac{2}{\lambda}\ \int_0^\infty\ \ln\ (\omega)\ \frac{\alpha^2 F(\omega)}{\omega}\ d\omega\right\} \tag{3.92}$$

Approximating $\alpha^2 F(\omega)$ by a δ-function at some tuned value of ω yields

$$T_c = \frac{2A}{1.2\lambda}\ \exp\left(\frac{-1.04\ (1+\lambda)}{\lambda - \mu^*(1+0.62\lambda)}\right) \tag{3.93}$$

with

$$A = \int_0^\infty\ \alpha^2\ F(\omega)\ d\omega \tag{3.94}$$

and for $1.2 < \lambda < 2.4 \qquad T_c \approx 0.148\ A$

Gap (see Fig. 3.28)

$$\frac{2\Delta_0}{k_B\ T_c} = 3.53\left\{1 + 12.5\left(\frac{T_c}{\omega_{\ln}}\right)^2\ \ln\left(\frac{\omega_{\ln}}{2\ T_c}\right)\right\} \tag{3.95}$$

Isotope effect (see Fig. 3.29)

$$\frac{M}{T_c}\ \frac{dT_c}{dM} = \frac{1}{2}\ \text{for}\ \mu^* = 0 \tag{3.96}$$

as in the BCS approximation. However deviations are observed at low values of λ when μ^* deviates from zero.

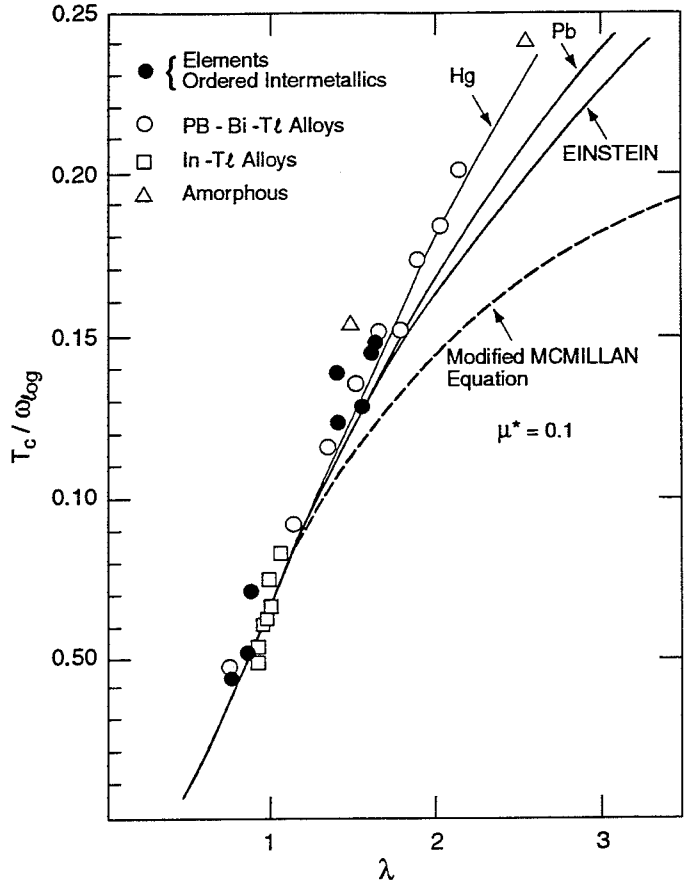

Figure 3.27: Critical temperatures.

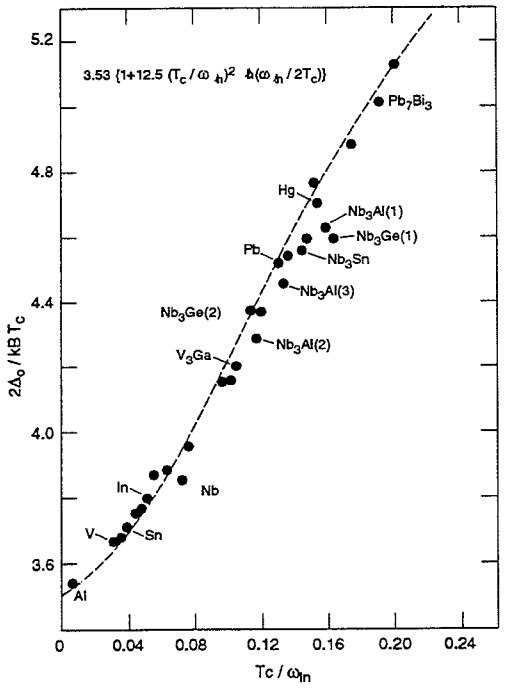

Figure 3.28: Gaps.

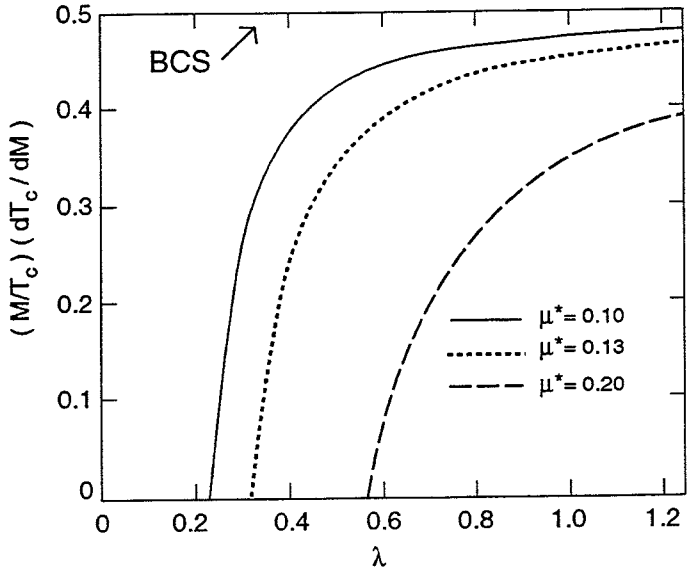

Figure 3.29: Isotope effect.

Critical thermodynamical field and electronic specific heat (Figs. 3.30 to 3.36)

$D(t) = H_c(T)/H_c(0) - (1 - (T/T_c)^2)$ is illustrated on Fig. 3.30 and the electronic specific heat on Figs. 3.31 and 3.32. Figures 3.33 to 3.36 illustrate regularities. In particular

$$\frac{Csc - Cn}{\gamma T_c} = f + (1-t)g \qquad t = T/T_c$$

$$f = 1.43\ (1 + 53\ (T_c/\omega_{\ln})^2\ \ln\ (\omega_{\ln}/3T_c))$$

$$g = -3.77\ (1 + 117\ (T_c/\omega_{\ln})^2 (\omega_{\ln}/2.9T_c))$$

$$\frac{\gamma T_c^2}{H_c^2(0)} = 0.168\ (1 - 12.2(T_c/\omega_{\ln})^2\ \ln\ (\omega_{\ln}/3T_c))$$

$$\frac{H_c(0)}{\frac{d}{dT} H_c(T)|_{T_c}} = 0.576\ T_c\ (1 - 13.4(T_c/\omega_{\ln})^2\ \ln\ (\omega_{\ln}/3.5T_c))$$

Finally Fig. 3.37 illustrates the T_c dependence of the jump at $V(\Delta)$ in the supercurrent of a junction.

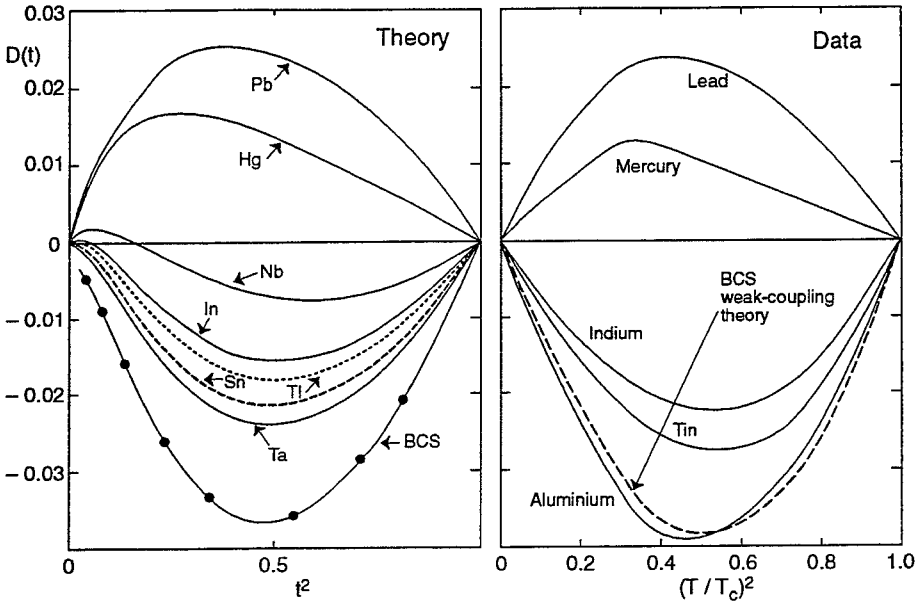

Figure 3.30: $D(t) = H_c(t)/H_c(0) - (1 - t^2)$.

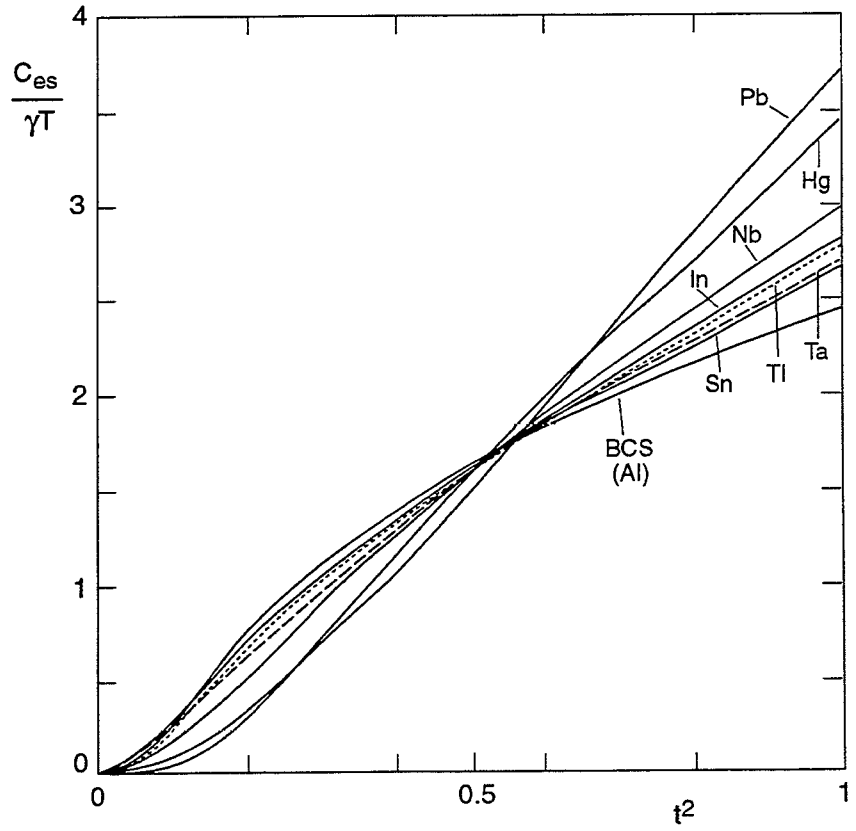

Figure 3.31: See text.

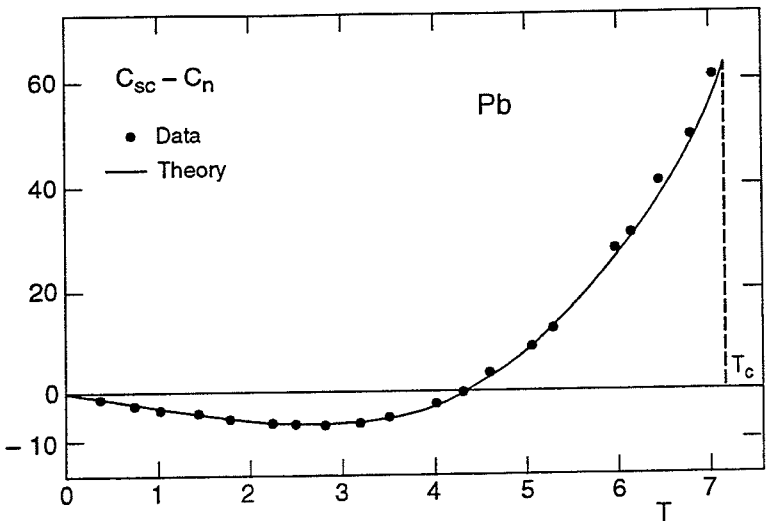

Figure 3.32: See text.

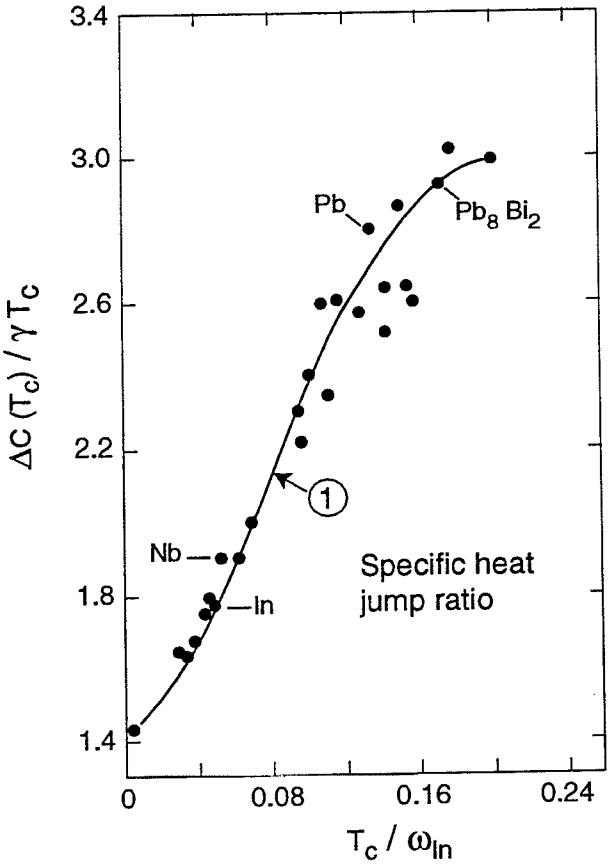

Figure 3.33: (1) is 1.43 $[1 + 53\ (T_c/\omega_{ln})^2 \ln\ (\omega_{ln}/3T_c)]$.

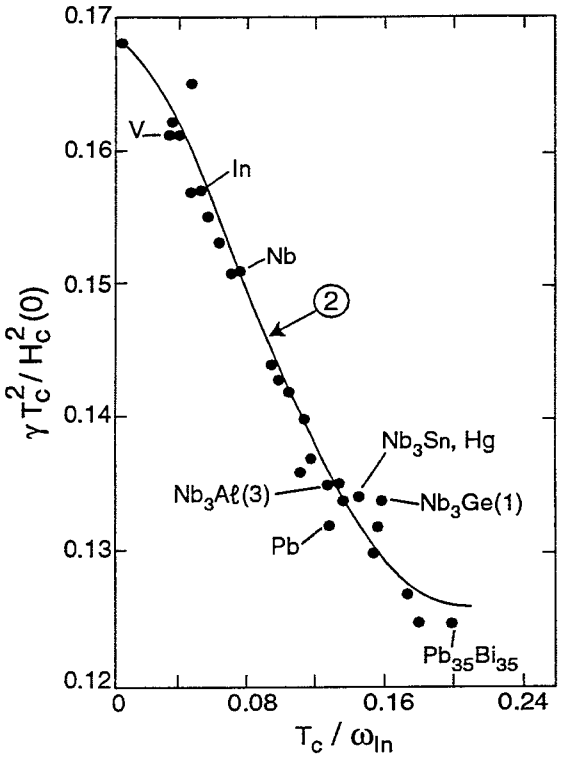

Figure 3.34: (2) is 0.168 (1–12.2 $(T_c/\omega_{\ln})^2$ ln $(\omega_{\ln}/3T_c)$.

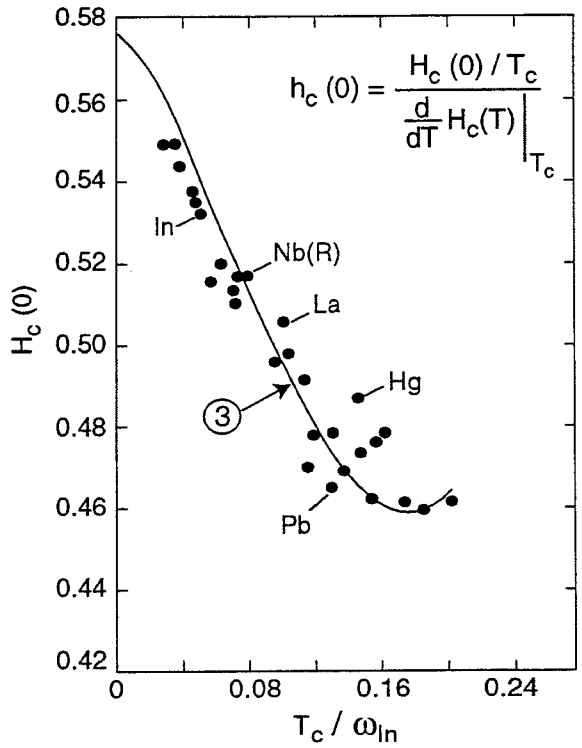

Figure 3.35: (3) is 0.576(1–13.4 $(T_c/\omega_{\ln})^2$ ln $(\omega_{\ln}/3.5\ T_c)$.

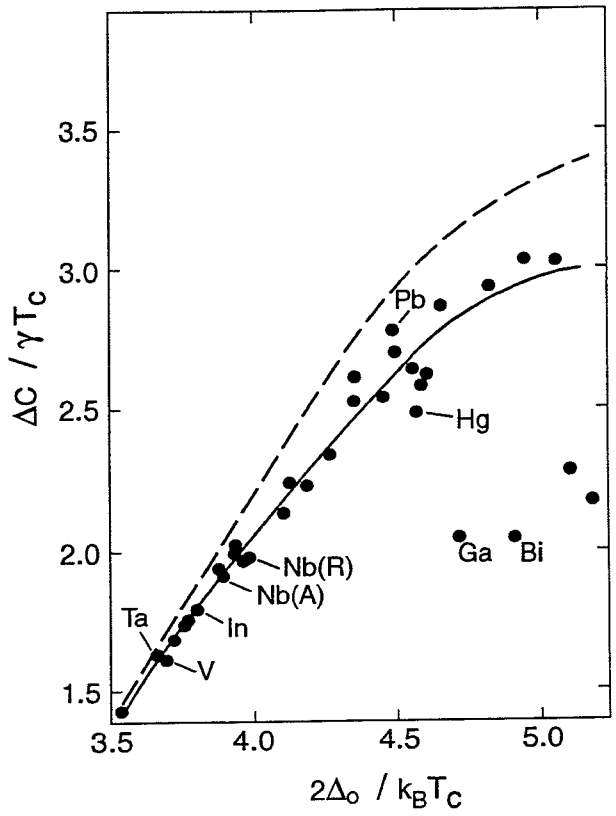

Figure 3.36: See text.

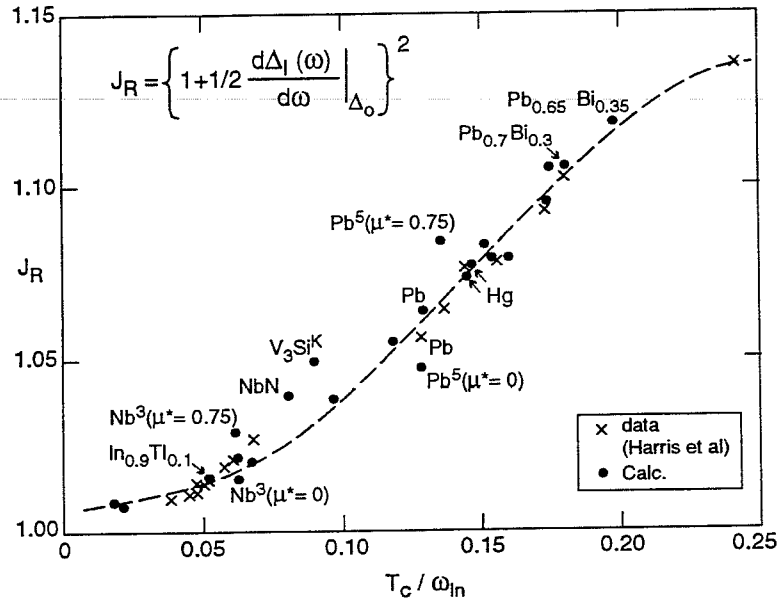

Figure 3.37: Jump at the energy-gap voltage in the quasiparticle current of a superconducting tunneling junction.

4 SUPERCONDUCTIVITY IN WEAK EXTERNAL FIELDS

4.1 Persistent currents

We consider a superconductor in which a constant electric field E is applied during a time t. As

$$E = -\frac{1}{c}\frac{\partial A}{\partial t}\ , \tag{4.1}$$

A being the vector potential,

$$-\frac{1}{c}A = \int_0^t E\ \mathrm{dt}\ ,\ \text{i.e.} \qquad A = -c\,Et = \text{cte}\ . \tag{4.2}$$

The hamiltonian is obtained from the zero field case by simply adding $-\frac{e}{c}A = e\,Et$ to each momentum. But the BCS groundstate is only trivially affected by a translation in momentum space, as the Fröhlich interaction depends only on the difference between momenta. Therefore the BCS ground state becomes

$$\Pi_m\ (\cos\theta_m + \sin\theta_m\ b^+_{m+k_0})|0\rangle \tag{4.3}$$

with

$$b^+_{m+k_0} = a^+_{m+k_0\uparrow}\ a^+_{-m+k_0\downarrow} \text{ and } k_0 = \frac{e\ Et}{\hbar} \tag{4.4}$$

While the potential energy is unaffected the kinetic energy increases as

$$2\frac{\hbar^2k^2}{2m} \rightarrow \frac{\hbar^2(k+k_0)^2}{2m} + \frac{\hbar^2(-k+k_0)^2}{2m} = 2\frac{\hbar^2}{2m}\ (k^2+k_0^2) \tag{4.5}$$

i.e. each pair acquires an additional kinetic energy $(\hbar^2/m)\ k_0^2$ (Fig. 4.1)

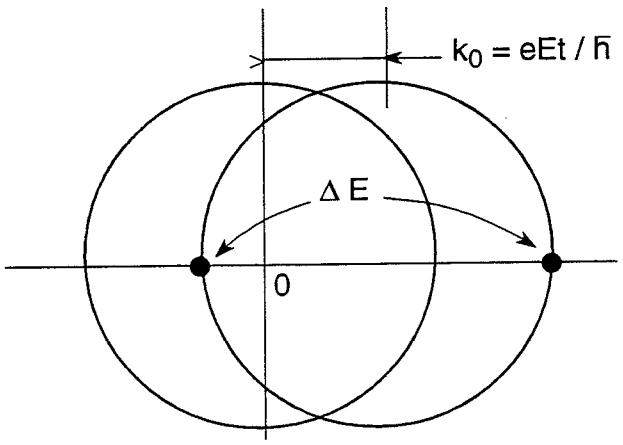

Figure 4.1: $\Delta E = 2\frac{\hbar^2}{m}\ k_0 k_F$.

As in the case of a perfect normal conductor the new state corresponds to a persistent current coherently carried by all conduction electrons (which remain paired in the superconducting case). The difference is that in the case of a real life normal conductor collisions induce transitions between excited states from the leading edge of the Fermi sphere to its trailing edge, thereby limiting the amount of translation in k-space which the Fermi sphere can afford. In the superconducting case, however, the gap prevents such transitions to occur as long as k_0 is small enough.

To bring a pair $(k_F + k_0, \ -k_F + k_0)$ from the leading edge to the trailing edge $(-k_F + k_0, -k_F + k_0)$ costs 2 Δ (to break the pair) $-\Delta E$ with (Fig. 4.2)

$$\frac{2m}{\hbar^2}\,\Delta E = 2(k_F^2 + k_0^2) - 2(-k_F + k_0)^2 = 4k_F k_0 \tag{4.6}$$

The condition for persistent current becomes

$$\Delta > \frac{\hbar^2}{m}\,k_F k_0, \text{ i.e. } p_0 < \frac{\Delta}{v_F},\ J_0 < \frac{ne}{m}\,\frac{\Delta}{v_F}\,. \tag{4.7}$$

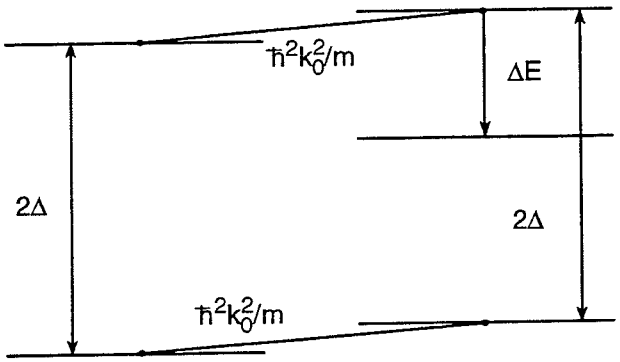

Figure 4.2: See text.

A more realistic evaluation of the critical current will be given in Section 5.6.

While the argument is solid at $T = 0$ it becomes a bit more handwaving for $T \neq 0$. It is customary to state that the Cooper pairs shunt any possible current carried by quasiparticles. Namely excited states carry a zero total momentum, as is intuitively reasonable but not trivially obvious. The only effect of a non vanishing temperature is to lower the critical current

$$J_C\,(T) = J_C\,(0)\,\Delta\,(T)/\Delta\,(0)\,. \tag{4.8}$$

4.2 Coherence effects

Consider a superconductor interacting with a field of frequency ω inducing transitions between a state of energy E to a state of energy $E + \hbar\omega$. The transition probability is

$$\begin{aligned} P \ = \ & \int N(E)\ f(E)\ |M|^2\ N(E + \hbar\omega)\ dE \\ & - \int N(E + \hbar\omega)\ f(E + \hbar\omega)\ |M|^2\ N(E)\ dE \end{aligned} \tag{4.9}$$

where the second term subtracts the transitions $E + \hbar\omega \rightarrow E$. Each term is summed over initial states (density of states N times occupation f at temperature T) and proportional to the density of available final states and to the square $|M|^2$ of the transition matrix element. Therefore

$$P = \int |M|^2\ (f(E) - f(E + \hbar\omega))\ N(E)\ N(E + \hbar\omega)\ dE \tag{4.10}$$

In the normal conducting case $|M|^2$ is simply $|\langle k'\sigma'|M|k\sigma\rangle|^2$, each contribution $k\sigma \rightarrow k'\sigma'$ being independent from each other. However, in the superconducting case, care must be taken to account for the coherence between $k\sigma \rightarrow k'\sigma'$ and $-k-\sigma \rightarrow -k'-\sigma'$.

Namely, a transition from a quasiparticle $k\uparrow$ to a quasiparticle $k'\uparrow$ may proceed in two ways: transfer of the $k\uparrow$ electron to the empty k' state or transfer of a $-k'\downarrow$ electron from a Cooper pair in k' to the singly occupied k state (Fig. 4.3)

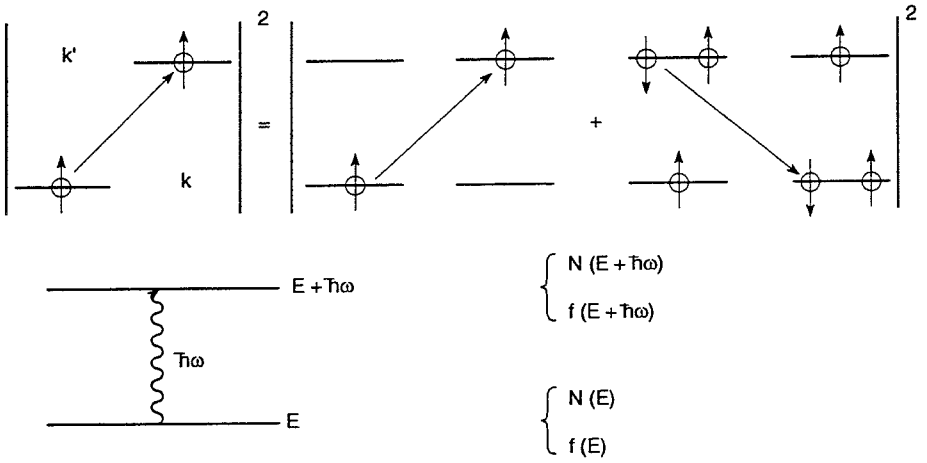

Figure 4.3: See text.

These amplitudes are coherent and must be added before taking the modulus squared. In most cases

$$|\langle k'\sigma'|M|k\sigma\rangle| = |\langle -k-\sigma|M|-k'-\sigma'\rangle|$$

$$\text{i.e. } \langle k'\sigma'|M|k\sigma\rangle = \text{sgn}\langle -k-\sigma|M|-k'-\sigma'\rangle \ . \tag{4.11}$$

Restricting the discussion to sgn = real $= \pm 1$ and to no spin-flip, $\langle k'\sigma'|M|k\sigma\rangle = M_{kk'}\delta_{\sigma\sigma'}$

$$M = \sum_{kk'} M_{kk'}\ (a^+_{k'}\ a_k + \text{sgn}\ a^+_{-k}\ a_{-k'}) \tag{4.12}$$

with, as usual, $a_k = a_k\uparrow$ and $a_{-k} = a_{-k}\downarrow$. Here the $M_{kk'}$ are taken between Bloch functions of the normal state and need to be transformed to a basis of quasi-particle states using the transformation equations

$$\begin{cases} a^+_m &= \cos\theta_m\gamma^+_m + \sin\theta_m\ \gamma_{-m} \\ a_{-m} &= \cos\theta_m\gamma_{-m} - \sin\theta_m\gamma^+_m \end{cases} \tag{4.13}$$

giving

$$\begin{aligned} a^+_{k'}\ a_k + sgn\ a^+_{-k}\ a_{-k'} &= (\cos\theta_{k'}\ \gamma^+_{k'} + \sin\theta_{k'}\gamma_{-k'})(\cos\theta_k\ \gamma_k + \sin\theta_k\ \gamma^+_{-k}) \\ &+ \text{sgn}(\cos\theta_k\ \gamma^+_{-k} - \sin\theta_k\ \gamma_k)(\cos\theta_{k'}\gamma_{-k'} - \sin\theta_{k'}\ \gamma^+_{k'}) \\ &= (\cos\theta_{k'}\ \cos\theta_k - \text{sgn}\ \sin\theta_{k'}\ \sin\theta_k)(\gamma^+_{k'}\gamma_k + \text{sgn}\gamma^+_{-k}\ \gamma_{-k'}) \\ &+ (\sin\theta_k\ \cos\theta_{k'} + \text{sgn}\ \cos\theta_k\ \sin\theta_{k'})(\gamma^+_{k'}\gamma^+_{-k} + \text{sgn}\ \gamma_{-k'}\gamma_k) \\ &= \cos\ (\theta_k + \text{sgn}\ \theta_{k'})(\gamma^+_{k'}\ \gamma_k + \text{sgn}\ \gamma^+_{-k}\gamma_{-k'}) \\ &+ \sin\ (\theta_k + \text{sgn}\ \theta_{k'})(\gamma^+_{k'}\ \gamma^+_{-k} + \text{sgn}\ \gamma_{-k'}\ \gamma_k)\ . \end{aligned} \tag{4.14}$$

Using (2.3.10) one obtains

$$\begin{cases} \cos^2\ (\theta_k + \text{sgn}\ \theta_{k'}) &= \frac{1}{2}(1 + \frac{\xi\xi'}{EE'} - \text{sgn}\frac{\Delta^2}{EE'}) \\ \sin^2(\theta_k + \text{sgn}\ \theta_{k'}) &= \frac{1}{2}(1 - \frac{\xi\xi'}{EE'} + \text{sgn}\ \frac{\Delta^2}{EE'}) \end{cases} \tag{4.15}$$

When replacing in the expression of P, the $\xi\xi'$ terms drop (once summed in the integral) and one is left with

$$P = \int |M_{kk'}|^2\ (f(E) - f(E+\hbar\omega))\ N(E)\ N(E+\hbar\omega)$$

$$\left\{\frac{1}{2}\left[1 - \text{sgn}\ \frac{\Delta^2}{E(E+\hbar\omega)}\right] + \frac{1}{2}\left[1 - \text{sgn}\ \frac{\Delta^2}{E(E-\hbar\omega)}\right]\right.$$
$$\left. + \frac{1}{2}\left[1 + \text{sgn}\ \frac{\Delta^2}{E(\hbar\omega - E)}\right] + \frac{1}{2}\left[1 + \text{sgn}\ \frac{\Delta^2}{E(-\hbar\omega - E)}\right]\right\} \tag{4.16}$$

where the four terms in the curly bracket correspond to $\gamma^+_{k'}\ \gamma_k$, $\gamma^+_{-k}\ \gamma_{-k'}$, $\gamma^+_{k'}\ \gamma^+_{-k}$ and $\gamma_{-k'}\ \gamma_k$ respectively, i.e. the curly bracket reduces to

$$1 - \text{sgn}\frac{\Delta^2}{E(E+\hbar\omega)} \tag{4.17}$$

for $E = \Delta$ to ∞ for the first and fourth terms and for $E = -\infty$ to $-\Delta - \hbar\omega$ for the middle terms. Writing $\int^* = \int_{-\infty}^{-\Delta-\hbar\omega} + \int_{\Delta}^{\infty}$

$$P = \int^*\ |M_{kk'}|^2 (f(E) - f(E+\hbar\omega))\ N_F^2\ \frac{E(E+\hbar\omega)}{\sqrt{E^2-\Delta^2}\sqrt{(E+\hbar\omega)^2-\Delta^2}} \frac{E(E+\hbar\omega) - \text{sgn}\ \Delta^2}{E(E+\hbar\omega)}\ dE \tag{4.18}$$

and changing from E to $E' = E + \hbar\omega/2$ which symmetrizes the integrand with respect to changes from E to $-E$

$$P = |M|^2 N_F^2\ 2\ \int_{\Delta+\hbar\omega/2}^{\infty} \frac{(E^2 - (\frac{\hbar\omega}{2})^2 - \text{sgn}\Delta^2)(f(E - \frac{\hbar\omega}{2}) - f(E + \frac{\hbar\omega}{2}))}{[(E - \frac{\hbar\omega}{2})^2 - \Delta^2]^{1/2}[(E + \frac{\hbar\omega}{2})^2 - \Delta^2]^{1/2}}\ dE \tag{4.19}$$

and finally, writing $\alpha = \frac{\hbar\omega}{2}$ and $E = \Delta + \alpha + x$

$$P = 2|M|^2 N_F^2 \int_0^{\infty} \frac{[(x+\Delta)(x+\Delta+2\alpha) - \text{sgn}\ \Delta^2]dx}{[x(x+2\alpha)(x+2\Delta)(x+2\Delta+2\alpha)]^{1/2}}\ [f(\Delta+x) - f(\Delta+2\alpha+x)] \tag{4.20}$$

with

$$f(E) = 1/(1 + \exp\ (E/k_BT))\ . \tag{4.21}$$

We have made the (reasonable) assumption that $|M|^2$ can be taken out of the integral.

For $\alpha = 0$ the fraction reduces to

$$\frac{(x+\Delta)^2 - \text{sgn}\ \Delta^2}{x(x+2\Delta)} \tag{4.22}$$

$$\text{i.e. } \equiv 1 \text{ for sgn} = +1 \text{ and } \equiv 1 + \frac{2\Delta^2}{x(x+2\Delta)} \text{ for sgn} = -1 \tag{4.23}$$

$$P_+ = 2|M|^2 N_F^2 \int_0^\infty -\frac{\partial f}{\partial E}\bigg|_{\Delta+x} 2\alpha \, dx = 2|M|^2 N_F^2 \, f(\Delta)\hbar\omega \tag{4.24}$$

while

$$P_- = P_+ - 2|M|^2 N_F^2 \int_0^\infty \frac{2\Delta^2}{x(x+2\Delta)} \left(-\frac{\partial f}{\partial E}\right)\bigg|_{\Delta+x}^{2\alpha dx} \tag{4.25}$$

which is dominated by the logarithmic divergence near $x = 0$:

$$\int_0^\infty \ldots \approx \Delta \, \frac{\partial f}{\partial E}\bigg|_\Delta 2\alpha \int_0 \frac{dx}{x}$$

As soon as $\alpha \neq 0$ the integral converges, but the effect will be a rise of P_- as soon as $T < T_C$ (which will then be quickly compensated by the contribution of f at low temperatures) in contrast with P_+ which drops as soon as $T < T_C$. This is illustrated in (Fig. 4.4) below

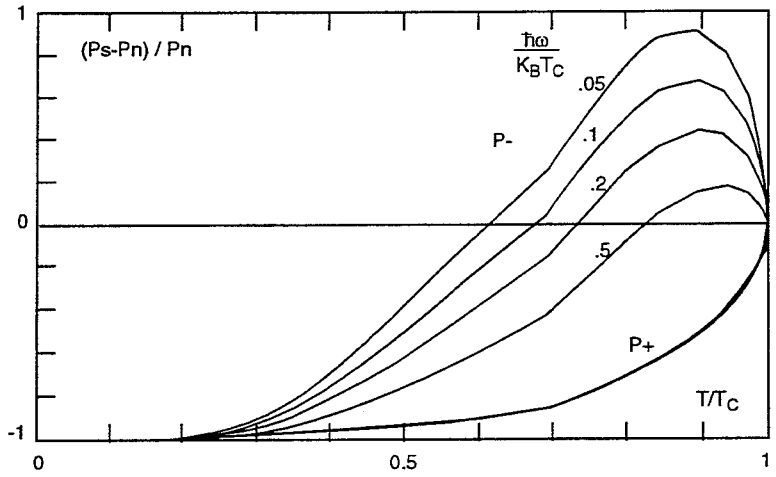

Figure 4.4: Temperature dependence of P_+ and P_-.

More generally, for $\Delta \gg \alpha$,

$$P_+ = 2|M|^2 N_F^2 \int_0^\infty (1 + O(\frac{\alpha^2}{\Delta^2}))2\alpha \frac{\partial f}{\partial E}\bigg|_{\Delta+x} dx \tag{4.26}$$

$$P_+ = 2|M|^2 N_F^2 \, \hbar\omega f(\Delta) \, (1 + O(\frac{\alpha^2}{\Delta^2}))$$

$$P_+ = 2 \, P_n \, f(\Delta)(1 + O(\frac{\alpha^2}{\Delta^2})) \tag{4.27}$$

where P_n is the normal state transition rate ($\Delta = 0$) and, assuming in addition $kT \ll \Delta$,

$$P_- \approx 2|M|^2 N_F^2 \int_0^\infty \exp\,(-[\Delta + x]/kT) \, \frac{\hbar\omega}{kT} \, \Delta \, \frac{dx}{\sqrt{x(x+2\alpha)}}$$

$$\approx 2|M|^2 N_F^2 \, \hbar\omega \, \frac{e^{-\Delta/kT}}{kT} \, \Delta \int_0^\infty \frac{e^{-u} du}{\sqrt{u(u + 2\alpha/kT)}} \tag{4.28}$$

4.3 Induced transitions

The developments of the preceding section have many experimental applications. Here we consider only three: ultrasonic attenuation, nuclear relaxation and absorption of microwaves.

At low temperatures, ultrasonic waves are absorbed by the perturbation induced on quasi-particles from the local distortion of the lattice field (typically a few meV for a permil local expansion of the lattice). This perturbation has sgn= +1 and relation (4.27) gives a good fit to the data with a sudden drop of the attenuation when crossing T_C from above (Fig. 4.5)

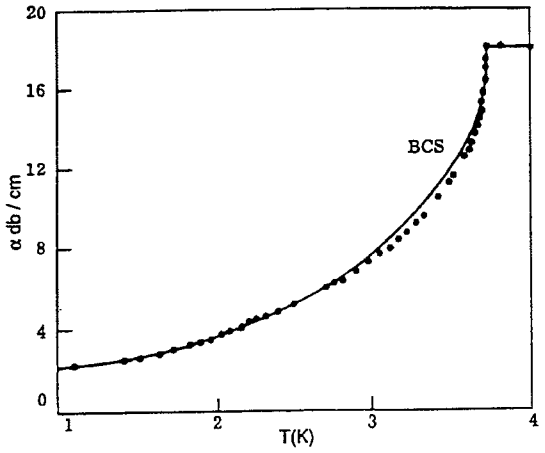

Figure 4.5: Ultrasonic attenuation.

On the contrary nuclear relaxation corresponds to sgn $= -1$. It results from the interaction between the lattice nuclear spins and the quasi-particles, the frequency of relevance being that governing spin-precession in the local nuclear environment. At low temperatures the relaxation rate is dominated by the exponential in Eq. (4.28).

However, when crossing T_C from above, the logarithm in Eq. (4.25) causes a sudden increase of the attenuation which is experimentally observed (Fig. 4.6) . This contrasting behaviour of ultrasonic attenuation and nuclear relaxation is a spectacular illustration of coherence and a major success of the BCS theory.

The absorption of microwaves has also sgn $= -1$. The surface resistance obeys a temperature dependence of the form

$$\frac{1}{k_B T} \exp\ (-\Delta/k_B T) \tag{4.29}$$

when both $k_B T$ and $\hbar\omega$ are well below Δ, as predicted by Eq. (4.28). Detailed calculations of the frequency and mean free path dependences of the surface resistance [22] give good fit to the data (Figs. 4.7 to 4.12). At high frequencies one can reach $\hbar\omega = 2\Delta$, and observe the disappearance of superconductivity. At $T = 0$ (no quasi-particles) this is the only absorption mechanism and the ratio of superconducting to normal state conductivities takes the simple analytical form ($\hbar\omega > 2\Delta_0$)

$$\frac{\sigma_1}{\sigma_n} = (1 + 2\frac{\Delta_0}{\hbar\omega})\ E(k) - 2(\frac{2\Delta_0}{\hbar\omega})\ K(k) \tag{4.30}$$

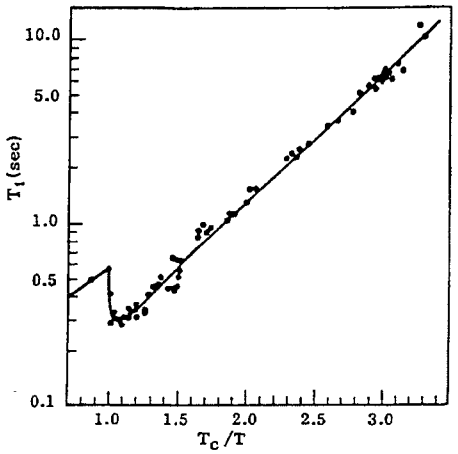

Figure 4.6: Nuclear relaxation.

with

$$k = |2\Delta_0 - \hbar\omega|/|2\Delta_0 + \hbar\omega| \tag{4.31}$$

Moreover one has for any $\hbar\omega$

$$\frac{\sigma_2}{\sigma n} = \frac{1}{2}\left\{\left[\frac{2\Delta_0}{\hbar\omega} + 1\right] E(K') + \left[\frac{2\Delta_0}{\hbar\omega} - 1\right] K(k')\right\} \tag{4.32}$$

with $k' = \sqrt{1-k^2}$, E and K are elliptic integrals and σ_1, σ_2 are the real and imaginary parts of the complex conductivity.

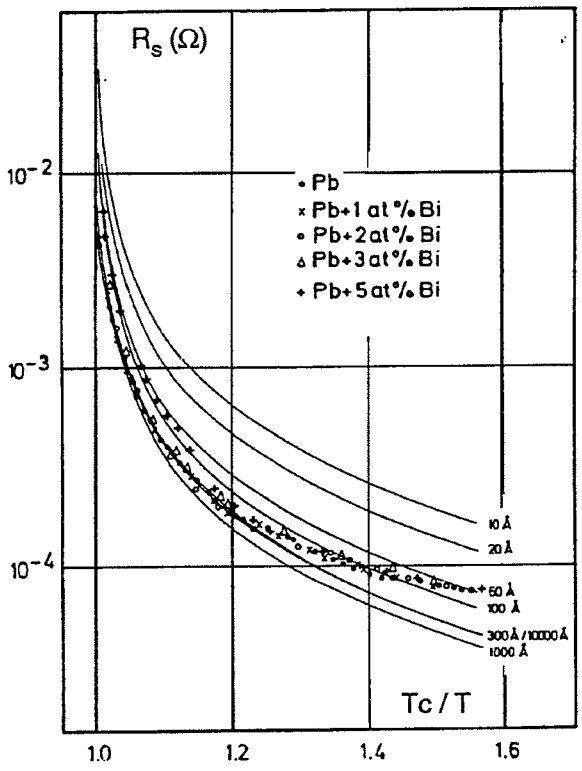

Figure 4.7: See text.

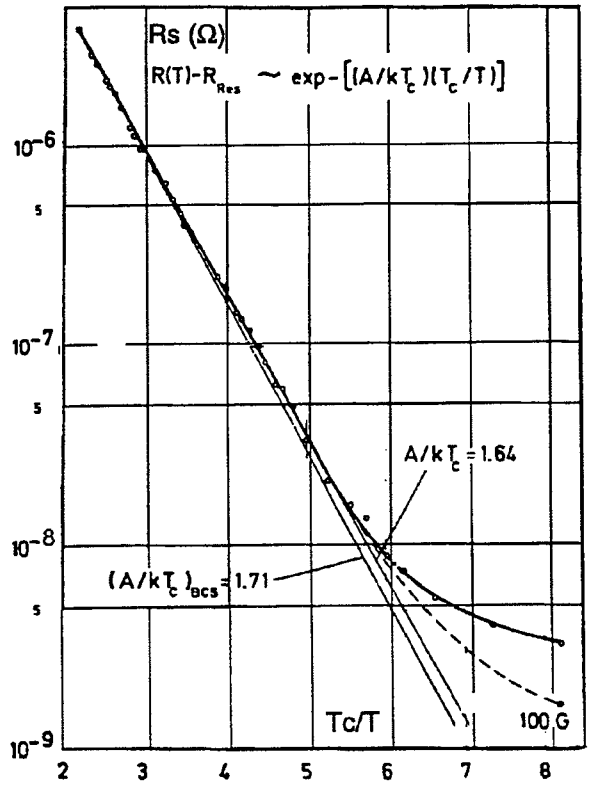

Figure 4.8: See text.

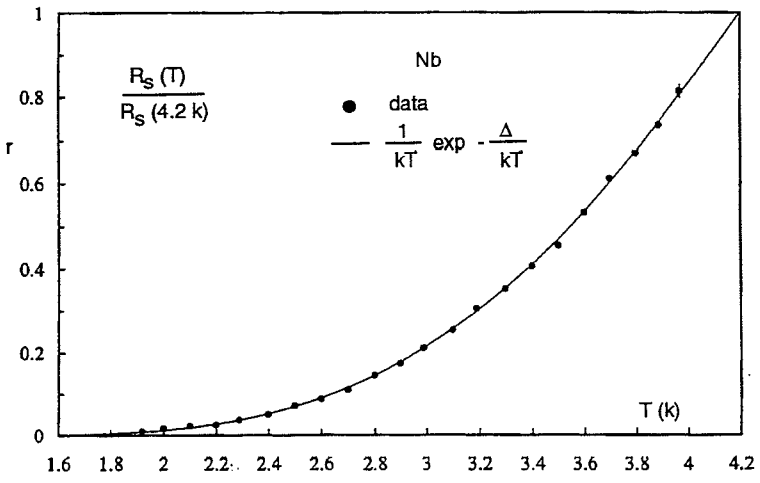

Figure 4.9: See text.

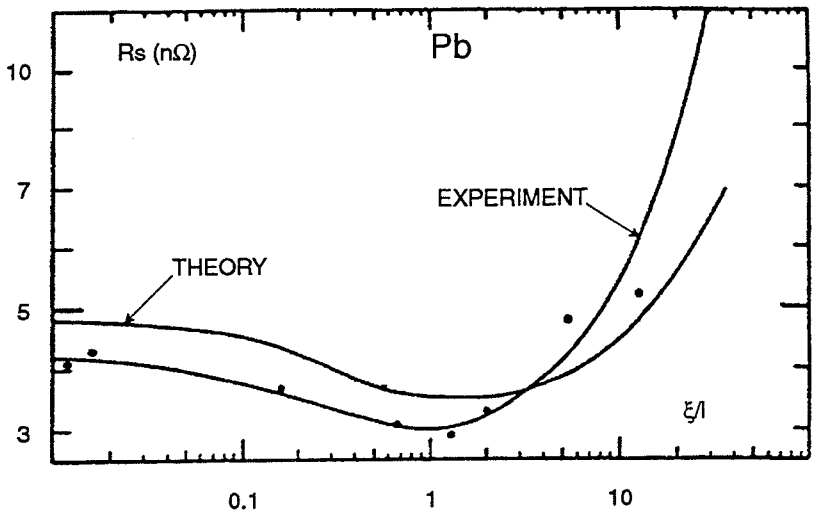

Figure 4.10: Mean free path dependence of R_s (Pb).

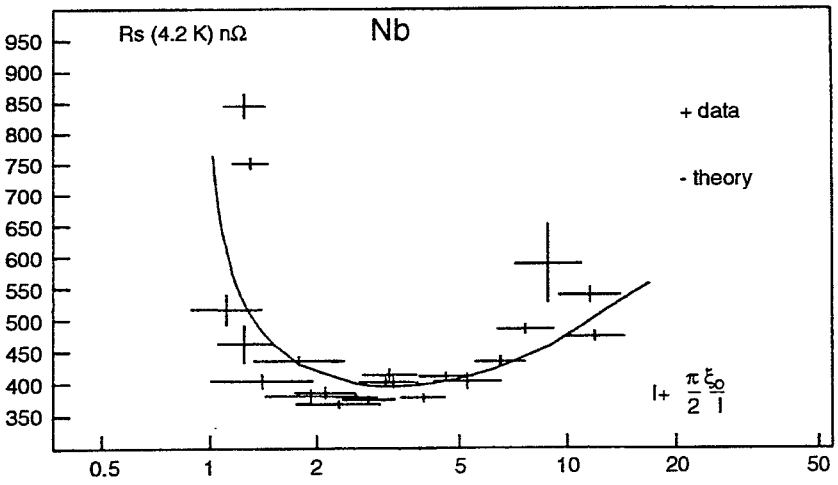

Figure 4.11: Mean free path dependence of R_s (Nb).

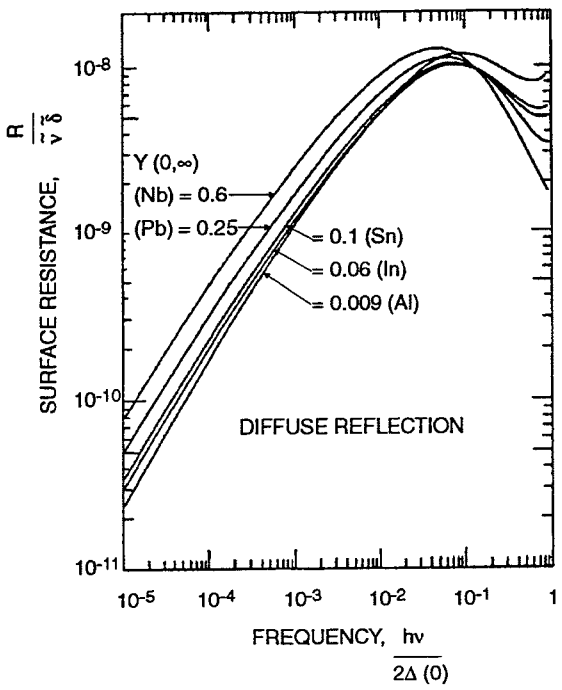

Figure 4.12: Frequency dependence of R_s

4.4 Meissner effect

The response of a free electron gas to a constant and uniform magnetic field H results in a quantification of the energy levels in the plane normal to H of the form $(n+\frac{1}{2})\hbar\omega_C$ with the cyclotron frequency $\omega_C = He/mc$. As a result, the current

$$J = \langle \frac{e}{m}\,(p - \frac{e}{c}\,A)\rangle \tag{4.33}$$

vanishes, the contributions from p and A cancelling each other (see relation 2.35). In the superconducting state, to the extent that $\hbar\omega_C \ll \Delta$, i.e. $H \ll (mc/\hbar e)\,\Delta$, the condensation will be inhibited and the wave function will stay at its $A = 0$ value for which $J = 0$. Then the current $J = -(e^2/mc)\langle A\rangle$ does not vanish and exactly cancels the field inside the sample. As $\hbar\omega_C = 1.16 \times 10^{-5}$ meV per Gauss of H and Δ is in the meV range the condition on H reads $H \ll 10^5$ Gauss, less restrictive than the condition $H \ll H_C$.

In order to better understand the mechanism of the Meissner effect, consider a sample with a flat surface in the y, z plane (Fig 4.13). To mimic the external field, one can introduce a current sheet J_{ext} on the sample surface and call J_{SC} the supercurrent. Then

$$\frac{4\pi}{c}\,(J_{\text{ext}} + J_{SC}) = \nabla_\wedge H = \nabla_\wedge\,\nabla_\wedge\,A = -\,\nabla^2\,A \tag{4.34}$$

where the first equation is from Maxwell, the second from $H = \nabla_\wedge A$ and the third from the choice of gauge $\nabla \cdot A = 0$.

Taking

$$J_{\text{ext}} = \frac{c}{2\pi}\,H_{\text{ext}}\,\delta(x) \tag{4.35}$$

corresponds to a boundary condition on the sample surface

$$H = H_{\text{ext}}\,\hat{y}\,. \tag{4.36}$$

It is convenient at this stage to take Fourier transforms

$$\nabla^2 \int e^{ik\cdot r}\, A(k)\, dk = -\int k^2\, A(k)\, e^{ik\cdot r}\, dk \tag{4.37}$$

and

$$-k^2\, A(k) = -\frac{4\pi}{c}\, J_{\text{ext}}\,(k) + K(k)\, A(k) \tag{4.38}$$

with the Kernel $K(k)$ defined from

$$J_{SC}(k) = -\frac{c}{4\pi}\, K(k)\, A(k) \tag{4.39}$$

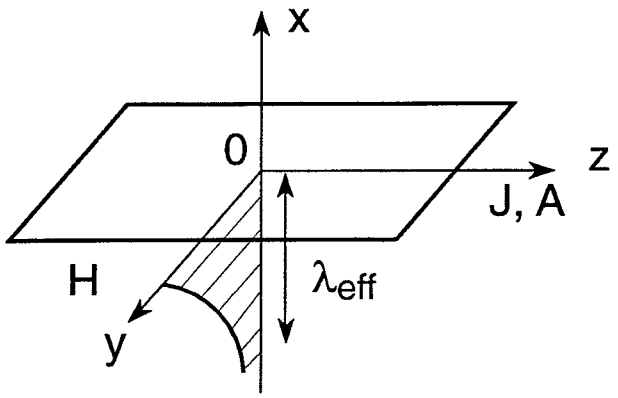

Figure 4.13: See text.

Then

$$A(k) = \frac{4\pi}{c}\, \frac{J_{\text{ext}}(k)}{K(k) + k^2} \tag{4.40}$$

But the Fourier transform of $\delta(x)$ is $1/2\pi$ so $J_{\text{ext}}(k) = (c/4\pi^2)\, H_{\text{ext}}$ and finally

$$A(k) = \frac{1}{\pi}\, \frac{H_{\text{ext}}}{K(k) + k^2} \tag{4.41}$$

Defining the penetration of the field inside the sample as a penetration depth

$$\lambda_{\text{eff}} = \frac{1}{H_{\text{ext}}} \int_0^\infty H(x)\, dx \tag{4.42}$$

From $H = \nabla_\wedge A \qquad H_y(k) = -ik\, A_z(k)$

$$H(x) = \int_{-\infty}^{\infty} H_y(k)\, e^{ik\cdot x}\, dk = -i \int_{-\infty}^{\infty} \frac{1}{\pi}\, e^{ik\cdot x} \frac{H_{\text{ext}}}{K(k) + k^2}\, k dk \tag{4.43}$$

$$\int_0^\infty H(x) dx = -i \int_0^\infty dx \int_{-\infty}^{\infty} dk\, \frac{H_{\text{ext}}}{\pi}\, \frac{k\, e^{ik\cdot x}\, dk}{K(k) + k^2}$$

$$= 2\, \frac{H_{\text{ext}}}{\pi} \int_0^\infty \frac{k dk}{K(k) + k^2} \int_0^\infty \sin kx dx = 2 \frac{H_{\text{ext}}}{\pi} \int_0^\infty \frac{dk}{K(k) + k^2}$$

$$\lambda_{\text{eff}} = \frac{2}{\pi} \int_0^\infty \frac{dk}{K(k) + k^2} \tag{4.44}$$

This result [23] is for specular scattering at the surface, as implicitely implied by the current sheet boundary condition. For diffuse scattering one obtains

$$\lambda_{\text{eff}} = \frac{\pi}{\int_0^\infty \ln\ [1 + \frac{K(k)}{k^2}]dk} \tag{4.45}$$

Both expressions are singular at $k = 0$ if $K(k) \leq 0$ and for λ_{eff} to be finite one needs $K(k) > 0$ when $k \to 0$. Namely as long as the kernel $K(k)$ defining the supercurrent is positive the field cannot penetrate into the sample beyond $\approx \lambda_{\text{eff}}$ and there is a Meissner effect.

Long before the kernel $K(k)$ was calculated by BCS one used to classify the superconductors in two families. The London family obeyed the simple London equation [6] $K(k) = \text{cte} = \frac{1}{\lambda_L^2}$

$$K_L(k) = \frac{1}{\lambda_L^2} = \frac{4\pi n e^2}{mc^2} \tag{4.46}$$

The Pippard family [8] obeyed instead a non-local relation between current and vector potential with a form similar to the Chambers' equation (2.37), the mean-free path ℓ being replaced by a coherence length $\xi_P \approx 0.15\ \hbar v_F / k_B T_C$

$$K_P(k) = \frac{1}{\lambda_L^2}\ \frac{3}{4\pi\xi_P} \int \frac{z^2 \exp\ (-R/\xi_P + ikx)}{R^4}\ dxdydz \tag{4.47}$$

which reduces to $K_P(k) = K_L(k)$ when $\xi_P \to 0$. Metals for which $\xi_P \ll \lambda_L$ were called London superconductors, metals for which $\xi_P \gg \lambda_L$ were called Pippard superconductors. Moreover, as T deviated from 0, λ_L was observed to evolve approximately as [7]

$$\lambda_L(T) \simeq \lambda_L(0)\{1 - [\frac{T}{T_C}]^4\}^{-1/2} \tag{4.48}$$

Finally ξ_P was observed to vary approximately as

$$\frac{1}{\xi_P} = \frac{1}{\xi_P}\bigg|_{\text{clean}} + \frac{1}{\ell} \tag{4.49}$$

when the mean-free path was decreased, with the result that dirty superconductors were ultimately all of the London family. These early results (Fig. 4.14) will get clarified as we now proceed with the BCS calculation of the kernel $K(k)$

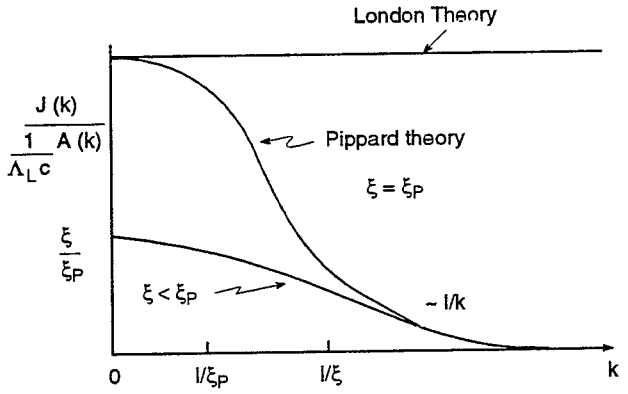

Figure 4.14: Schematic illustration of the London and Pippard models. Here $\Lambda_L = 4\pi\lambda_L^2/c^2$.

In this BCS calculation we allow for T to deviate from 0 and for H_{ext} to deviate from uniformity.

Treating the interaction with the field as a perturbation to first order in A

$$H_A = -\int dr\ a^+(r)(\frac{e\hbar}{2imc}[A\cdot\bigtriangledown + \bigtriangledown\cdot A])\ a(r) \tag{4.50}$$

with[2] $a(r) = \sum_{k\sigma}\ a_{k\sigma}\ e^{-ik\cdot r}|\sigma\rangle$ and using the gauge condition $\bigtriangledown.A = 0$

$$H_A = \frac{e\hbar}{mc}\sum_{kk'\sigma\sigma'}\int dr\ a^+_{k'\sigma'}\ e^{+ik'\cdot r}\ A\cdot k\ a_{k\sigma}\ e^{-ik\cdot r}\ \delta_{\sigma\sigma'}$$

$$= \frac{e\hbar}{mc}\sum_{kk'\sigma} a^+_{k'\sigma'}\ a_{k\sigma}\left\{\int dr\ e^{-i(k-k')\cdot r}A(r)\right\}\cdot k \tag{4.51}$$

and writing $k = k' - q$ and Fourier transforming

$$H_A = \frac{e\hbar}{mc}\sum_{kq\sigma} a^+_{k+q\sigma}\ a_{k\sigma}\ A(q)\cdot k \tag{4.52}$$

The total current reads

$$\left\{\begin{array}{lcl} J(r) & = & J_P(r) + J_D(r) \text{ with} \\ J_P(r) & = & \frac{e\hbar}{2m}\ \sum_{kq\sigma}\ a^+_{k+q\sigma}\ a_{k\sigma}\ e^{+iq\cdot r}\ (2k+q) \\ J_D(r) & = & -\frac{e^2}{mc}\ \sum_{kq\sigma}\ a^+_{k+q\sigma}\ a_{k\sigma}\ e^{+iq\cdot r}\ A \end{array}\right. \tag{4.53}$$

and the piece of wave function added by H_A is

$$\phi = \sum_{i\neq 0}\ \frac{\langle\psi_i|H_A|\psi_0\rangle}{E_0 - E_i}\ |\psi_i\rangle \tag{4.54}$$

where the $|\psi_i\rangle$ are the unperturbed states having unperturbed energies E_i.

After some arithmetics one obtains

$$\left\{\begin{array}{lcl} J_D(r) & = & -\frac{ne^2}{mc}\ A(r) \\ J_P(r) & = & \frac{e^2\hbar^2}{2m^2c}\ \sum_{kq}\ (2k+q)\cdot A(-q)\ e^{-iq\cdot r}\ L(\epsilon_k,\ \epsilon_{k+q}) \\ & & \text{with } L(\epsilon,\epsilon') = \frac{1}{2}\left\{\frac{1-f-f'}{\epsilon+\epsilon'}\left[1 - \frac{\xi\xi' + \Delta_0^2}{\epsilon\epsilon'}\right] + \frac{f'-f}{\epsilon-\epsilon'}\left[1 + \frac{\xi\xi'+\Delta_0^2}{\epsilon\epsilon'}\right]\right\} \end{array}\right. \tag{4.55}$$

Fourier transforming $J_P(r)$ gives

$$J_P(q) = \frac{e^2\hbar^2}{m^2c}\ \frac{1}{(2\pi)^3}\ \int dk(2k+q)\ k\cdot A(q)\ L_{\epsilon_k,\epsilon_{k+q}} \tag{4.56}$$

[2] Up to powers of (2π) all along.

and

$$\begin{cases} \lim_{q\to 0}\ J_P(q) & = \frac{ne^2}{mc}\left(1-\frac{\Lambda_L}{\Lambda_T}\right) A(q) \\ 1-\frac{\Lambda_L}{\Lambda_T} & = 2\int_0^\infty dy\ \frac{\exp\ [y^2+\beta^2\Delta_0^2]^{1/2}}{(1+\exp\ [y^2+\beta^2\Delta_0^2]^{1/2})^2} \\ \text{or equivalently } \Lambda_T & = \Lambda_L\left(1+\frac{\beta}{\Delta_0}\ \frac{d\Delta_0}{d\beta}\right) \\ \text{and } \Lambda_L & = \frac{m}{ne^2}=\frac{4\pi}{c^2}\ \lambda_L^2 \text{ and } \beta = 1/k_BT \end{cases} \tag{4.57}$$

$$As\ q\to 0\ J_P(q)+J_D(q)\to -\frac{\Lambda_L}{\Lambda_T}\ \frac{ne^2}{mc}\ A(q) = -\frac{1}{c\Lambda_T}\ A(q) \tag{4.58}$$

$$\begin{cases} As\ T\to 0\ \Lambda_T\to\Lambda_L \\ As\ T\to T_c\ \Lambda_T\to\infty \end{cases} \tag{4.59}$$

Therefore the Meissner effect always occurs for $T < T_c$ with a penetration depth increasing from λ_L at $T = 0$ to ∞ at $T = T_c$.

Not restricting any longer the discussion to $q \to 0$, one finds for the current a general non-local expression *à la* Pippard

$$J(r) = \frac{-3\pi\Delta}{4\pi c\,\Lambda_T\,\hbar v_F}\int dr' \frac{K_J(R,T)\vec{R}(\bar{A}(r')\cdot\bar{R})}{R^4} \qquad (R = r-r') \tag{4.60}$$

and

$$K_J(R,T) = \frac{\Lambda_T}{\Lambda_L}\ \frac{\Delta(T)}{\Delta(0)}\left\{th\frac{\Delta(T)}{2k_BT} - \frac{2\Delta(T)}{\pi}\int_0^\infty d\epsilon' \sin\frac{2R\epsilon'}{\hbar v_F}\ \frac{1-2f(E')}{\epsilon' E'}\right\} \tag{4.61}$$

which is a kernel (Fig. 4.15) very close to

$$\exp\ (-\frac{R}{\xi_0}) \tag{4.62}$$

with

$$\xi_0 = \frac{\hbar v_F}{\pi\Delta_0} = 0.18\frac{\hbar v_F}{k_BT_c} \tag{4.63}$$

called the BCS coherence length.

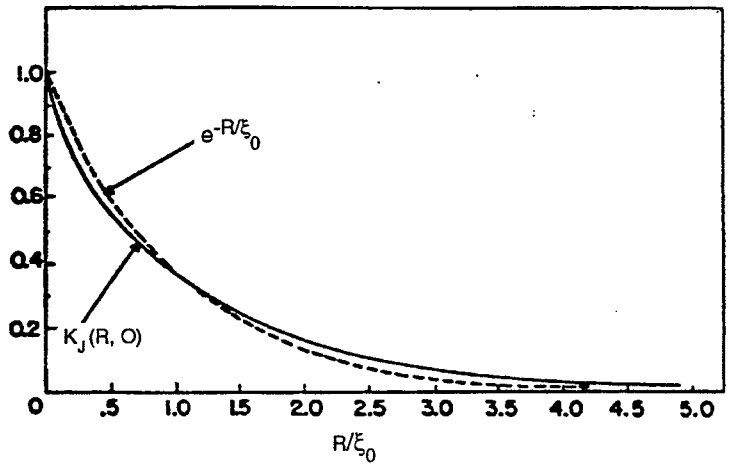

Figure 4.15: The BCS kernel.

The Kernel $K_J\ (R,T)$ is negligibly dependent on temperature and the BCS coherence length is very close to the Pippard coherence length (0.18 instead of 0.15). Both are related to the extension of a Cooper pair calculated in (3.18),

$$\xi_{\text{naive}} = \frac{\hbar v_F}{\sqrt{3}\,\Delta} = \frac{\pi}{\sqrt{3}}\,\xi_0\ . \tag{4.64}$$

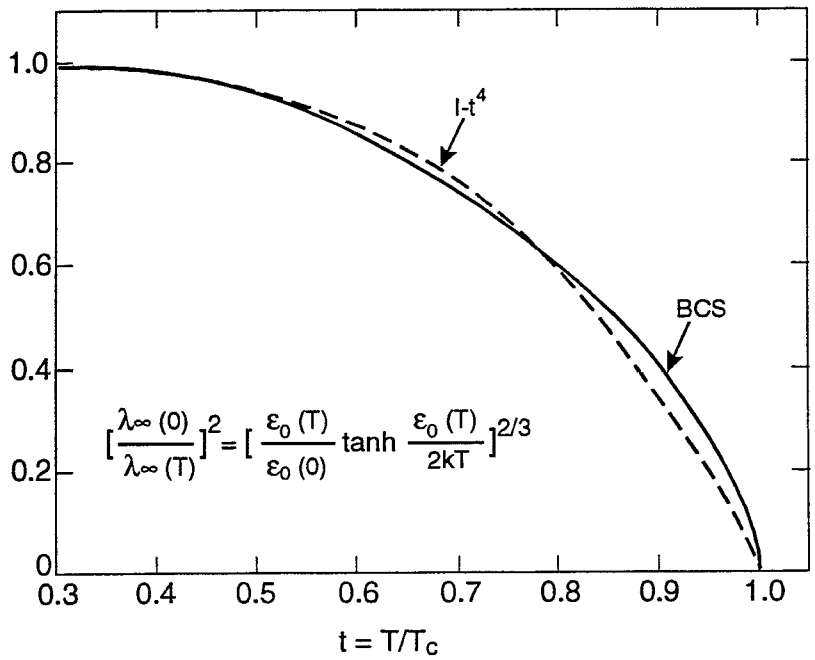

Figure 4.16: Temperature dependence of the BCS penetration depth in the limit $\xi_0 \gg \lambda$.

Having calculated the current versus vector potential relation one can now calculate the penetration depth $\lambda(T)$ using (4.44 and 4.45). In the London limit ($\xi_0 \ll \lambda$) $\lambda(T)$

reduces to λ_L at $T = 0$ (for a free electron gas) and depends on T as

$$\lambda_L(T) = \lambda_L \left(\frac{\Lambda_T}{\Lambda_L} \right)^{1/2} . \tag{4.65}$$

In the Pippard limit the temperature dependence of $\lambda(T)$ is displayed in Fig. 4.16 and found very close from the two fluid model result [7].

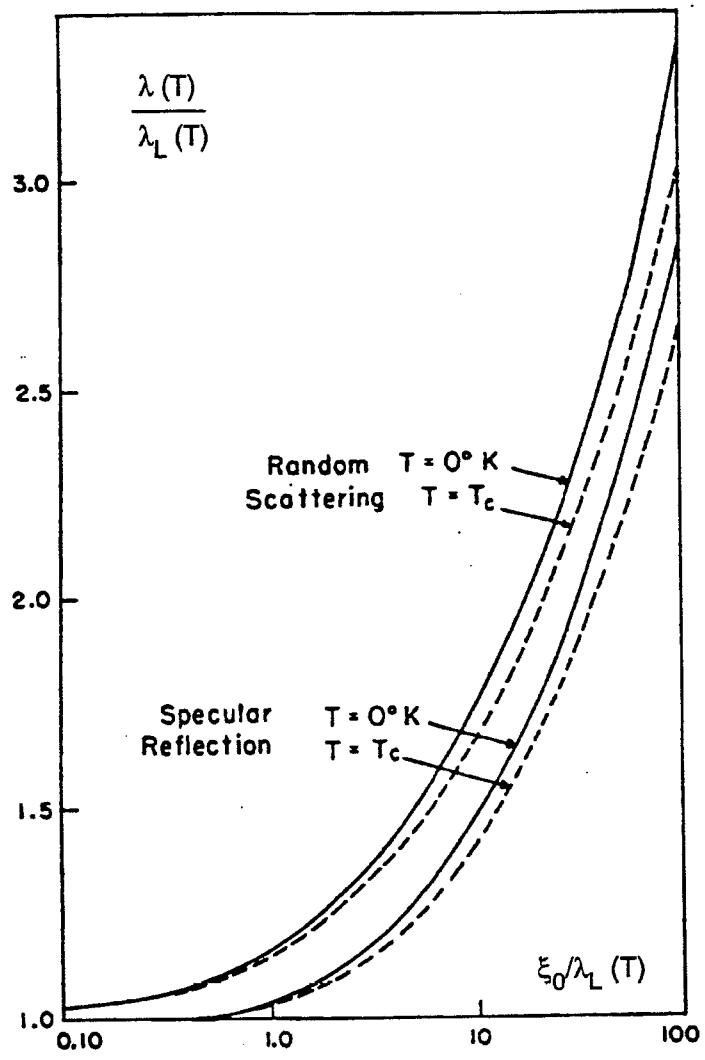

Figure 4.17: In general the penetration depth $\lambda(T)$ is related to $\lambda_L(T) = \lambda_L \left(\frac{\Lambda_T}{\Lambda_L} \right)^{1/2}$ as shown in the figure.

In the presence of impurities λ and ξ_0 are modified approximately as

$$\begin{cases} \lambda^2(\ell) = \lambda^2(\infty)\{1 + \frac{\pi}{2} \frac{\xi_0}{\ell}\} \\ \xi_0^{-1}(\ell) = \xi_0^{-1}(\infty) + \ell^{-1} \end{cases} \tag{4.66}$$

Calculations using the Eliashberg equations show relatively modest deviations with respect to the BCS results. Figure 4.18 illustrates results on the penetration depth.

Defining

$$\omega_{\ln} = \exp\left(\frac{2}{\lambda}\int_0^\infty \ln\omega \frac{\alpha^2 F(\omega)}{\omega}\, d\omega\right) \tag{4.67}$$

as in (3.92) (here λ is the coefficient in the Eliashberg equations, not the penetration depth!) one can find rather general expressions describing the deviation with respect to BCS

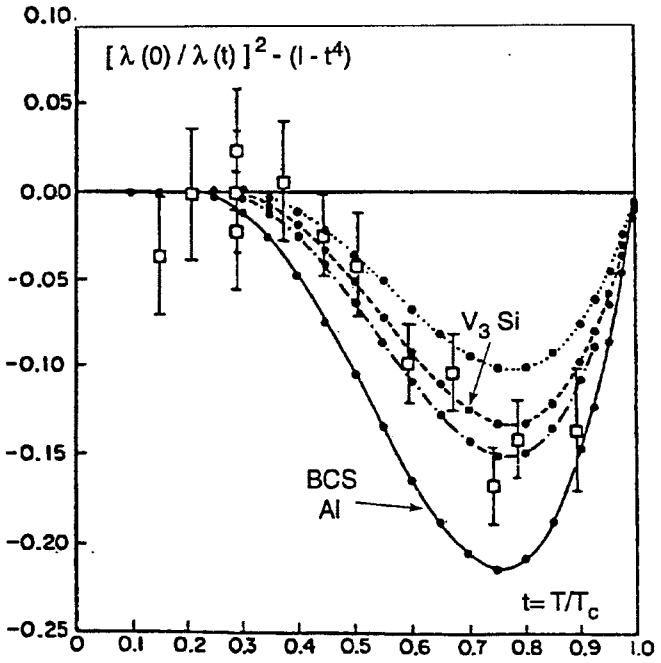

Figure 4.18: Deviation of $\left(\frac{\lambda(0)}{\lambda(t)}\right)^2$ from the two fluid model for the BCS approximation, for V_3Si data and related Eliashberg calculations.

$$\begin{cases} \delta\lambda_L(T_c)/\lambda_L(T_c) &= 1 - 16\left(\frac{T_c}{\omega_{\ln}}\right)^2 \ln\left(\frac{\omega_{\ln}}{3.5T_c}\right) \\ \delta\,\lambda_\ell(0)/\lambda_\ell(0) &= 1 + 5\left(\frac{T_c}{\omega_{\ln}}\right)^2 \ln\left(\frac{\omega_{\ln}}{3.8\,T_c}\right) + 0.4\left(\frac{T_c}{\omega_{\ln}}\right) \\ \delta\,\lambda_\ell(T_c)/\lambda_\ell(T_c) &= 1 - 2.5\left(\frac{T_c}{\omega_{\ln}}\right)^2 \ln\left(\frac{\omega_{\ln}}{1.9T_c}\right) \\ \delta\,\xi_0(0)/\xi_0(0) &= 1 + 11\left(\frac{T_c}{\omega_{\ln}}\right)^2 \ln\left(\frac{\omega_{\ln}}{4.2T_c}\right) + 1.5\left(\frac{T_c}{\omega_{\ln}}\right) \\ \delta\,\xi_0(T_c)/\xi_0(T_c) &= 1 + 17\left(\frac{T_c}{\omega_{\ln}}\right)^2 \ln\left(\frac{\omega_{\ln}}{3.4T_c}\right) + 1.5\left(\frac{T_c}{\omega_{\ln}}\right) \end{cases} \tag{4.68}$$

and, defining $y_L = 1/\lambda_L^2$, one finds (Fig. 4.19)

$$\frac{y_L(0)}{T_c|y_L'(T_c)|} = 0.5\left\{1 - 2\frac{T_c}{\omega_{\ln}} - 11\left(\frac{T_c}{\omega_{\ln}}\right)^2 \ln\left(\frac{\omega_{\ln}}{4.5T_c}\right)\right\} \tag{4.69}$$

and (Fig. 4.20)

$$\xi_0(0)/\xi_0(T_c) = 1.33\left\{1 - 0.83\frac{T_c}{\omega_{\ln}} - 0.75\left(\frac{T_c}{\omega_{\ln}}\right)^2 \ln\left(\frac{\omega_{\ln}}{40T_c}\right)\right\} \tag{4.70}$$

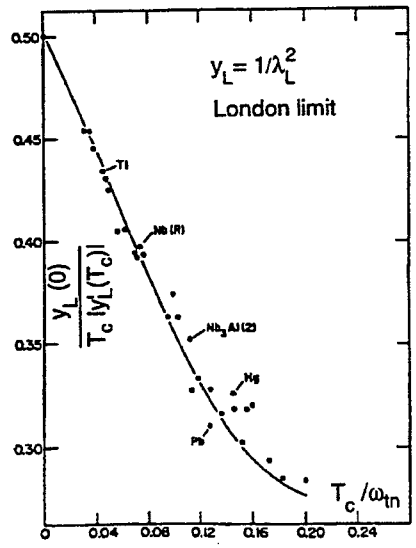

Figure 4.19: See text.

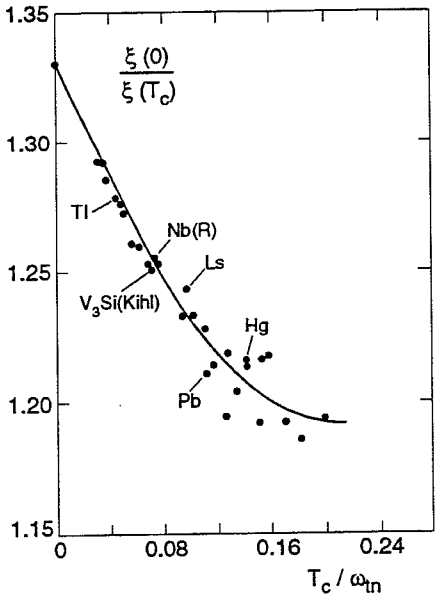

Figure 4.20: See text.

5 SUPERCONDUCTIVITY WITH A VARIABLE GAP

5.1 Bogolioubov equations [24]

In Section 3.3 we saw that the pair interaction $\sum_{k\ell}\ V_{k\ell}\ b_\ell^+\ b_k$ reduces to a single particle potential energy, $\sum_k\ \Delta\ b_k^+$ when calculated in the BCS ground state. This suggests a Hartree Fock approach using a potential of the form

$$V_{HF} = U(a_{k\uparrow}^+\ a_{k\uparrow} + a_{-k\downarrow}^+\ a_{-k\downarrow}) + \Delta\ a_{k\uparrow}^+\ a_{-k\downarrow}^+ + \Delta^*\ a_{k\uparrow}a_{-k\downarrow} \tag{5.1}$$

where allowance has been made for Δ to be complex and where U accounts for renormalization effects which had been neglected in the BCS approximation.

While retaining the basic BCS approximation ($V_{k\ell} = -V$ for $|\xi_k|,\ |\xi_\ell| < \hbar\ \omega_D$), such a generalization would make it possible to take proper account of the effect of the lattice (Bloch functions), of impurities and of a possible external field (electromagnetic or whatever). In order to do so it is convenient to work in the $\{r\}$ rather than $\{k\}$ representation, i.e. to use operators

$$a_{r\alpha} = \sum_k\ e^{ik\cdot r}\ a_{k\alpha} \tag{5.2}$$

where α stands for the spin index.

Then the Hamiltonian can be written

$$\left\{\begin{array}{lcl} H & = & H_0 + H_1 \\ H_0 & = & \int\ dr\ \sum_\alpha\ a_{r\alpha}^+\left(-\frac{\hbar^2\nabla^2}{2m} + V_{\text{ext}} + V_0 - E_F\right)\ a_{r\alpha} \\ H_1 & = & -\frac{V}{2}\ \int\ dr\ \sum_{\alpha\beta}\ a_{r\alpha}^+\ a_{r\beta}^+\ a_{r\beta}\ a_{r\alpha} \end{array}\right. \tag{5.3}$$

where the pair interaction has been split off and will be approximated by a Hartree Fock potential of the form given above.

The procedure consists in minimizing the free energy calculated with $H = H_0 + H_1$ on a set of eigenstates of $H_0 + V_{HF}$ used as trial functions.

Having solved the eigenvalue problem of $H_0 + V_{HF}$ one can write

$$H_0 + V_{HF} = E_{g.s.} + \sum_{n\alpha}\ E_n\ \gamma_{n\alpha}^+\ \gamma_n \tag{5.4}$$

where $E_{g.s.}$ is the ground state energy and $\gamma_{n\alpha}^+$ creates a quasiparticle $(n\alpha)$ of excitation energy E_n. Then, using

$$\left\{\begin{array}{lcl} a_{r\uparrow} & = & \sum_n \gamma_{n\uparrow}\ u_n(r) - \gamma_{n\downarrow}^+\ v_n^*(r) \\ a_{r\downarrow} & = & \sum_n\ \gamma_{n\downarrow}\ u_n(r) + \gamma_{n\uparrow}^+ v_n^*(r) \end{array}\right. \tag{5.5}$$

one can write (Bogolioubov equations)

$$E_n\begin{pmatrix} u_n(r) \\ v_n(r) \end{pmatrix} = \begin{pmatrix} H_0 + U & \Delta \\ \Delta^* & -H_0^* - U \end{pmatrix}\begin{pmatrix} u_n(r) \\ v_n(r) \end{pmatrix} \tag{5.6}$$

Given Δ and U the Bogolioubov equations allow for calculating the eigenfunctions and eigenvalues of $H_0 + V_{HF}$ and the functions u_n and v_n play the rôle of $\cos\ \theta_n$ and $\sin\ \theta_n$

in the simple BCS approach. Then, minimizing the free energy $F = \langle H_0 + H_1 \rangle - TS$ one obtains the self-consistency relations which define U and Δ from u_n and v_n

$$\begin{cases} U &= -V \sum_n \{|u_n(r)|^2 \ f_n + |v_n(r)|^2 (1 - f_n)\} \\ \Delta &= V \ \sum_n \ (1 - 2 \ f_n) \ v_n^*(r) \ u_n(r) \end{cases} \tag{5.7}$$

with, as usual, $f_n = 1/(1 + \exp \ [E_n/k_B T])$.

Taken together, the Bogolioubov equations and the self-consistency equations are the solution of the problem. By construction they reduce to the results of Section 3.3 in the free electron gas case when neglecting renormalization terms.

For $V = 0$ the Bogolioubov equations reduce to

$$\begin{cases} E_n \ u_n(r) = H_0 \ u_n(r) \\ -E_n \ v_n^*(r) = H_0 \ v_n^*(r) \end{cases} \tag{5.8}$$

i.e. u_n and v_n^* are both H_0 eigenstates with respectively positive and negative eigenvalues.

For the normal metal, with a vector potential A,

$$\xi_n \ \phi_n^A(r) = H_0 \ \phi_n^A(r) \tag{5.9}$$

and the solution of the Bogolioubov equations is

$$\begin{cases} u_n(r) = \dfrac{|\xi_n| + \xi_n}{2|\xi_n|} \ \phi_n^A(r) \\ \\ v_n(r) = \dfrac{|\xi_n| - \xi_n}{2 \ |\xi_n|} \ \phi_n^{A*}(r) \\ \\ E_n = |\xi_n| \end{cases} \tag{5.10}$$

5.2 Landau Ginzburg equations [9], [25]

The developments of the preceding section are quite general and introduce a pair potential $\Delta(r)$ which can be expected to generalize the condensation amplitude introduced in (3.48) and to serve as a kind of wave function for the Cooper pairs. This can be made explicit in situations where $\Delta(r)$ becomes small, e.g. when $T \to T_c$ or $H \to H_c$ or in the vicinity of the boundary with a normal conducting or insulating medium. In such cases a perturbative expansion in terms of Δ (rather than A as was done in 3.4) is appropriate. Working on the ϕ_n^A basis

$$\begin{cases} u_n(r) &= \dfrac{|\xi_n| + \xi_n}{2|\xi_n|} \ \phi_n^A(r) + \sum_{n \neq m} \ \tilde{u}_{nm} \ \phi_m^A(r) \\ \\ v_n(r) &= \dfrac{|\xi_n| - \xi_n}{2|\xi_n|} \ \phi_n^{A*}(r) + \sum_{n \neq m} \ \tilde{v}_{nm} \ \phi_m^{A*}(r) \end{cases} \tag{5.11}$$

Inserting these expressions in the Bogolioubov equations yields

$$\begin{cases} \tilde{u}_{nm} &= \dfrac{|\xi_n| - \xi_n}{2|\xi_n|(|\xi_n| - \xi_m)} \displaystyle\int \Delta(r) \ \phi_n^{A*}(r) \ \phi_m^{A*}(r) \ dr \\ \\ \tilde{v}_{nm} &= \dfrac{|\xi_n| + \xi_n}{2|\xi_n|(|\xi_n| + \xi_m)} \displaystyle\int \Delta^*(r) \ \phi_n^A(r) \ \phi_m^A(r) \ dr \end{cases} \tag{5.12}$$

and the pair potential obeys the integral equation

$$\Delta(r) = \int K^A(r,r')\ \Delta(r')dr' \tag{5.13}$$

with

$$K^A(r,r') = V\sum_{nm} \frac{(1-2f(|\xi_n|))}{2|\xi_n|}\ \phi_m^A(r)\ \phi_m^{A*}(r')\ \phi_n^A(r)\ \phi_n^{A*}(r')\left\{\frac{|\xi_n|+\xi_n}{|\xi_n|+\xi_m} + \frac{|\xi_n|-\xi_n}{|\xi_n|-\xi_m}\right\} \tag{5.14}$$

which, after some arithmetics, reduces to

$$K^A(r,r') = \frac{V}{2}\sum_{nm} \frac{\mathrm{th}\frac{\beta\xi_n}{2}\ \mathrm{th}\frac{\beta\xi_m}{2}}{\xi_n+\xi_m}\ \phi_n^{A*}(r')\ \phi_m^{A*}(r')\phi_n^A(r)\ \phi_m^A(r) \tag{5.15}$$

The A dependence of K^A can be made explicit if A can be taken constant over the range of the kernel K^A. Then, as

$$H_0 = \frac{1}{2\,m}\ (p - \frac{e}{c}\ A)^2 + V_0 - E_F \tag{5.16}$$

the wave functions ϕ_n^A are obtained from the Bloch functions ϕ_n^0 by a simple phase rotation corresponding to the constant translation in p by $\frac{e}{c}\ A$

$$\phi_n^A(r) = \phi_n^0(r)\exp\ (i\frac{eA}{\hbar c}\cdot r) \tag{5.17}$$

Moreover, it will be useful to push the perturbative expansion further, which introduces another kernel $K'(r,r',r'',r''')$ whcih we do not calculate explicitely here.

The pair potential can now be expressed as

$$\begin{aligned}\Delta(r) &= \int K(r,r')\Delta(r')\exp(-\frac{2ie}{\hbar c}\ A\cdot[r'-r])dr' \\ &+ \int K'(r,r',r'',r''')\Delta^*(r')\Delta(r'')\Delta(r''')dr'dr''dr'''\end{aligned} \tag{5.18}$$

Assuming that $\tilde{\Delta}(r) \equiv \Delta(r)\exp\ (-\frac{2ie}{\hbar c}\ A\cdot r)$ varies slowly over the range of the kernel one can expand it in Taylor series

$$\tilde{\Delta}(r') = \tilde{\Delta}(r) + (r'-r)\cdot\nabla\tilde{\Delta}(r) + \frac{1}{2}\sum_{ij}(r'-r)_i(r'-r)_j\ \frac{\partial^2\tilde{\Delta}(r)}{\partial r_i\ \partial r_j} \qquad i,j = x,y,z \tag{5.19}$$

and, noting that

$$\nabla\tilde{\Delta}(r) = \exp\ (-\frac{2ie}{\hbar c}\ A.r)\ \frac{i}{\hbar}(p - 2\frac{eA}{c})\Delta(r) \tag{5.20}$$

where $(p - 2\frac{e}{c}\ A)$ corresponds to the current of a charge $2\ e$ (Cooper pair) particle, and after some arithmetics, one finds

$$\Delta(r) = A_0\Delta(r) + B_0|\Delta(r)|^2\Delta(r) + C_0(\nabla - 2\frac{ie}{\hbar c}\ A)^2\Delta(r) \tag{5.21}$$

with

$$\begin{cases} A_0 &= \int K(r,r')dr' \\ B_0 &= \int\ K'(r,r',r'',r''')\ dr'\ dr''\ dr''' \\ C_0 &= \frac{1}{3}\ \int\ K(r,r')(r-r')^2\ dr' \end{cases} \tag{5.22}$$

which can be rewriten as

$$\left\{\frac{(p-2\frac{e}{c}A)^2}{2\,m}+\frac{\hbar^2}{2mC_0}\,(1-A_0-B_0|\Delta(r)|^2)\right\}\Delta(r)=0 \tag{5.23}$$

which looks like a Schrödinger equation for a charge 2 e. The presence of 2 e instead of e is non-trivial, at variance with the possibility of introducing 2 m instead of m at the price of an *ad hoc* renormalization.

Similarly, one finds for the current

$$J(r)\propto\frac{2e\hbar}{m}\,\mathrm{Re}\,(\Delta^*(r)\frac{\nabla}{i}\,\Delta(r))-\frac{(2e)^2}{mc}\,\Delta^*(r)\Delta(r)\;A\;, \tag{5.24}$$

again corresponding to a charge 2 e particle. For $\Delta\,(r)$ to be interpreted as a wave function, it should be properly normalized, which is not the case in the above expressions. Hence the proportionality (rather than equality) sign in Eq. (5.24).

The Ginzburg-Landau equations [9] were postulated in 1950, long before BCS. The interpretation of $\Delta(r)$ as a pair potential and its relation to the energy gap was not clear by then and the wave-function was named the 'order parameter'. The Ginzburg-Landau equations, 5.23 and 5.24, clarify the meaning of the interpretation of $\Delta(r)$ as a pair wave function. For this to be possible, two conditions must be realized: $\Delta\,(r)$ must be small enough and $\Delta\,(r)$ and $A\,(r)$ must vary slowly enough. These restrictions are made clearer in the next section.

5.3 Relevant length scales, types I and II

Explicit calculations of the Ginzburg-Landau kernels $K(r,r')$ and $K'(r,r',r'',r''')$ show that their range is $\approx\xi_0$ in the clean limit. This comes about because the coherence time near T_c is $\hbar/k_B\,T_c$ corresponding to a coherence length

$$\frac{v_F\hbar}{k_BT_c}\approx\xi_0\;. \tag{5.25}$$

The same argument applies to the BCS kernel. However, while the Ginzburg-Landau kernels are density correlation functions (relating $\phi\phi^*$ factors) the BCS kernel is a velocity correlation function (relating $\phi^*\,\nabla\,\phi$ factors). In the dirty limit the density correlation is conserved at each scattering but the velocity correlation is destroyed. As a result the range of the BCS Kernel reduces to ℓ in the dirty limit while that of the Ginzburg Landau kernels is only reduced by a random walk factor $\sim\sqrt{\ell/\xi_0}$ bringing the kernel range to

$$\sqrt{\xi_0\ell} \tag{5.26}$$

(see Table on next page).

In the absence of field, for $A=0$ and $\Delta=$ real constant, Eq. (5.23) reduces to

$$\Delta=A_0\Delta+B_0\Delta^3 \tag{5.27}$$

but from (3.71) it also reduces to

$$\Delta=\mathcal{N}_F\;V\int_0^{\hbar\omega_D}\Delta\frac{d\xi}{\sqrt{\Delta^2+\xi^2}}\;\mathrm{th}\;\frac{\sqrt{\Delta^2+\xi^2}}{2k_BT} \tag{5.28}$$

Relevant length scales

Penetration depths	$\lambda = \int_0^\infty H(x)dx/H(0)$	(4.42)
Kernel K	$J(k) = -(c/4\pi)\ K(k)\ A(k)$	(4.39)
Specular [23]	$\lambda = (2/\pi)\ \int_0^\infty dk/(K(k)+k^2)$	(4.44)
Diffuse [23]	$\lambda = \pi/\int_0^\infty \ln\ (1+K(k)/k^2)dk$	(4.45)
London [6]	$K_L(k) = \lambda_L^{-2} = 4\pi n\ e^2/(m\ c^2)$	(4.46)
Pippard [8]	$K_P = \text{Chambers}\ (K_L,\ \xi_p)$	(4.47)
Gorter-Casimir [7]	$\lambda_L^2(t) = \lambda_L^2\ (1-t^4)^{-1}$	(4.48)
BCS [5]	$K_{BCS} = \text{Chambers}\ (K_L, \xi_0)$	(4.61)
$(h \ll 1)$	$\lambda^2(t) = \lambda_L^2(1+\beta d\Delta/[\Delta d\beta])$	(4.57)
	$\lambda^2(\theta) = \lambda_L^2/(2\theta)\ ,\ \ell \gg \xi_0$	$\theta \ll 1$
	$= (0.64\lambda_L)^2\ \xi_0/(\ell\theta)\ ,\ \ell \ll \xi_0$	
	$\lambda^2(\ell) = (1+\pi\xi_0/[2\ell])$	(4.66)
Coherence lengths		
Definition of $\xi(T)$	$\left\{\left(p-\frac{2eA}{c}\right)^2+\frac{1}{\xi^2(t)}\left(1-0.107\ \frac{\lvert\Delta\rvert^2}{(k_BT_c)^2}/\theta\right)\right\}\Delta = 0$	(5.32)
Cooper pair [14]	$\langle R^2\rangle^{1/2} = \hbar v_F/(\sqrt{3}\ \Delta)$	(3.18)
Pippard [8]	$\xi_p = 0.15\ \hbar v_F/(k_BT_c),\ \ell = \infty$	(4.47)
	$\xi_p^{-1}(\ell) = \xi_p^{-1}\ (\infty) + \ell^{-1}$	(4.49)
BCS [5] $(h \ll 1)$	$\xi_0 = 0.18\ \hbar v_F/(k_B\ T_c)$	(4.63)
	$\xi_0^{-1}(\ell) \simeq \xi_0^{-1}\ (\infty) + \ell^{-1}$	(4.66)
Ginzburg-Landau [9][25] $(\theta \ll 1)$		
	$\sqrt{\theta}\xi(\theta) = 0.74\ \xi_0 \qquad \ell \gg \xi_0$	(5.33)
	$= 0.85\ \sqrt{\xi_0\ell} \qquad \ell \ll \xi_0$	
	$\kappa = 0.96\ \lambda_L/\xi_0\ (\ell=\infty) = 0.75\ \lambda_L/\ell\ (\ell \ll \xi_0)$	(5.37,38)

$t = T/T_c \qquad \theta = 1-t \qquad h = H_{\text{ext}}/H_c\ (\text{type I}) = H_{\text{ext}}/H_{c2}\ (\text{type II})$
Chambers (K,ξ) = Chambers convolution of range ξ (2.37)

By equating the coefficients of Δ and Δ^3 in the two above expressions, it is easy to evaluate A_0 and B_0. In fact, using Eq. (5.25) one finds

$$\begin{aligned} A_0 &= \mathcal{N}_F\, V\, \ln\left(\frac{1.14\hbar\,\omega_D}{k_B T_c}\,\frac{T_c}{T}\right) = 1 + \mathcal{N}_F V\, \ln\left(1+\frac{T_c-T}{T}\right) \\ A_0 &= 1 + \mathcal{N}_F\, V\, \frac{T_c-T}{T_c} \qquad T_c - T \ll T_c \end{aligned} \tag{5.29}$$

For B_0, (5.27) gives $\Delta^2 = (1-A_0)/B_0$ but from Eq. (3.75) $\Delta^2 = (3.2\ k_B\ T_c)^2(1 - T/T_c)$ giving

$$B_0 = -0.107\ N_F\ V/(k_B\ T_c)^2 \tag{5.30}$$

(Note that $0.107 = 7\,\zeta(3)/8\pi^2$ where ζ is the Riemann zeta function).

The calculation of C_0 is less straightforward and depends on the purity of the sample. It gives as a result

$$2\ C_0 = N_F\ V\ 0.107\ \frac{1}{3}\left(\frac{\hbar\ v_F}{k_B\ T_c}\right)^2 = 1.10\ N_F\ V\ \xi_0^2 \tag{5.31}$$

in the pure case. In the dirty limit ξ_0^2 is replaced by $1.454\ \xi_0\ell$.

It is now possible to rewrite Eq. 5.23 as

$$\left\{\left[\frac{\nabla}{i} - 2\frac{e}{\hbar c}\,A\right]^2 + \frac{1}{\xi^2(T)}\left(1 - 0.107\,\frac{T_c}{T_c-T}\,\frac{|\Delta(r)|^2}{(k_B\ T_c)^2}\right)\right\}\Delta(r) = 0 \tag{5.32}$$

with

$$\begin{aligned} \sqrt{\frac{T_c-T}{T_c}}\,\xi(T) &= 0.74\ \xi_0 \text{ in the pure case} \\ &= 0.85\ \sqrt{\xi_0\ell} \text{ in the dirty limit.} \end{aligned} \tag{5.33}$$

The space variation of the pair potential is therefore governed, in the absence of field, by a scale $\xi(T)$ which diverges like $(T_c - T)^{-1/2}$ when T approaches T_c and which is proportional to ξ_0 in the pure case. In the preceding section we noted that the penetration depth was close to

$$\lambda_L(T) = \lambda_L\left(1 + \frac{\beta}{\Delta}\,\frac{d\Delta}{d\beta}\right)^{1/2} \tag{5.34}$$

Near T_c (3.75) $\Delta = 3.2\ k_B\ T_c\sqrt{1-\frac{T}{T_c}}$ and

$$\frac{d\Delta}{\Delta} = -\frac{1}{2}\,\frac{dT}{T_c - T}\,, \qquad \frac{d\beta}{\beta} = -\frac{dT}{T}\,, \tag{5.35}$$

giving

$$\lambda(T) \approx \lambda_L(T) = \lambda_L\sqrt{\frac{T_c}{2(T_c-T)}} \qquad T_c - T \ll T_c \tag{5.36}$$

Both $\xi(T)$ and $\lambda(T)$ diverge the same way when T approaches T_c but their ratio remains constant. This ratio is called the Ginzburg–Landau parameter

$$\kappa = \frac{\lambda(T)}{\xi(T)} = \frac{1}{0.74\sqrt{2}}\,\frac{\lambda_L}{\xi_0} = 0.96\,\frac{\lambda_L}{\xi_o} \tag{5.37}$$

for a pure metal. In the dirty limit

$$\kappa = 0.75 \, \frac{\lambda_L}{\ell} \, . \tag{5.38}$$

The Ginzburg–Landau parameter plays an essential rôle in differentiating between London and Pippard superconductors. Developing the free energy in powers of Δ (assumed $=$ cte, $A = 0$)

$$F = \sum_0^\infty f_n \, \Delta^n \tag{5.39}$$

it should be minimal with respect to variations of Δ

$$\frac{\partial F}{\partial \Delta} \equiv \sum_0^\infty n \, f_n \, \Delta^{n-1} = 0 \tag{5.40}$$

This equation must be identical to 5.21 up to a factor, implying that

$$F = F_0 + \mu \left(\frac{A_0 - 1}{2} \, \Delta^2 + \frac{B_0}{4} \, \Delta^4 + \ldots \right) \tag{5.41}$$

where one can easily verify that $\mu = \frac{2}{V}$. The original Ginzburg-Landau approach was in fact to start from such a postulated expression of the free energy. As $F = F_n$ for $\Delta = 0$

$$F = F_n + N_F \Delta^2 \left(\frac{T_c - T}{T_c} - 0.107 \, \frac{\Delta^2}{2(k_B \, T_c)^2} \right) + \ldots \tag{5.42}$$

$F_n - F$ is minimal for $2\Delta^2 = \frac{2}{0.107}(k_B T_c)^2 \, \frac{T_c - T}{T_c}$ by construction and its minimum value is

$$-\frac{1}{2} \, \frac{N_F}{0.107} \, (k_B \, T_c)^2 \left(\frac{T_c - T}{T_c} \right)^2 \tag{5.43}$$

which, by definition of the thermodynamical critical field must equal $H_c^2/8\pi$

$$H_c(T) = \sqrt{\frac{4\pi N_F}{0.107}} \, (k_B \, T_c) \left(\frac{T_c - T}{T_c} \right) \tag{5.44}$$

which can be rewritten as

$$\lambda(T)\xi(T)H_c(T) = \frac{0.74}{\sqrt{2}} \, \xi_0 \lambda_L \sqrt{\frac{4\pi N_F}{0.107}} \, (k_B \, T_c) \tag{5.45}$$

and replacing ξ_0 and λ_L by their values in (4.46) and (4.63) one obtains useful relations

$$\begin{cases} H_c(T) & = & \dfrac{\phi_0}{2\pi\sqrt{2} \, \xi(T)\lambda(T)} \text{ with } \phi_0 = \dfrac{hc}{2e} \\ \\ \kappa & = & 2\sqrt{2} \, \dfrac{e}{\hbar c} \, H_c(T) \, \lambda^2(T) \end{cases} \tag{5.46}$$

Consider a superconductor which has been driven to its normal conducting state by a strong enough external magnetic field H. By decreasing H one will restore superconductivity. If the whole sample were to switch in a single shot, the transition would occur when $H = H_c(T)$. It may be, however, that some regions switch before H reaches $H_c(T)$

if this is energetically more favourable. At the time of switching Δ is very small and one can use the linear part of (5.23)

$$\frac{1}{2m}\left(p - 2\frac{e}{c}A\right)^2 \Delta = \frac{\hbar^2}{m}\frac{A_0 - 1}{2\,C_0}\,\Delta \tag{5.47}$$

Moreover Δ is small enough for the supercurrents to have a negligible effect, i.e. $H = H_{\text{ext}} = \nabla_\wedge A$. Equation (5.47) is then a Schrödinger equation for a free particle of mass m and charge $2\,e$ in an external field H. The transition will take place when the particle energy, $(\hbar^2/m)\,(A_0 - 1)/(2\,C_0)$, equals the cyclotron energy, $\hbar\omega_c/2 = (e\hbar/mc)\,H$, i.e.

$$e\,H = \hbar\frac{A_0 - 1}{2\,C_0} = \hbar\frac{T_c - T}{T}\,\frac{1}{1.10\xi_0^2} = \hbar\frac{(0.74)^2}{1.10}\,\frac{1}{\xi^2(T)} \tag{5.48}$$

and, using (5.46), $1/\xi^2(T) = 2\sqrt{2}\,(e/\hbar c)\,H_c(T)\kappa$ one obtains

$$H = \frac{\hbar}{e}\,\frac{(0.74)^2}{1.10}\,2\sqrt{2}\,\frac{e}{\hbar c}\,H_c(T)\,\kappa$$

$$H = \kappa\sqrt{2}\,H_c\,(T) \tag{5.49}$$

For $\kappa\sqrt{2} \geq 1$ the transition will occur at a field $H_{c2} = \kappa\sqrt{2}\,H_c(T) > H_c(T)$, called the upper critical field, and the sample will be only partially superconducting until H reaches the lower critical field H_{c1}. The next sections study this transition state in more detail.

5.4 Fluxons

When H reaches $H_{c2} = \kappa\sqrt{2}\,H_c$, the field penetrates in some regions of the sample. What happens in the vicinity of the boundary between the normal conducting (N) and superconducting (S) regions? There will be a loss of condensation energy over a distance $\approx \xi$ but a gain of magnetic energy over a range $\approx \lambda$. For a type II ($\kappa > 1/\sqrt{2}$) superconductor, as considered here, the balance will be positive and the equilibrium state will maximize the total area of the $N-S$ separation for a given volume. For a same penetration over a radius λ, one can imagine having small S-filaments in an N-environment or small N-filaments in a S-environment (Fig. 5.1). The latter solution yields a loss of condensation energy typically $\approx 2\,\kappa$ times smaller than the former and is therefore prefered.

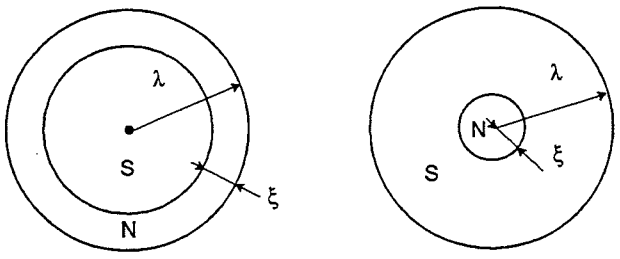

Figure 5.1: See text.

One would then conclude from this simple argument that the field penetrates in the form of a huge number of very tiny filaments. However there is a lower limit to the magnetic flux carried by each single filament which we now examine.

The Bogolioubov equations

$$\begin{cases} E_n\, u_n &= \left(\frac{1}{2m}\left(p-\frac{e}{c}\,A\right)^2+V_0+U-E_F\right) u_n+\Delta\, v_n \\ E_n\, v_n &= \Delta^* u_n-\left(\frac{1}{2m}\left(p+\frac{e}{c}\,A\right)^2+V_0+U-E_F\right) v_n \end{cases} \tag{5.50}$$

should give solutions which should not depend on the choice of gauge, i.e. which should not change when the vector potential A is incremented by a term $\nabla\chi(r)$, a gauge transformation which does not affect $H = \nabla_\wedge A$. For $\Delta = 0$ such a change of gauge changes $p \pm \frac{e}{c}\,A = \frac{\hbar}{i}\nabla \pm \frac{e}{c}\,A$ into

$$\frac{\hbar}{i}\left(\nabla \pm \frac{ie}{\hbar c}\nabla\chi\right) \pm \frac{e}{c}\,A \tag{5.51}$$

and therefore u_n into u_n exp $(i\frac{e}{\hbar c}\chi(r))$ and v_n into v_n exp $(-i\frac{e}{\hbar c}\chi(r))$.

This result remains valid when $\Delta \neq 0$ as long as Δ is changed into Δ exp $(2\frac{ie}{\hbar c}\,\chi(r))$. Namely the wave functions and the pair potential are gauge covariant while the eigenvalues are gauge invariant. However the pair potential must be a single valued function of r, even if $\chi(r)$ is not.

Consider now a filament and a contour C around it, at a distance $\gg \lambda$, such that C is free of magnetic field and of super currents (Fig. 5.2). For some particular gauge $A = \theta = 0$ on C.

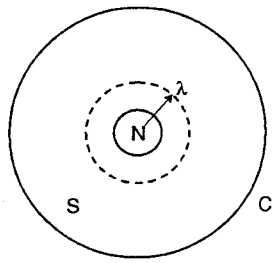

Figure 5.2: See text.

Writing $\Delta = |\Delta|$ exp $(i\theta)$ let

$$\mathcal{I} = \hbar\nabla\theta - 2\frac{e}{c}\,A \tag{5.52}$$

Adding $\nabla\chi$ to A multiplies Δ by exp $(2i\frac{e}{\hbar c}\chi)$ and increments therefore $\nabla\theta$ by $2\frac{e}{\hbar c}\nabla\chi$ leaving $\mathcal{I}$ invariant. Therefore $\int_c \mathcal{I}.d\ell$, which vanishes for the particular gauge $A = \theta = 0$, also vanishes for any other gauge and

$$\frac{\hbar c}{2e}\int_c \nabla\theta\; d\ell = \int_c A\; d\ell\;. \tag{5.53}$$

The integral on the left-hand side is $\frac{\hbar c}{2e}$ times the phase change of Δ after one turn, which must be an integer multiple of 2π. The integral on the right-hand side is the magnetic flux ϕ carried by the filament. Hence

$$\phi = \frac{\hbar c}{2e}\,2n\pi = n\phi_0, \qquad \phi_0 = \frac{hc}{2e}\;. \tag{5.54}$$

The magnetic flux carried by a filament must be an integer multiple of the elementary fluxoid

$$\phi_0 = \frac{hc}{2e} \approx 20.7 \text{ Gauss microns}^2 \ . \tag{5.55}$$

This quantity is large enough to be measurable [26] and the validity of the above result has been confirmed experimentally (see Fig. 5.3)

Filaments which carry a flux ϕ_0 will therefore populate the mixed phase (also called Schubnikov phase from the name of the physicist who discovered its existence in 1936 [27]). They are called fluxons or vortices.

The radial structure of a fluxon is characterized by a normal conducting hard core of radius $\approx \xi$ and a field penetration over a range $\approx \lambda$, the core being surrounded by super currents which shield the outside space from the core field. In the limiting case where $\lambda \gg \xi$ the fluxon energy per unit length reads

$$E = \int dr\ n \frac{mv^2}{2} + \int dr \frac{H^2}{8\pi} \tag{5.56}$$

and, as $\nabla_\wedge H = \frac{4\pi}{c} J$

$$E = \frac{1}{8\pi} \int \{H^2 + \lambda_L^2 \ (\nabla_\wedge H)^2\} \ dr \ . \tag{5.57}$$

Note that minimizing E with respect to H gives the London equation and modelling the hard core with a delta function $\delta(x)\delta(y)$ one obtains

$$E = \left(\frac{\phi_0}{4\pi\lambda_L}\right)^2 \ln\left(\frac{\lambda}{\xi}\right) . \tag{5.58}$$

The quadratic dependence on ϕ_0 shows that when doubling the flux, $\phi_0 \rightarrow 2\phi_0$, it is more economic to have two filaments ($2\ \phi_0^2$) rather than a single filament with twice the flux ($4\phi_0^2$), confirming the nucleation into fluxons.

In the same approximation of infinitely thin cores, the interaction energy between two parallel fluxons distant by r is

$$E_{int} = \frac{\phi_0}{4\pi} \frac{\phi_0}{2\pi\lambda^2} K_0\left(\frac{r}{\lambda}\right) \tag{5.59}$$

which decreases as $\frac{1}{\sqrt{r}} \exp\ (-\frac{r}{\lambda})$ for $r \gg \lambda$.

As it is repulsive, it implies that the fluxons arrange themselves in a triangular lattice, which is the configuration minimizing the interaction energy. This result was predicted by Abrikosov [28] in 1956 before the publication of the BCS theory. Its validity has been confirmed by various experiments such as slow neutron diffraction and, most spectacularly, by decoration experiments (see Figs. 5.4 to 5.6). In cases where κ is close to $1/\sqrt{2}$ nucleation may however occur in a non-uniform manner (but where it occurs it does it in the form of a fluxon lattice, see Figs. 5.7 and 5.8). This is at variance with the situation of type I superconductors where partial penetration may also occur on a macroscopic scale, in particular as a result of geometry, but where nucleation into fluxons does not happen (Figs. 5.9 and 5.10).

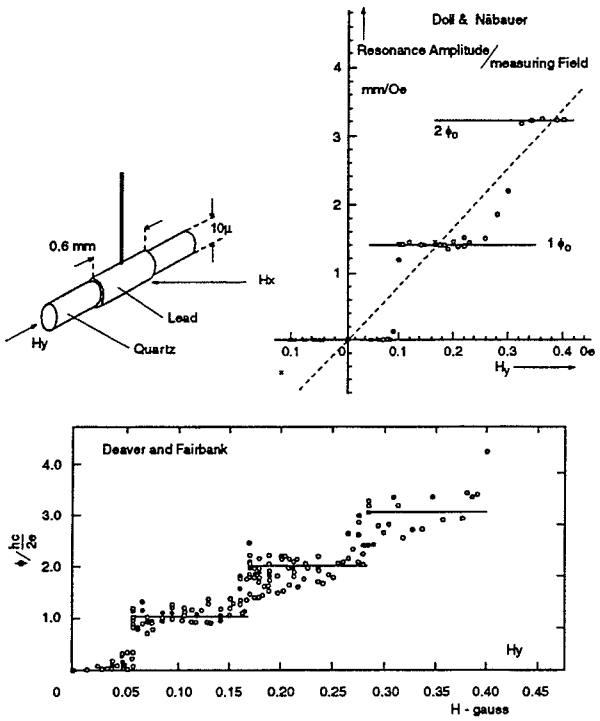

Figure 5.3: Experimental evidence for flux quantization. A small cylinder is cooled below T_c in a field H_y along its axis. The trapped flux is measured by oscillating the hollow cylinder and measuring the induced current. Top left: Doll and Näbauer arrangement, Top right: their data. Bottom: Deaver and Fairbank data. They used a tin cylinder $\phi_{\text{in}} = 13.3$ μm, $\phi_{\text{out}} = 23.3$ μm, length = 8 mm.

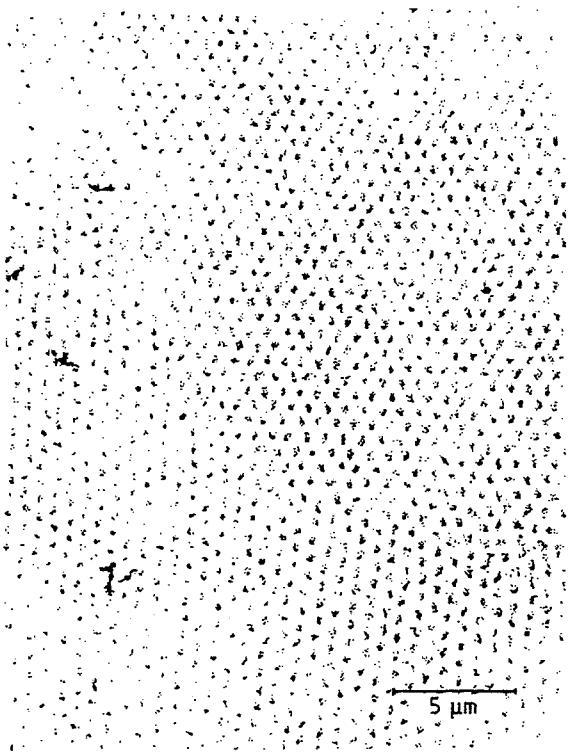

Figure 5.4: Pb In 1.2 K 70 G.

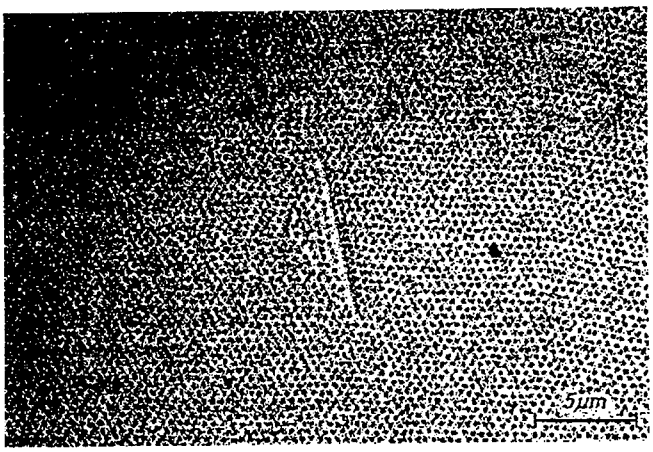

Figure 5.5: Va 1.2 K 130 G.

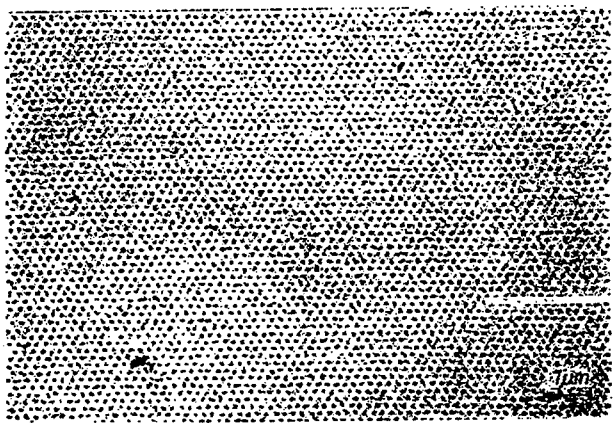

Figure 5.6: Nb 1.2 K 80 G.

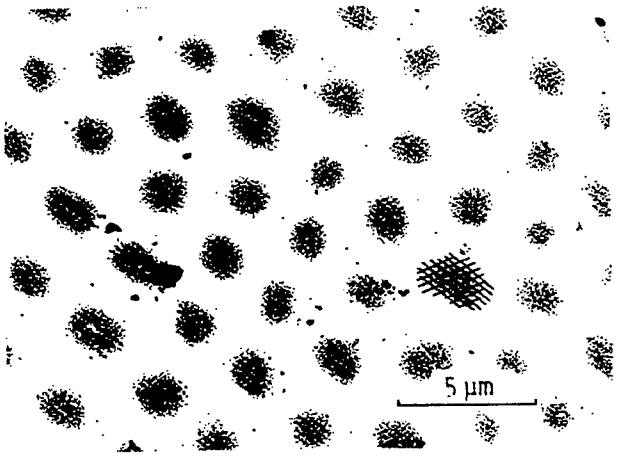

Figure 5.7: Nb.

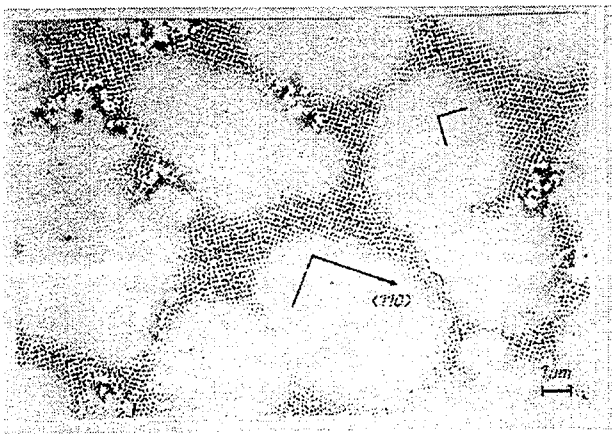

Figure 5.8: Nb.

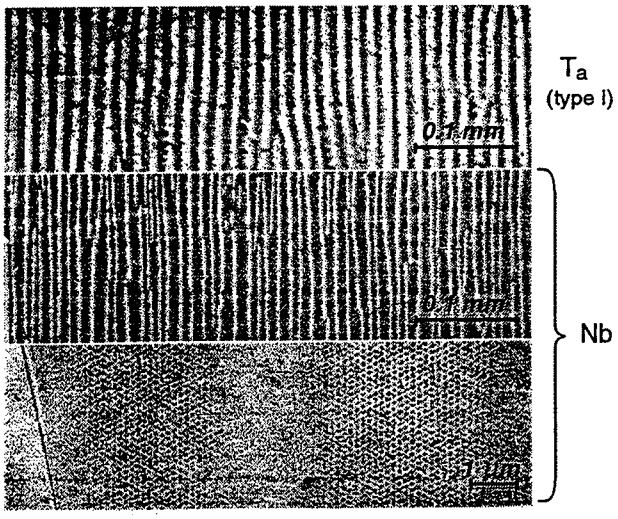

Figure 5.9: Ta versus Nb.

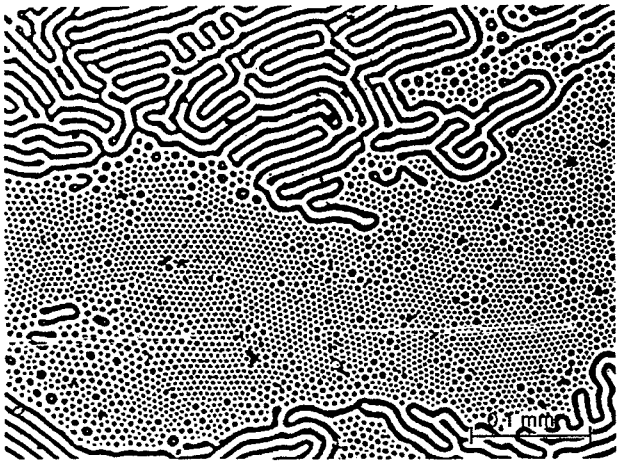

Figure 5.10: Partial penetration in a type I superconductor (Ta).

5.5 Critical fields

From relation (5.46) $\phi_0 = 2\pi\sqrt{2}\, H_c \lambda\xi$ and using (5.49) one has

$$H_{c2} = \kappa\sqrt{2}\, H_c = \frac{\phi_0}{2\pi\xi^2} \tag{5.60}$$

which implies that the fluxon cores are closely packed against each other when the field starts penetrating at $H = H_{c2}$. When H decreases the fluxon lattice gets more diluted and the flux ϕ_0 spreads over a broader area saturating at

$$\approx \pi\lambda^2 \text{ with a core field} \approx \frac{\phi_0}{\pi\lambda^2}\ . \tag{5.61}$$

When H reaches H_{c1} all fluxons have been expelled and the Meissner state is complete. While $\frac{\phi_0}{\pi\lambda^2}$ gives the scale of H_{c1} an exact calculation is not straightforward and requires a model for the fluxon energy.

For a δ-function core Abrikosov finds

$$H_{c1} = \frac{\phi_0}{4\pi\lambda^2}\ (\ln\ \kappa + 0.08) \tag{5.62}$$

In the limit $\lambda \gg \xi,\ (T_c - T) \ll T_c,\ \ell \gg \xi$ one has therefore

$$\begin{cases} H_{c1} & = \dfrac{\phi_0}{4\pi\lambda^2}\ (\ln\ \kappa + 0.08) = \dfrac{H_c}{\sqrt{2}\kappa}(\ln\kappa + 0.08) \\ H_c & = \dfrac{\phi_0}{2\sqrt{2}\pi\lambda\xi} \\ H_{c2} & = \dfrac{\phi_0}{2\pi\xi^2} = H_c\ \sqrt{2}\ \kappa \\ H_{c1}\ H_{c2} & = H_c^2\ (\ln\ \kappa + 0.08) \\ H_{c2}/H_{c1} & = 2\ \kappa^2/(\ln\ \kappa + 0.08) \end{cases} \tag{5.63}$$

More realistic and general expressions are examined below.

In the mixed phase of type II superconductors it is convenient to define an 'induction' B, the macroscopic average of the penetrating field, and a magnetization

$$M = \frac{B - H}{4\pi} \tag{5.64}$$

see Fig. 5.11. The free energy difference between normal and superconducting states is

$$F_n - F_s = \frac{(H - B)^2}{8\pi} \tag{5.65}$$

giving

$$\frac{\partial}{\partial H}\ (F_n - F_s) = \frac{B - H}{4\pi} = M\ . \tag{5.66}$$

As

$$\int_0^{H_{c2}} dH\ \frac{\partial}{\partial H}\ (F_n - F_s) = [F_n - F_s]_0^{H_{c2}} = -\frac{H_c^2}{8\pi} \tag{5.67}$$

$$\int_0^{H_{c2}} M dH = -\frac{H_c^2}{8\pi} , \tag{5.68}$$

independent of κ.

The area under the magnetization curve between 0 and H_{c2} is an invariant and is the same as for a type I superconductor having the same value of H_c.

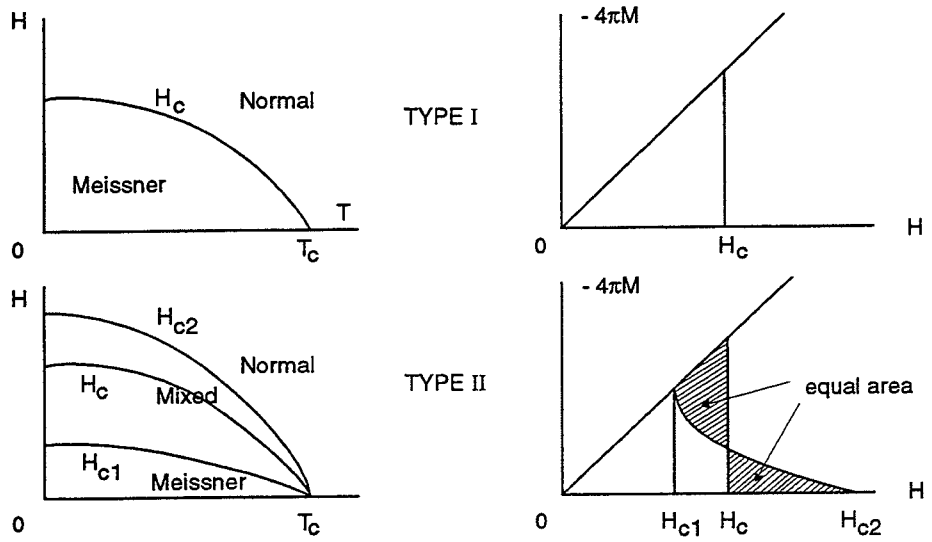

Figure 5.11: See text.

The slope of the magnetization curve near $H = H_{c2}$ can be calculated in the Ginzburg–Landau regime once the structure of the fluxon lattice is known. One finds

$$\left.\frac{\partial M}{\partial H}\right|_{H_{c2}} = \frac{1}{4\pi\beta_A(2\kappa^2 - 1)} \tag{5.69}$$

where the Abrikosov parameter β_A depends only on the structure of the fluxon lattice and is 1.16 for a triangular lattice. When relaxing the conditions under which the Ginzburg–Landau equation is valid it is convenient to introduce two generalized Ginzburg–Landau parameters. One

$$\kappa_1(T) = H_{c2}(T)/\sqrt{2}H_c(T) \tag{5.70}$$

and another $\kappa_2(T)$ such that

$$\left.\frac{\partial M}{\partial H}\right|_{H_{c2}} = \frac{1}{4\pi\beta_A\,(2\kappa_2^2(T) - 1)} . \tag{5.71}$$

Both $\kappa_1(T)$ and $\kappa_2(T)$ tend to κ when $T \to T_c$. In the same spirit one introduces $\kappa_3(T)$ obeying

$$H_{c1}(T) = \frac{H_c(T)}{\sqrt{2}\;\kappa_3(T)} \ln\, \kappa_3(T) . \tag{5.72}$$

The Ginzburg–Landau equations have been generalized to apply to the whole temperature range and to include dirty superconductors [29]. This is straightforward in the vicinity of $H_{c2}(T)$ where the small value of Δ justifies the perturbative treatment and, in the case where $\ell \ll \xi$, the penetration depth increases faster than the coherence length

when impurities are added, allowing for a London treatment when necessary. In the vicinity of H_{c1}, however, the problem is more difficult, as Δ is large. There, progress has required a deeper understanding of the structure of a vertex line and of its free energy. The main results are summarized below in terms of approximate expressions of the generalized Ginzburg–Landau parameters in the clean and dirty limits for $t = \frac{T}{T_c} \ll T_c$ or for $\theta = 1 - t \ll T_c$.

Dirty limit (Figs. 5.12 to 5.14)

	$t \ll 1$	$\theta \ll 1$
κ_1/κ	$1.20(1 - 0.06t^2)$	$1 + 0.13\theta$
κ_1/κ	(all $t's$) $1.25 - 0.30t^2 + 0.05t^4$	
κ_2/κ	$0.69(1 + 10.3t^2)$	$1 - 0.85\theta$
κ_3/κ	$1.53\left(1 - \frac{2}{3}\left[\frac{\pi T}{\Delta}\right]^2\right)^{1/2}$	$1 + 0.032\theta$

(5.73)

Clean limit

κ_1/κ	$1.25\ (1{+}0.65\ t^2 \ln t)$	$1{+}0.41\ \theta$
κ_2/κ	$1.22\ (\ln 1/t)^{1/2}$	$1{+}2.36\ \theta$

More general results are illustrated in Figs. 5.15 to 5.17. Figures 5.18 to 5.22 illustrate results on the structure of an isolated vertex and the dependences on κ of the hard core radius, r_N, and of the field penetration range, r_H, are displayed in Figs. 5.23 and 5.24.

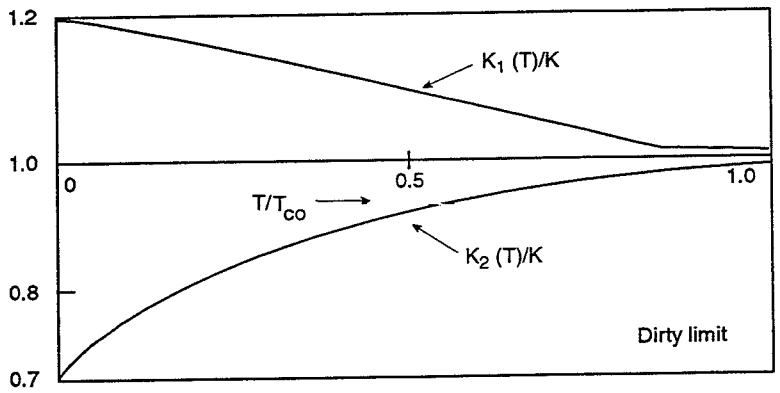

Figure 5.12: Dirty limit.

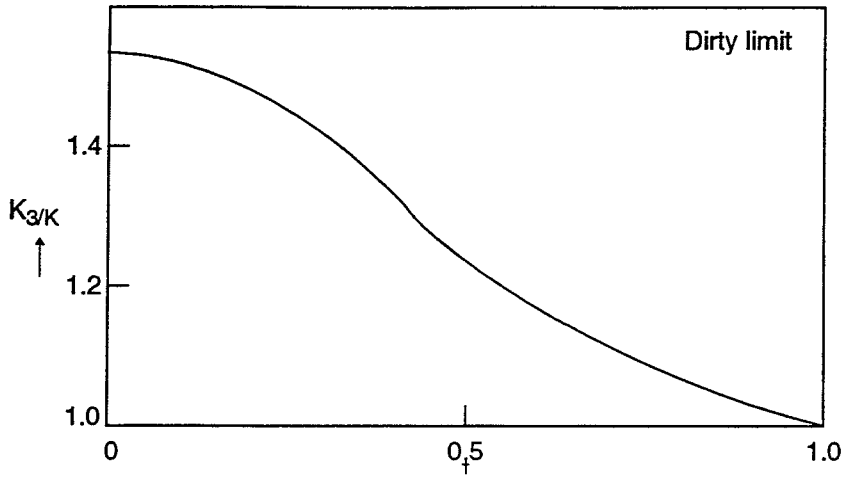

Figure 5.13: Dirty limit.

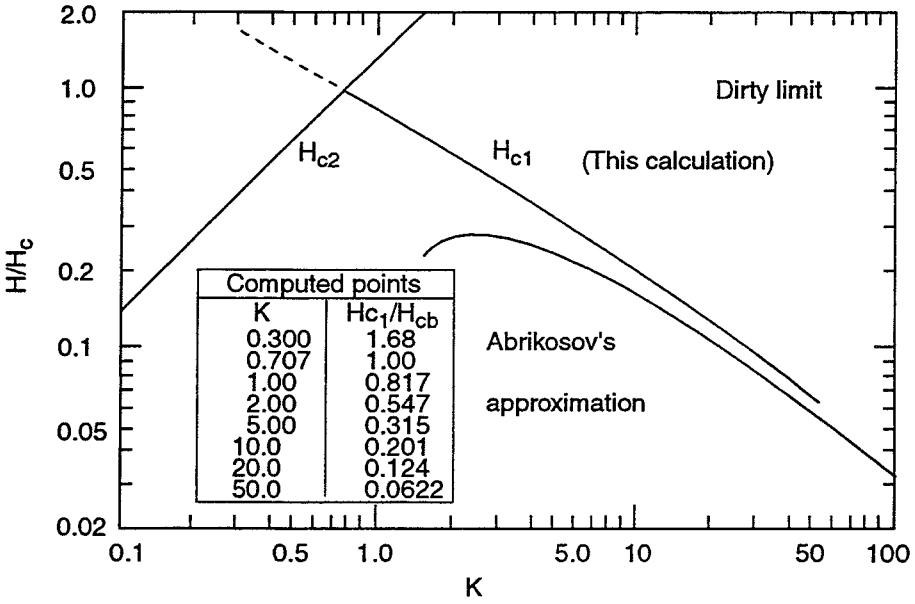

Figure 5.14: Dirty limit.

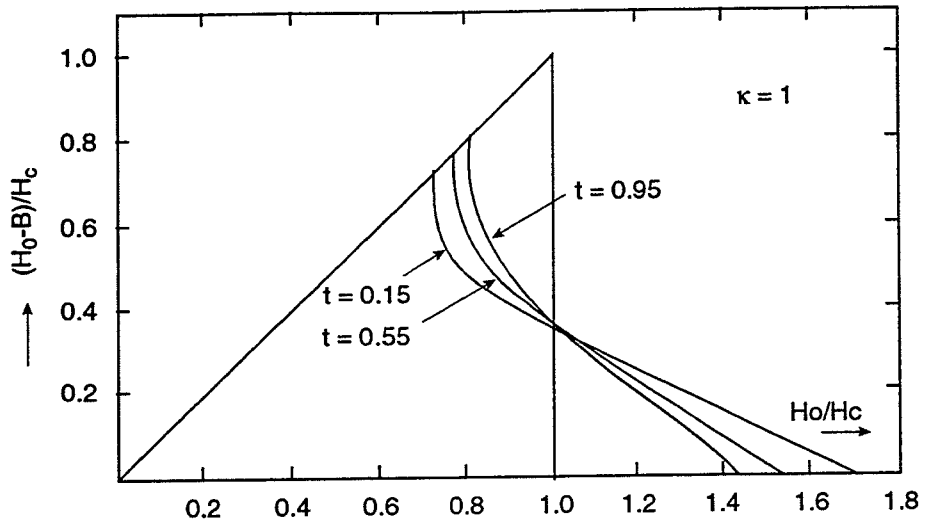

Figure 5.15: See text.

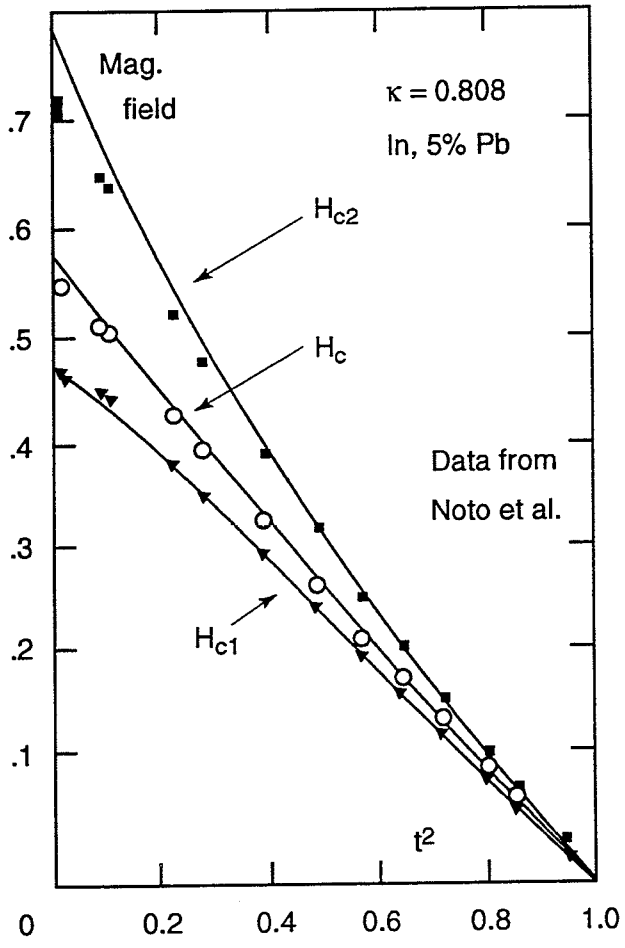

Figure 5.16: See text.

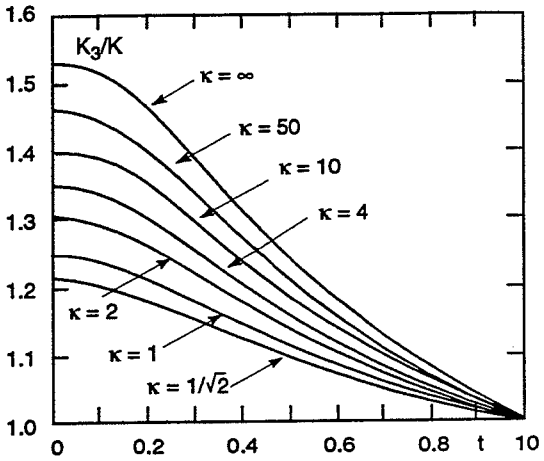

Figure 5.17: See text.

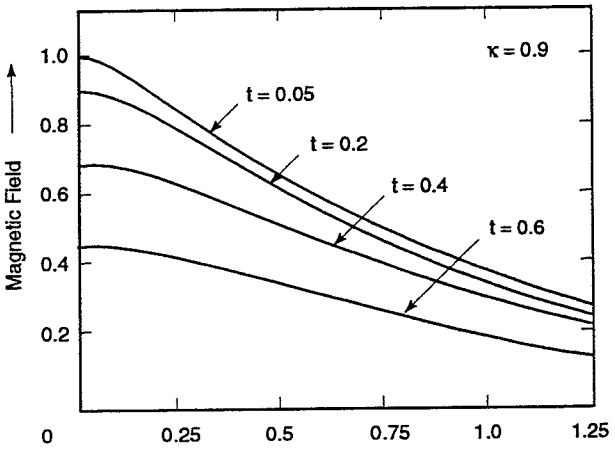

Figure 5.18: See text.

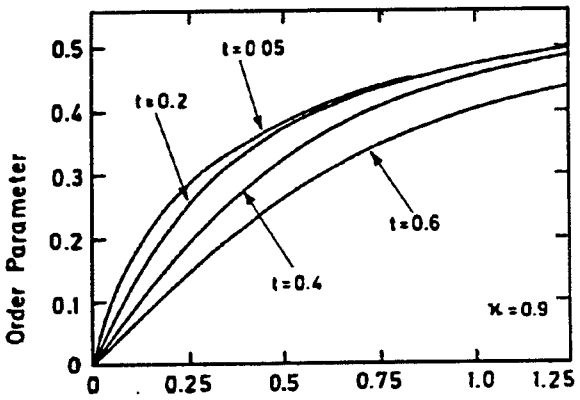

Figure 5.19: See text.

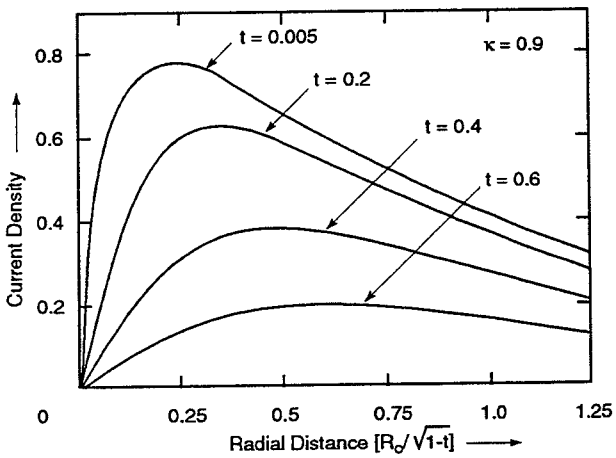

Figure 5.20: See text.

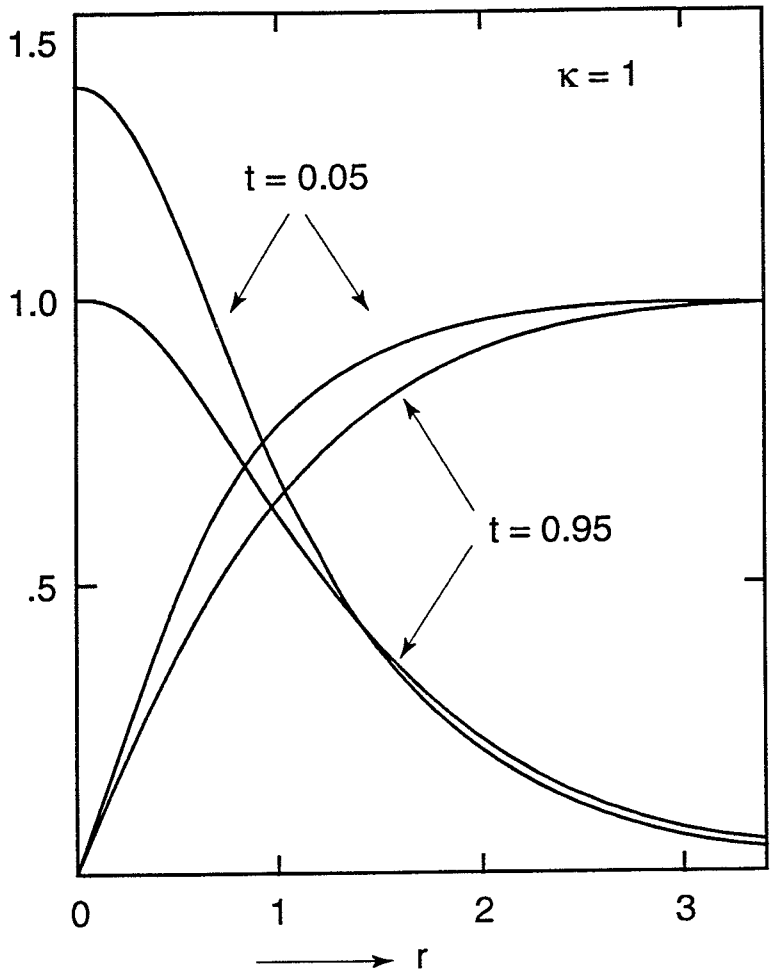

Figure 5.21: See text.

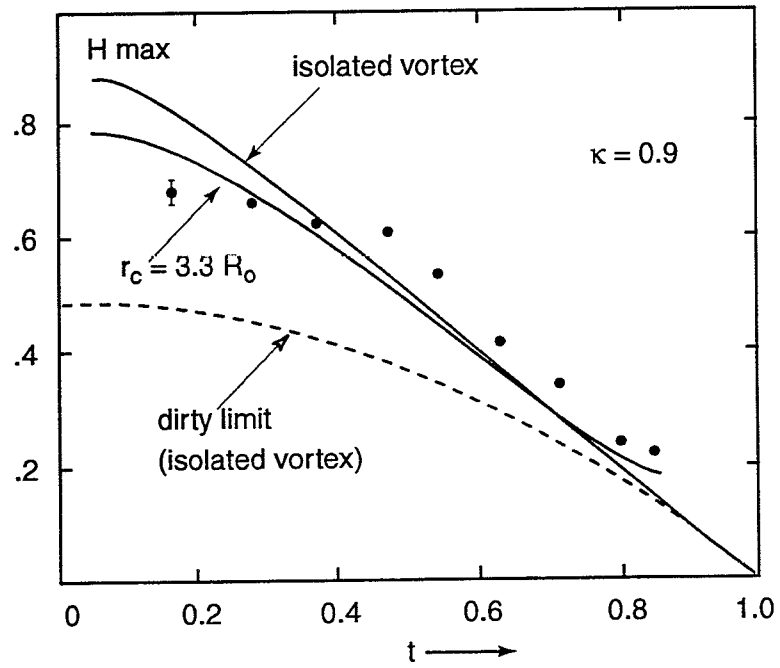

Figure 5.22: See text.

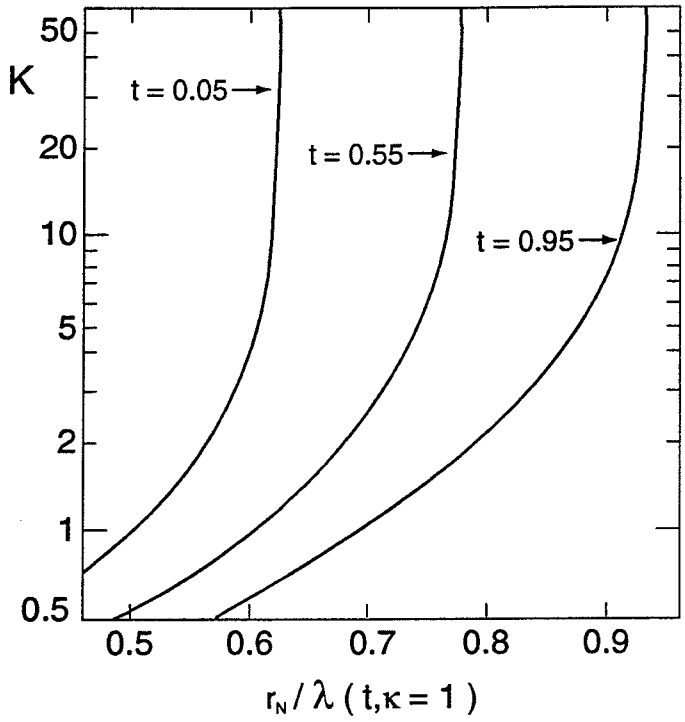

Figure 5.23: See text.

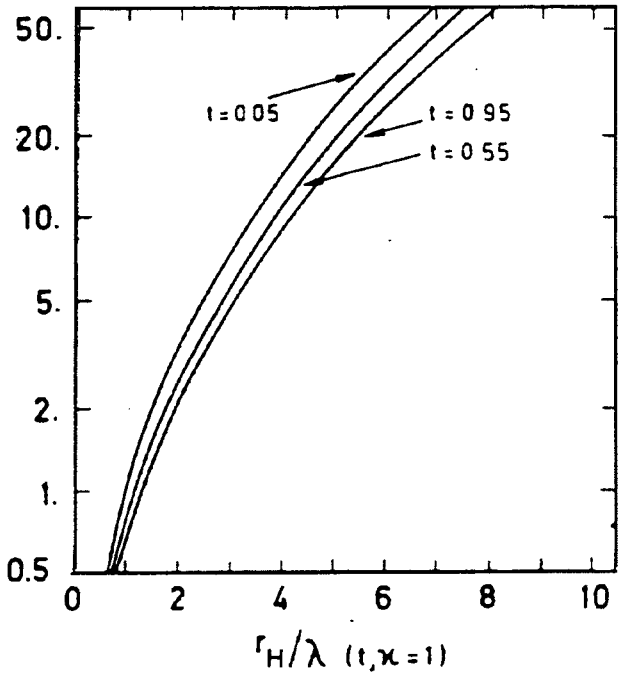

Figure 5.24: See text.

Figures 5.25 and 5.26 display results spanning the whole range of mean-free path. There λ is

$$0.882\ \xi_0/\ell\ ,\ h^* = H_{c2}/(-dH_{c2}/dt)|_{t=1} \tag{5.74}$$

and $\kappa^* = \kappa_1(t)/\kappa_1(1)$

The same authors [29] study spin effects which are usually unimportant. In a normal metal the parameter of relevance is the Pauli paramagnetic susceptibility of the conduction electrons near the Fermi surface

$$\chi = \frac{3N_F\mu^2}{2\ E_F}\ (\mu = \text{ Bohr magneton}). \tag{5.75}$$

Electrons inside the Fermi sphere do not contribute as they cannot align, all states being occupied. In the superconducting metal one introduces the mean-free times for spin-independent and spin-orbit scattering respectively, τ_1 and τ_2, and

$$\tau^{-1} = \tau_1^{-1} + \tau_2^{-1}\ . \tag{5.76}$$

Results and comparisons to experimental data are shown in Figs. 5.27 and 5.28

$$\left(h^* \text{ as in Fig. 5.25}, \alpha = 3/4\tau\ E_F,\ \lambda_{so} = \frac{1}{3\pi T_c\ \tau_2}\right) \tag{5.77}$$

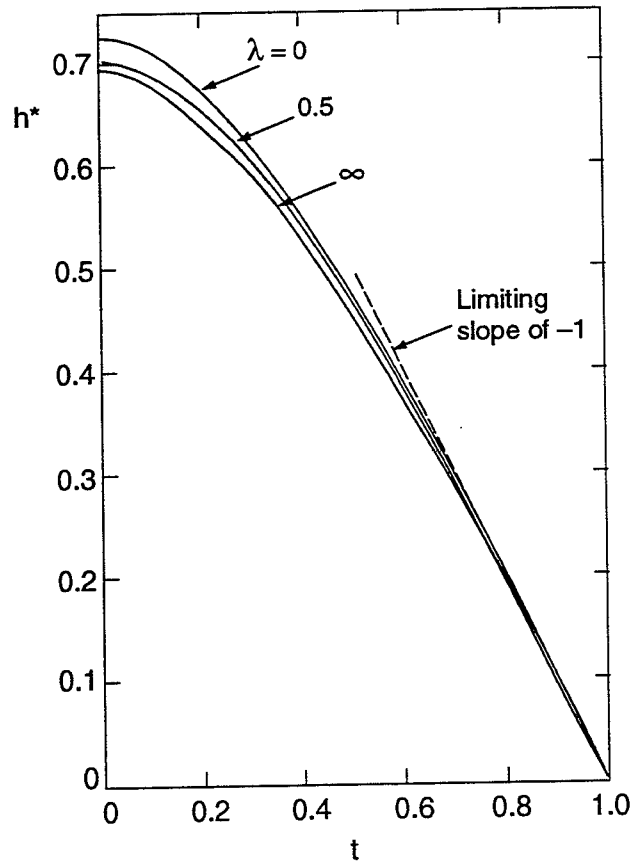

Figure 5.25: See text.

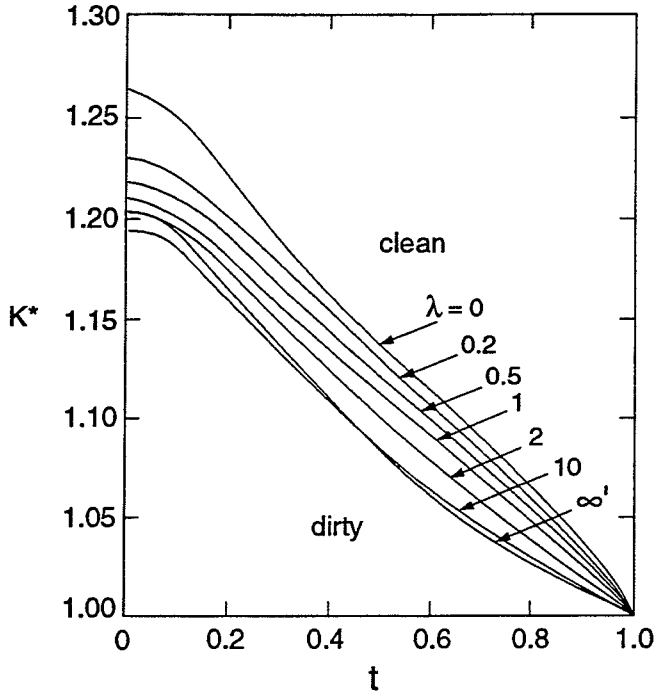

Figure 5.26: See text.

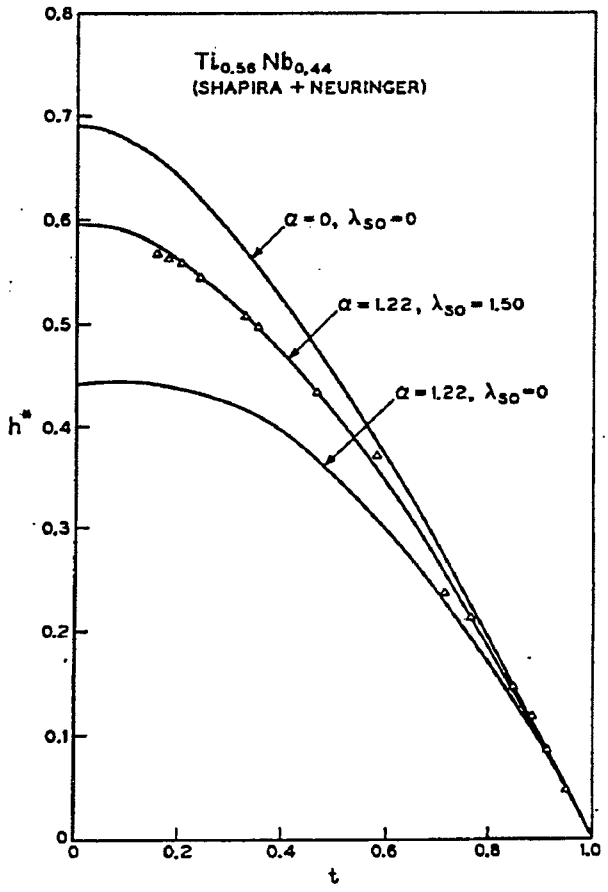

Figure 5.27: See text.

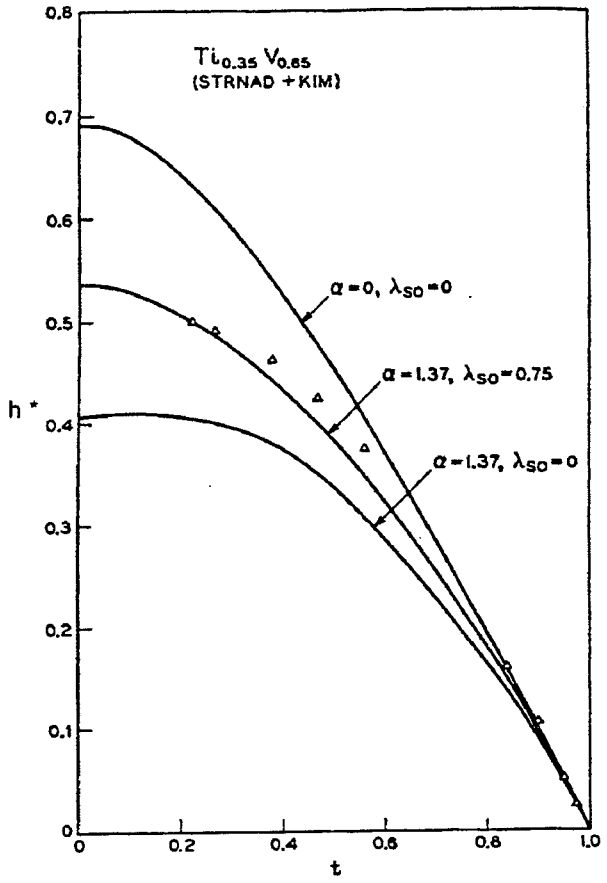

Figure 5.28: See text.

Calculations using the Eliashberg equations have been made, to account for strong coupling. The main effect is a renormalization of various parameters by powers of $(1+\lambda)$. Using a two square-wells approximation as was done in Section 3.7 one finds regularities allowing for general empiric relations. Defining $h_{c2}(T) = H_{c2}(T)/\frac{dH_{c2}}{dt}\ (T_c)$ and $k(T) = \kappa_1(T)/\kappa_1(T_c)$,

$$\begin{cases} h_{c2}^{\text{dirty}}(0) &= 0.69\left(1 - 1.5\frac{T_c}{\omega_{\ln}} + 2.0\left(\frac{T_c}{\omega_{\ln}}\right)^2 \ln\left(\frac{\omega_{\ln}}{0.8\ T_c}\right)\right) \\ h_{c2}^{\text{clean}}(0) &= 0.727\left(1 - 2.7\left(\frac{T_c}{\omega_{\ln}}\right)^2 \ln\left(\frac{\omega_{\ln}}{20\ T_c}\right)\right) \\ h^{\text{dirty}}(0) &= 1.2\left(1 + 2.3\left(\frac{T_c}{\omega_{\ln}}\right)^2 \ln\left(\frac{\omega_{\ln}}{0.2\ T_c}\right)\right) \\ h^{\text{clean}}(0) &= 1.26\left(1 + 12\left(\frac{T_c}{\omega_{\ln}}\right)^2 \ln\left(\frac{\omega_{\ln}}{2\ T_c}\right)\right) \end{cases} \tag{5.78}$$

Also the following universal relation

$$\frac{2\Delta_0}{k_B T_c} = 2.9\ k_{(0)}^{\text{clean}} - 0.13 \tag{5.79}$$

is found to apply.

These results are illustrated in Figs. 5.29 to 5.33.

Figure 5.34 shows the results of a full Eliashberg calculation using $\alpha F^2(\omega)$ from tunneling data and comparing it to the result of a simple renormalization by the proper $(1+\lambda)^x$ factors.

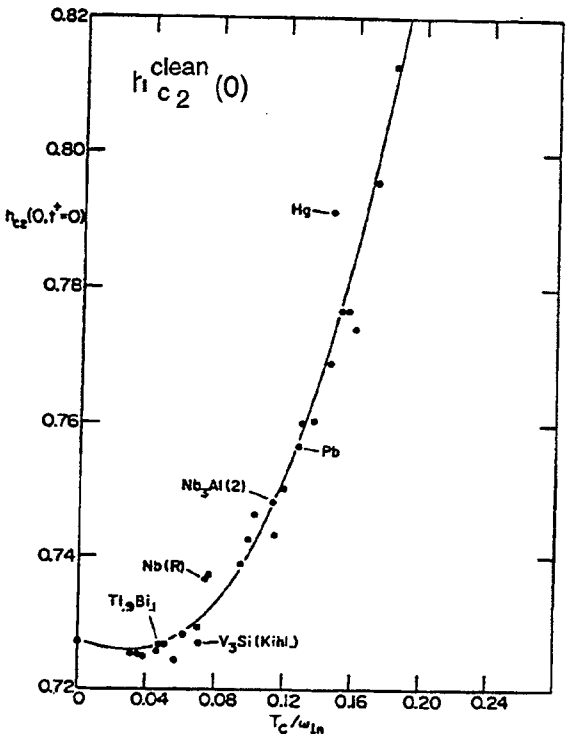

Figure 5.29: See text.

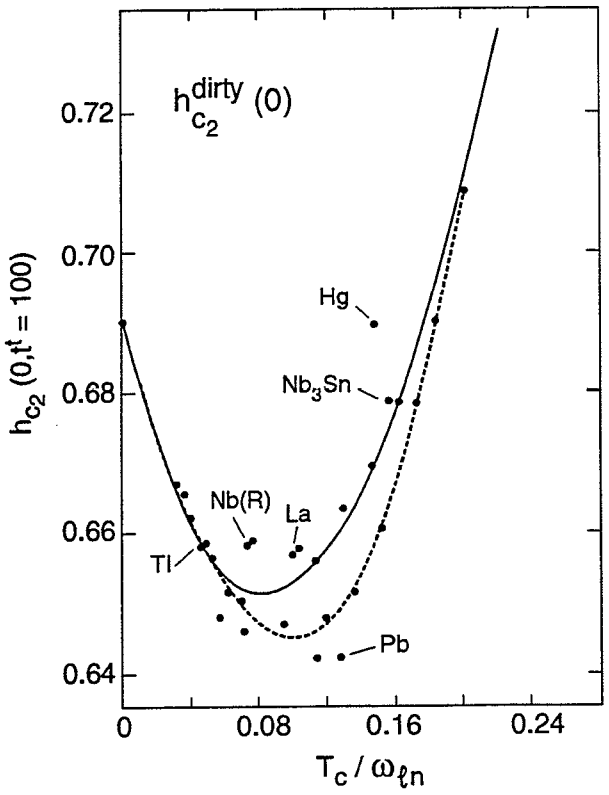

Figure 5.30: See text.

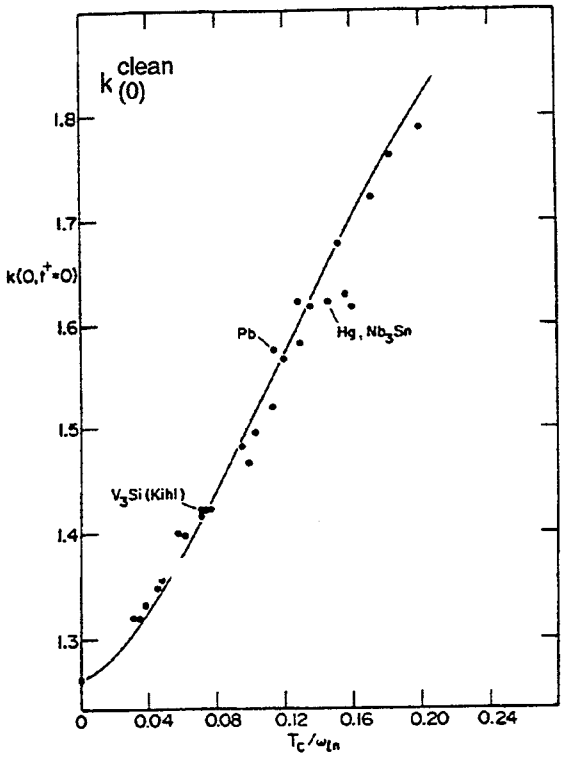

Figure 5.31: See text.

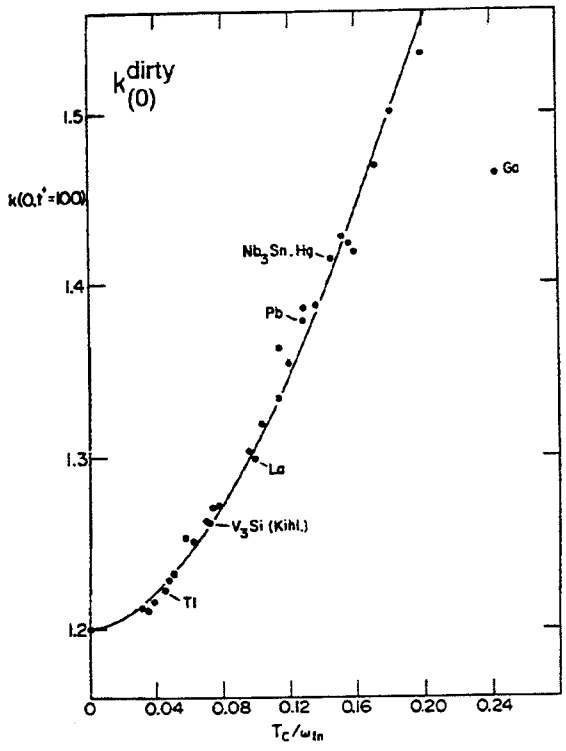

Figure 5.32: See text.

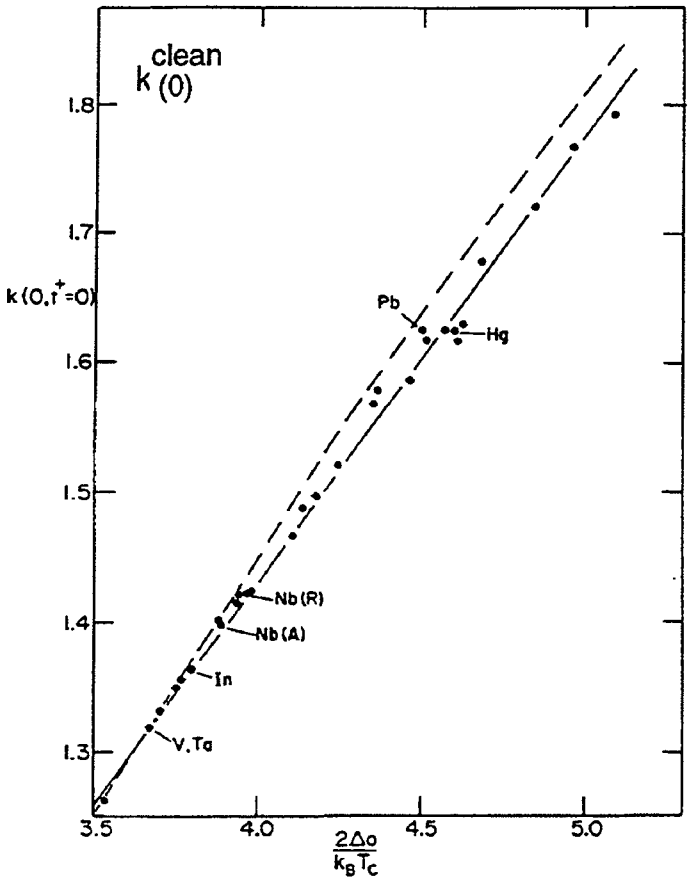

Figure 5.33: Universal relation $k_{(0)}^{\text{clean}}$ *vs* $\frac{2\Delta_0}{k_B T_c}$

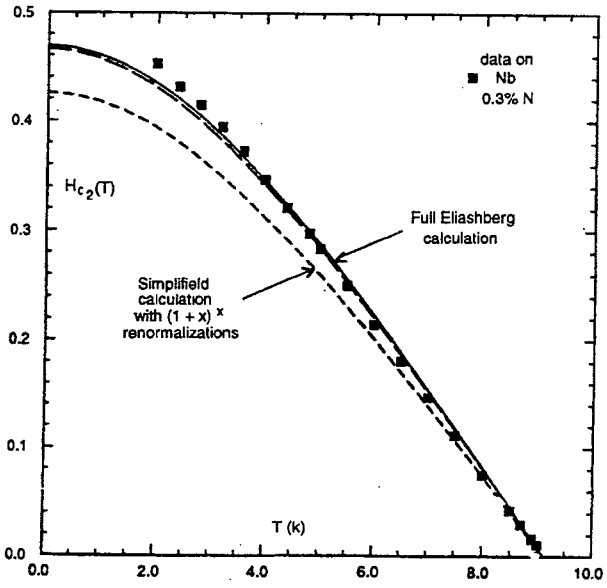

Figure 5.34: See text.

5.6 Fluxon dynamics [30]

In Eq. (4.7) we calculated a critical current density $J_c = \frac{ne}{m}\frac{\Delta}{v_F}$ above which depairing takes place. However this critical depairing current is largely irrelevant. Long before the current density reaches J_c the field produced by the current will exceed H_c (or H_{c1}) and at least part of the conductor will become normal. For example, in the simple case of a cylindrical type I wire carrying a current density J the field at a distance r from the axis (Fig. 5.35) is $\frac{2\pi}{c} Jr$, implying a critical current density

$$J_c = \frac{cH_c}{2\pi R} \qquad R = \text{wire radius} \tag{5.80}$$

much smaller than the depairing critical current calculated in Eq. 4.7 which is in fact (using Eqs. 4.46, 3.81 and 2.22)

$$\frac{1}{2\sqrt{3}}\,\frac{cH_c}{2\pi\lambda_L}\,. \tag{5.81}$$

As soon as $R \gg \lambda_L$ the relevant critical current is that of Eq. 5.80. Actually, when J exceeds J_c the conductor does not switch to the normal state in its totality but only in an outer shell and partially in the inner core.

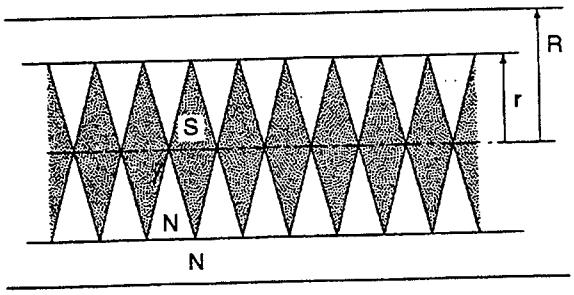

Figure 5.35: Type I cylindrical conductor of radius R. The grey regions are superconducting, the others are normal $H(r) = H_{c1}$.

Such a simple example illustrates the relevance of critical magnefic fields in calculating critical currents and how easily a simple geometry can lead to rather complex configurations.

In order to achieve high critical current densities, one is led in practice to use type II superconductors. The problem is then to understand the fluxon dynamics in the mixed phase in the presence of a transport current. It is essentially governed by two mechanisms: viscous flow and pinning.

A clear qualitative picture of the mechanism of viscous flow is given by Bardeen and Stephen [31].

They consider an isolated fluxon in a superconducting slab where a constant current J_T is established (Fig. 5.36).

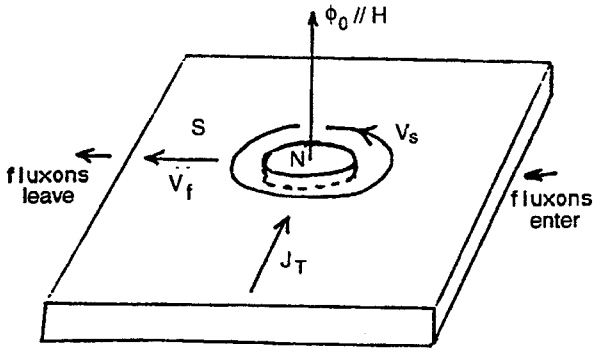

Figure 5.36: Bardeen-Stephen model of viscous flow.

The fluxon is modelled by a cylindrical normal conducting core of radius a, around it there are supercurrents obeying London equation, i.e. the slab is a London superconductor outside the core (and its boundary): if dissipation occurs it can only be inside the core and/or at its boundary. The fluxon may be generated by the transport current itself (H_{c1} is exceeded) but this is irrelevant: the fluxon is sufficiently isolated from other fluxons (in particular a possible gradient in the fluxon lattice density is ignored as it would have no effect). Moreover the transport current is supposed to be small enough to leave the structure of supercurrents unchanged as it sets the fluxon into motion. The Lorentz force exerted on the fluxon is $\frac{1}{c}\ J_T \wedge \phi_0$, inducing a velocity V_f parallel to it (i.e. the Hall effect is neglected). The velocity of the supercurrents, V_s, is accordingly shifted

$$\frac{\partial V_s}{\partial t} = -(V_f.\nabla)V_s = -\nabla\,(V_f \cdot V_s) - \frac{e}{mc}\ V_f \wedge H \tag{5.82}$$

The second term is simply the acceleration produced by a moving field, it is relatively small. The first term however can be rewritten as

$$F = m\frac{\partial V_s}{\partial t} = -e\,\nabla\,\varphi = e\,E \tag{5.83}$$

i.e. it corresponds to an electric field E derived from a scalar potential (Fig. 5.37).

$$\varphi = \frac{m}{e}\ V_f \cdot V_s\ ,\ E = -\nabla\,\varphi \tag{5.84}$$

The field E is uniform inside the core and parallel to the transport current

$$E_{\text{inside}} = \frac{\hbar|V_f|}{2ea^2} \tag{5.85}$$

It is dipolar outside the core and corresponds to a static charge distribution on the core boundary

$$\frac{\hbar V_F}{4\pi e\ a^2}\ \sin\theta \tag{5.86}$$

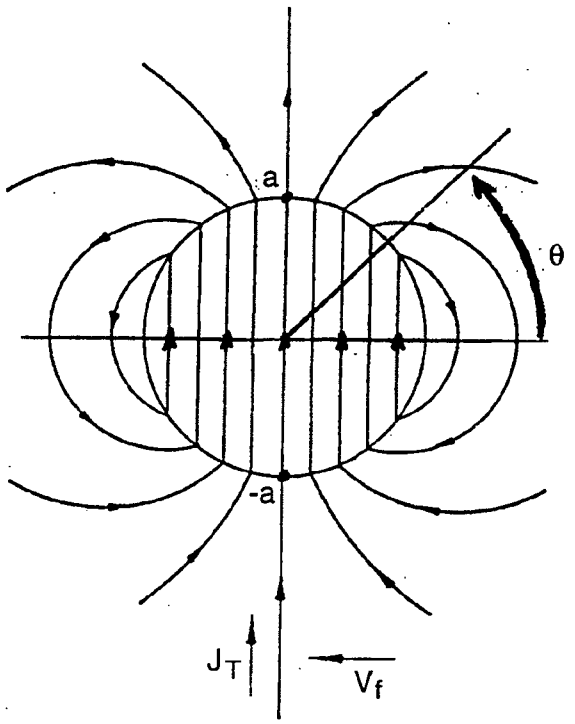

Figure 5.37: Force field in the fluxon core region induced by a fluxon velocity V_f.

As $E = -\nabla(\frac{m}{e}V_f \cdot Vs)$ is porportional to V_f, the energy dissipation is proportional to V_f^2, implying that the presence of E causes the fluxon motion to become viscous and the Lorentz force is opposed by the viscous drag:

$$\frac{1}{c}\, J_{T\wedge}\, \phi_0 = -\eta\, V_f \tag{5.87}$$

The value of the viscosity coefficient η is obtained by calculating the energy dissipation inside the core and on the boundary

$$\eta = \frac{2\pi n a^2}{m}\left(\frac{\hbar}{2a^2}\right)^2 \tau\left(1 + \frac{eH}{\hbar c}a^2\right) \tag{5.88}$$

In Eq. (5.88) τ describes the electron-lattice relaxation time. As soon as $V_f \neq 0$ current flows through the normal core of the fluxon (but when $V_f = 0$ the current avoids the fluxon core). There is therefore a constant depairing and repairing going on in the core and at its boundary, the relevant time constant for this is $\approx V_F^{-1}\xi \approx \frac{\hbar}{\Delta}$, much smaller than $V_f^{-1}a$, as it should for the model to make sense. Finally we note that about half of the dissipation occurs within the normal core and about half in the transition region just outside the core (in real life the sharp core boundary is smeared over $\approx$ one coherence length).

In actual experimental situations one has to face much more complex situations than described by this simple model, in particular because of less ideal geometries, but the relevant underlying physics is all contained in the model.

In order to reach high critical currents in type II superconductors it is therefore essential to stop the fluxons from moving. As long as $V_f = 0$ there is no energy dissipation and the fluxons are bypassed by the supercurrents. This is possible by pinning the fluxon lattice, the second essential topic in the game.

That pinning a fluxon is possible is evident when one considers the effect of a thin cylindrical hole of radius ρ on a parallel fluxon at distance r ($\rho < r < \lambda$) (Fig. 5.38). The r-dependence of the free energy is easily calculated to be of the form

$$\propto \ \ln\ [1 - \frac{\rho^2}{r^2}] + n\ K_0(r) \tag{5.89}$$

where n is the number of fluxons previously trapped in the hole and K_0 is the Hankel function

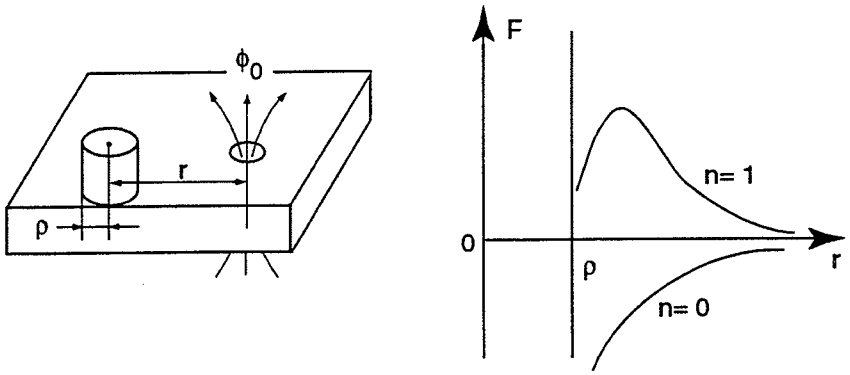

Figure 5.38: See text.

A hole acts as an attractive pin but as soon as it has trapped a fluxon it acts as a repulsive pin. The force needed to free a trapped fluxon is $\approx \frac{1}{2}\ H_c^2\ \xi(T)(n = 0)$ which means a depinning current density (using Eq. 5.87) of the order of the depairing one (Eq. 5.81)

$$J_D \simeq \frac{cH_c^2\xi}{2\phi_0} = \frac{cH_c}{4\sqrt{2}\pi\lambda}\ . \tag{5.90}$$

In practice impurities, defects, surface imperfections, etc... are potential pinning sites. There exists an abondant literature on this subject (see [30] for references). But the interaction between a pin and a single fluxon is not the only ingredient in the understanding of the pinning of a lattice. Indeed, if the lattice is rigid (which it is when it is dense enough) it will feel a zero total pinning force if the pinning sites are randomly distributed. Understanding the pinning of the lattice implies therefore understanding how it can deform. Figure 5.39 gives a good feeling for the complexity of the problem. The string of originally equally spaced weights f_i linked by springs represent the fluxon lattice (even though the forces between fluxons are repulsive). The weights slide on a rail with randomly distributed valleys P_i which represent the pinning centres, more precisely their potentials. Pulling on the string with a force F will cause the string to jump to a new equilibrium position if F exceeds some depinning force F_p. Then, for $F > F_p$, the string is free to move. Of course F mimics the Lorentz force induced by the transport current. This picture gives a feeling for the dependence of F_p on the density of pins, on the depth and breadth of their potentials, on the distance between fluxons and on the elasticity of the fluxon lattice. In three dimensions, the increased degree of freedom in the fluxon lattice movement comes together with additional elasticity parameters (essentially shear and tilt) and with the possibility to bend the fluxons (depending on the line tension). To first order in the fluxon displacements (i labels the fluxons)

$$u_i(z) = r_i(z) - R_i = (u_{xi},\ u_{yi},\ 0)$$

from their ideal positions $R_i = (X_i,\ Y_i,\ z)$, the elastic energy reads

$$F_{\text{elastic}} = \frac{1}{2}\int_{BZ} \frac{d^3k}{(2\pi)^3}\ u_\alpha(k)\ \phi_{\alpha\beta}(k)\ u^*_\beta(k) \tag{5.91}$$

where

- $u(k) = \frac{\varphi_0}{B}\ \sum_i \int\ dz\ u_i(z)\ e^{-ikR_i}$
- $\alpha,\ \beta = x,\ y$
- the integral is on the first Brillouin zone of the reciprocal fluxon lattice
- $\Phi_{xy} = \Phi_{yx} = (C_{11} - C_{66})K_xK_y$

  $\Phi_{xx} = C_{11}\ K_x^2 + C_{66}\ K_y^2 + C_{44}\ K_z^2 + \alpha_L(K)$

  $\Phi_{yy} = C_{66}\ K_x^2 + C_{11}\ K_y^2 + C_{44}\ K_z^2 + \alpha_L(K)$

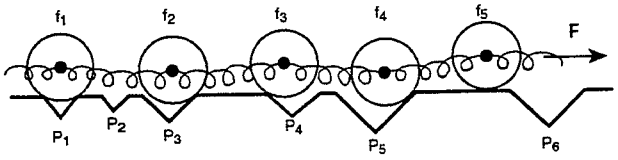

Figure 5.39: See text.

Here C_{11}, C_{66} and C_{44} are the elastic moduli for uniaxial compression, shear and tilt respectively. $\alpha_L(K)$ is the so-called Labusch parameter [32] which describes the elastic interaction of the fluxon lattice with the pinning potential.

The literature is full of calculations of the depinning force (per unit volume) F_P, all of them being approximate and rarely much more illuminating than Fig. 5.39 is. Returning to Eq. 5.87 one sees that the fluxon lattice does not move until the transport current reaches the critical value (see Fig. 5.40)

$$J_c = \frac{c\ F_p}{n\ \phi_0} \tag{5.92}$$

where n is the fluxon density per unit area, F_p the depinning force per unit volume and J_c the current density. When the transport current J_T exceeds J_c the fluxon lattice is set in motion and its viscous flow is governed by the viscosity coefficient η (Eq. 5.88). Using Eqs. 2.26 and 5.63 we can rewrite

$$\eta = \sigma_n\ H_{c2}\ \phi_0/c^2\ (1 + \frac{1}{2}\ \frac{H}{H_{c2}}) \tag{5.93}$$

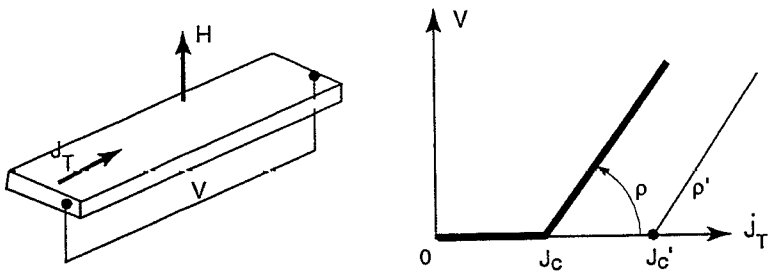

Figure 5.40: See text.

When measuring the voltage-current curve one finds a resistivity ρ such that

$$\text{Power} = \rho\, J_T^2 = n\, \eta\, V_f^2 \tag{5.94}$$

and using $V_f = J_T \phi_0/(\eta c)$ from Eq. 5.87

$$\sigma = \frac{1}{\rho} = \frac{\eta\, c^2}{n\, \phi_0^2} \tag{5.95}$$

and replacing η by its expression (5.93) and $n\phi_0$ by H one finds

$$\begin{cases} \dfrac{\sigma}{\sigma_n} &= \dfrac{H_{c2}}{H}\,(1 + \dfrac{1}{2}\,\dfrac{H}{H_{c2}}) \\ \dfrac{\rho}{\rho_n} &= \dfrac{H}{H_{c2}}/(1 + \dfrac{1}{2}\,\dfrac{H}{H_{c2}}) \end{cases} \tag{5.96}$$

Namely when changing J_c by changing F_p one maintains the same universal relation Eq. (5.96) between ρ/ρ_n and H/H_{c2} (see Fig. 5.41)

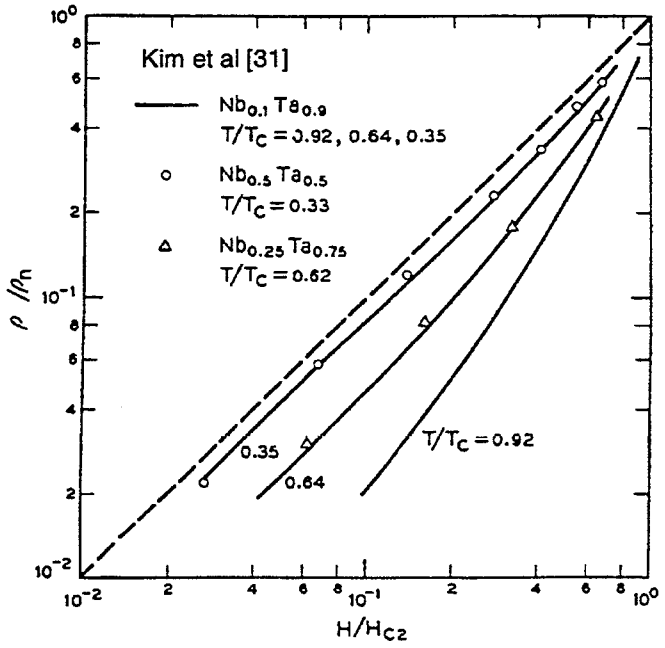

Figure 5.41: See text.

Moreover, as η and ρ depend essentially on H_{c2} (Eq. 5.93), changes in the pinning which do not affect H_{c2} significantly will result in large changes in J_c but modest changes in ρ (Fig. 5.42).

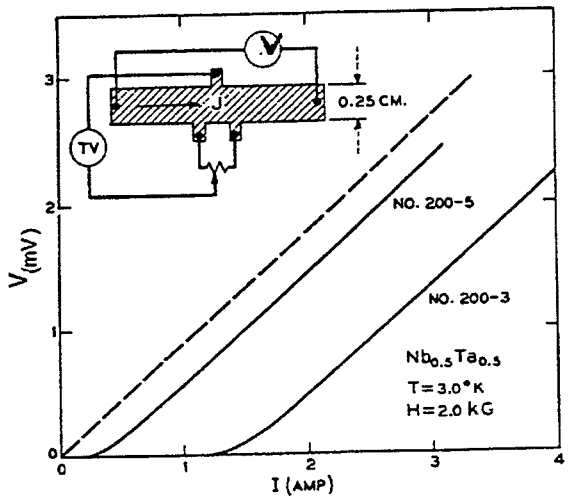

Figure 5.42: Pioneer data of Strnad et al. (PRL13 (1964)794) V vs. I for two NbTa samples containing different amounts of defects.

The approximate relation $\rho/\rho_n \simeq H/H_{c2}$ corresponds to the fact that the dissipation is associated with the normal cores which indeed occupy a fraction $\approx H/H_{c2}$ of the conductor area.

In the neighbourhood of the transition the sharp corner depicted in Fig. 5.40 is rounded by a number of effects. The most important is related to thermally induced transitions and is named flux creep. It becomes particularly important for high T_c superconductors but its study goes beyond the scope of these lectures.

For geometries more general than the slab geometry considered above the situation is still governed by the critical state Eq. 5.92

$$BJ_c = c\,F_p \tag{5.97}$$

Here $B = n\,\phi_0$ gives the average local field inside the conductor. Equation (5.97) is written for currents normal to the field (otherwise it would read $B_\wedge Jc = cFp$).

When currents and/or fields are changed shielding currents adapt to maintain the Meissner state until they reach J_c defined by (5.97). At which point fluxons nucleate on the conductor surface and migrate inside as J is further increased. When the trend is reversed the pinned fluxons will not move until J reaches $-Jc$, implying an hysteresis effect directly porportional to the critical current. This simple description is refered to as the Bean model [33].

Figure 5.43 is a standard illustration.

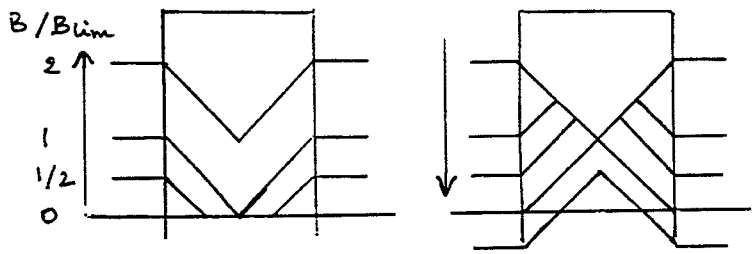

Figure 5.43: B penetration in a slab.

Before closing this section a few words on microwaves are in order. Keeping the simple geometry of Fig. 5.40, one replaces the transport current by the magnetic component of an electromagnetic wave incident on the sample surface. The external field is large enough to penetrate the sample in the form of fluxons while the RF field is supposed to be $\ll H_{c1}$.

Consider first the case of perfect pinning. Here, contrary to the DC case, one expects dissipation from the normal fluxon cores (even though they do not move).

The surface resistance will have the form

$$R_s = R_n \frac{H}{H_{c2}} f(\omega) \tag{5.98}$$

where H/H_{c2} is the fraction of the sample area occupied by normal fluxon cores and where $f(\omega)$ is the frequency dependence calculated in 4.3 for quasi particles (see Fig. 5.44). If instead the fluxons are perfectly free to move one expects R_s to stay at the DC value when ω is increased, i.e.

$$R_s = R_n \frac{H}{H_{c2}} \tag{5.99}$$

(see Fig. 5.45). Inbetween these extreme cases one expects a transition of the form [34]

$$R_s = R_n \frac{H}{H_{c2}} \frac{\omega^2}{\omega^2 + \omega_0^2} \tag{5.100}$$

with

$$\omega_0 \propto \frac{J_c}{\eta} \tag{5.101}$$

where η is the viscosity coefficient (Eq. 5.888) and J_c the critical current (Eq. 5.92). Such transitions have been observed (Fig 5.46)

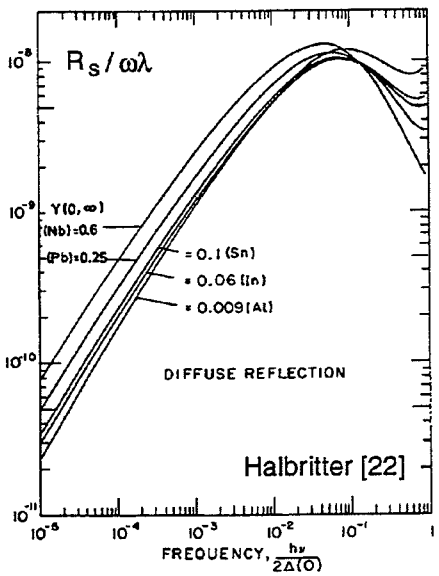

Figure 5.44: Frequency dependence of the surface resistance of quasi-particles.

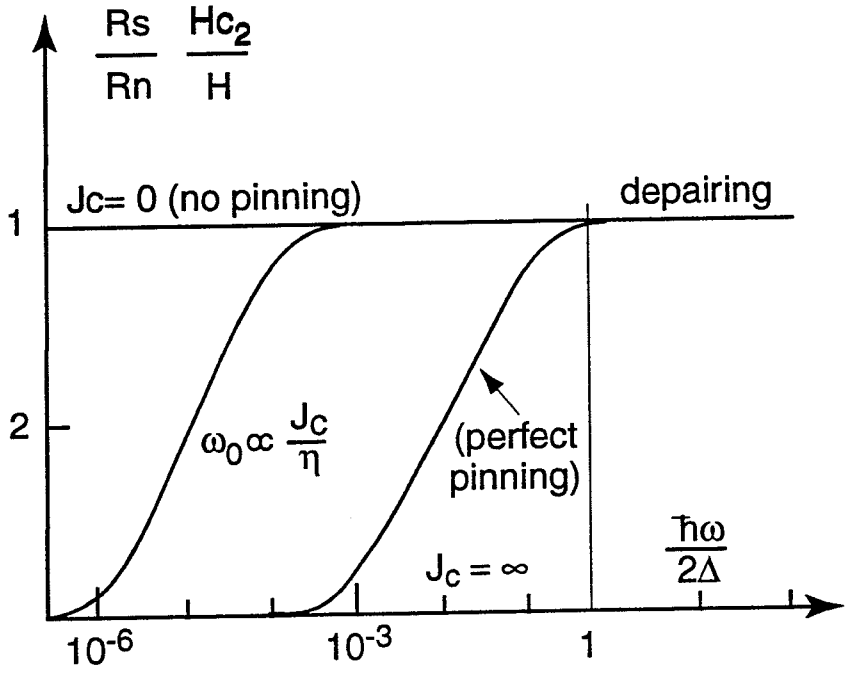

Figure 5.45: Schematic dependence of $\frac{R_s}{R_n}\ \frac{H_{c2}}{H}$ on $\frac{\hbar\omega}{2\Delta}$.

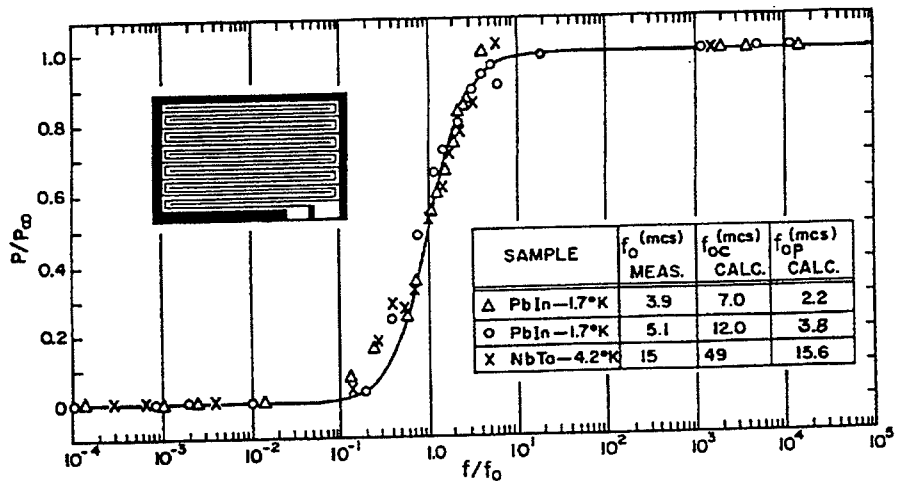

Figure 5.46: Low frequency transitions (Ref. [34])

5.7 Junctions, Josephson effects

This section deals with junctions of the MIM' type where M and M' are metals, either in the normal state (N, N') or in the superconducting state (S, S') and I is a thin (10 to 50 Å) layer of insulator (usually an oxide of M or M'). The current I flowing through a junction in response to an applied voltage V is expected to be proportional to

$$\int \rho'(E-V)\ \rho(E)\{f(E-V)-f(E)\}\ dE \tag{5.102}$$

where ρ and ρ' are the densities of states in M and M' and f the usual Fermi function. As illustrated in Fig. 5.47 different types of V-I characteristics are expected in the NIN', NIS' and SIS' cases.

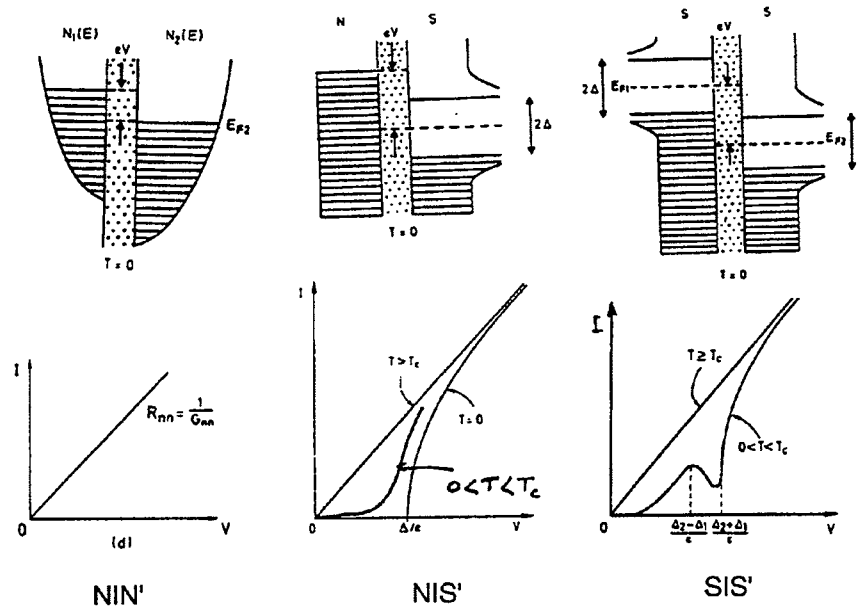

Figure 5.47: See text.

Early experiments [35] have shown that quasi-particle tunneling through the insulating barrier was indeed proceding as expected from Eq. 5.101 (Figs. 5.48 to 5.50). For $T = 0$, in the SIN' case, Eq. (5.101) reduces to $\frac{dI}{dV} = 0$ for $V < \Delta$ and $\frac{dI}{dV} \propto \rho(E)$ for $V > \Delta$ (see Fig. 5.48). More generally V versus I curves provide a way to measure accurately the gap $\Delta(T)$ and the quasi-particle density of states, ρ.

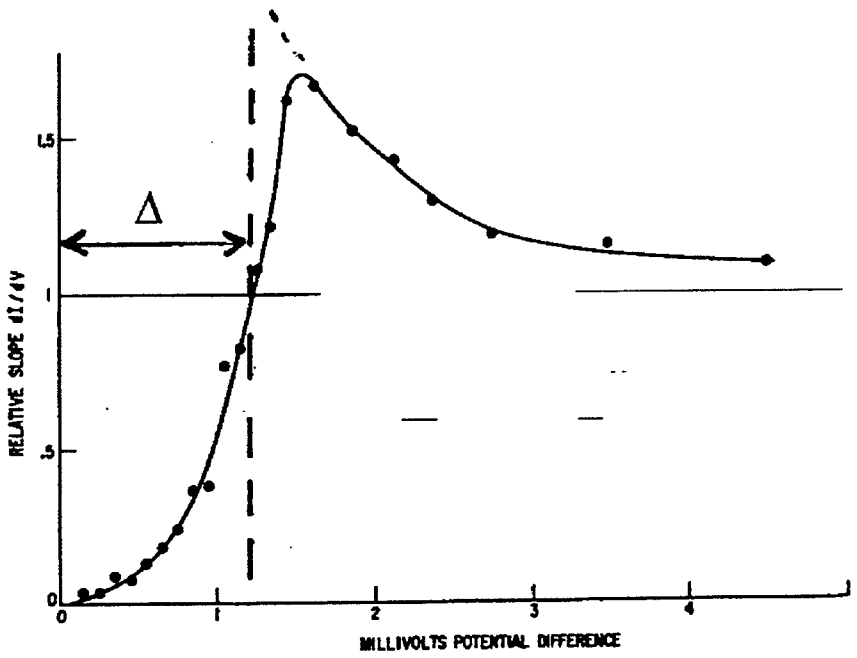

Figure 5.48: Al/Pb.

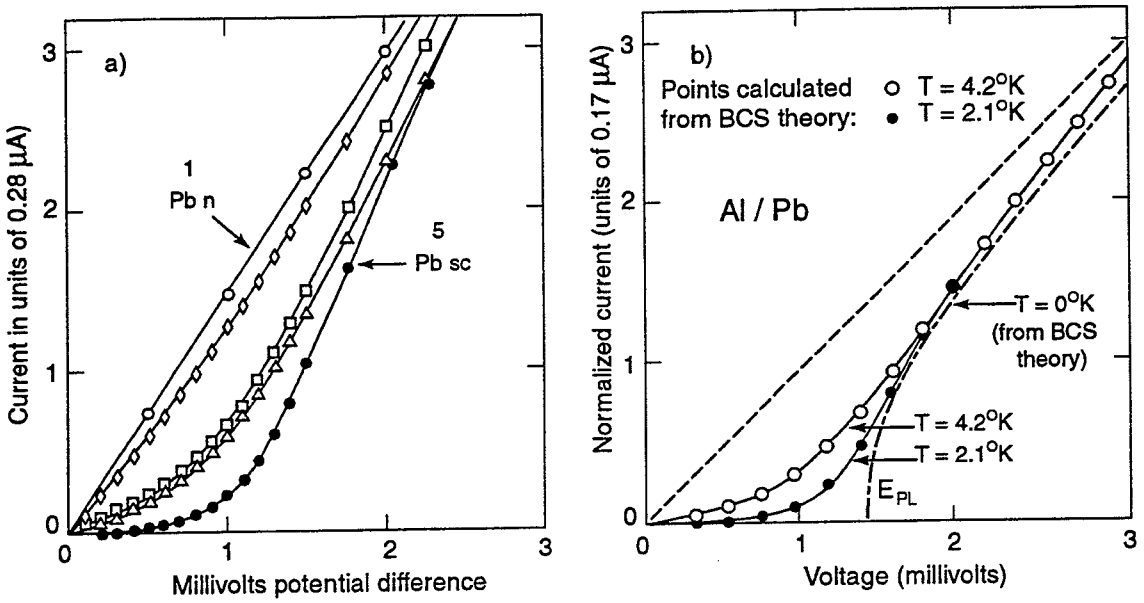

Figure 5.49: SIN'.

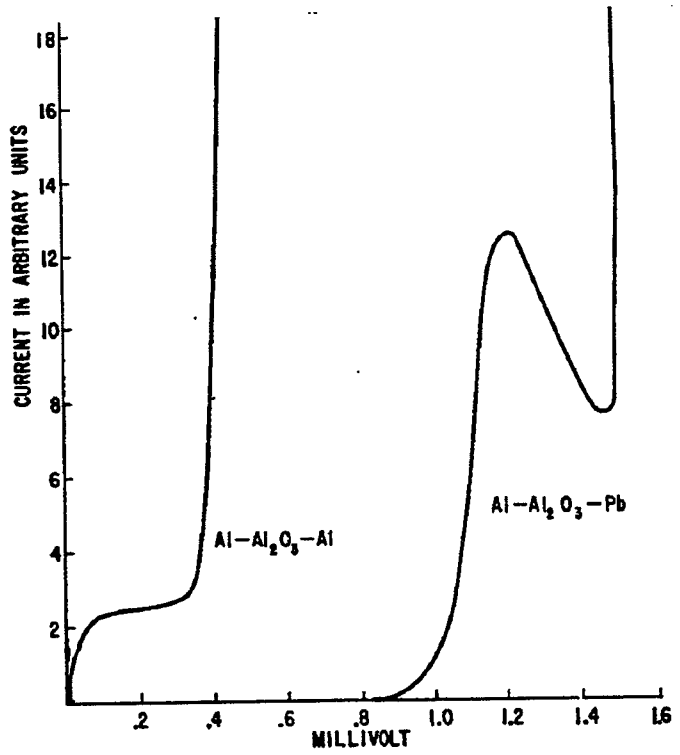

Figure 5.50: SIS'.

With improving experimental accuracy finer structure can be observed which is related to $\alpha^2 F(\omega)$ and allows for it to be measured [36]. This was already mentioned in Section 3.7. Pioneer data are illustrated below (Figs. 5.51 and 5.52).

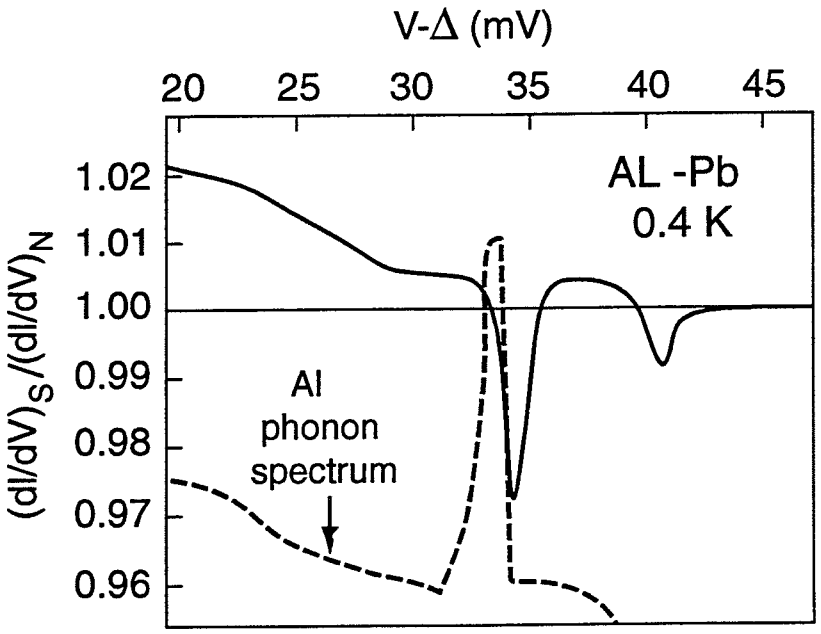

Figure 5.51: I'_s/I'_N *vs* V compared to the phonon spectrum.

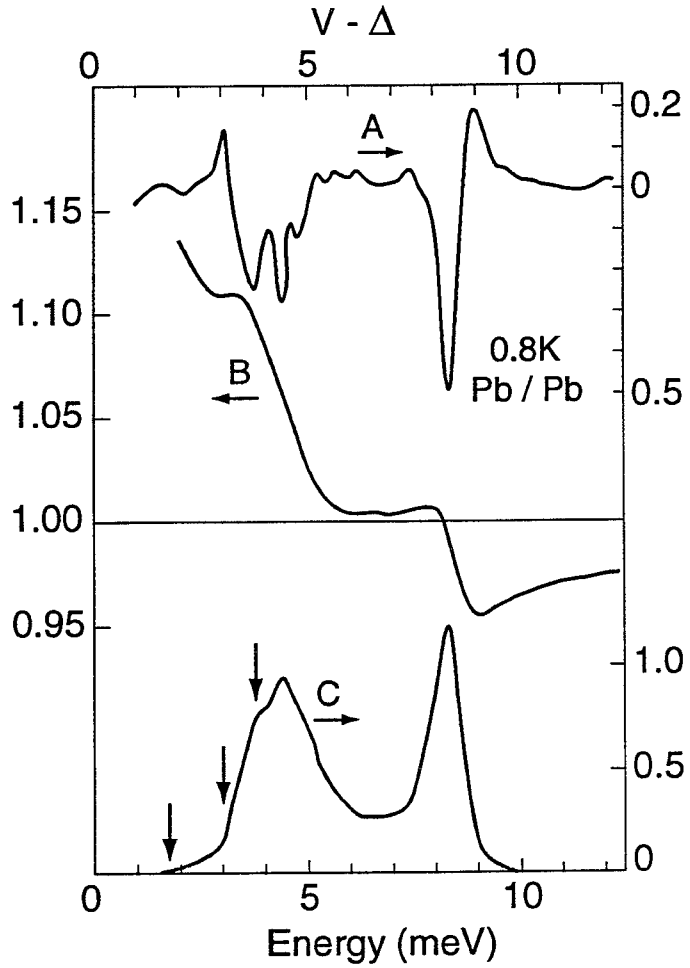

Figure 5.52: $\frac{d}{dV}(I'_S/I'_N)$ (A), ρ_s/ρ_N (B), $\alpha^2F(\omega)$ (C) for lead.

Early tunneling experiments failed to observe supercurrent tunneling before its existence was predicted by Josephson [10]. But soon after, the Josephson's effects were experimentally confirmed [37].

Consider a junction of the SIS' type, the thickness of I being much smaller than the coherence lengths and penetration depths in each of S and S'.

In each of S and S', Δ and Δ' obey the Ginzburg Landau equations and the effect of the barrier (if it is transparent enough!) is simply to correlate the boundary conditions on Δ and Δ' at the barrier (Fig. 5.53).

For A = 0 and z being the axis normal to the barrier this correlation can be written as

$$\begin{cases} \Delta' &= m_{11}\,\Delta + m_{12}\,\dfrac{\partial\Delta}{\partial Z} \\ \dfrac{\partial\Delta'}{\partial Z} &= m_{21}\,\Delta + m_{22}\,\dfrac{\partial\Delta}{\partial Z} \end{cases} \tag{5.103}$$

where the m_{ij} are real coefficients. The current J flowing across the barrier is (Eq. 5.24) $\frac{2e\hbar}{m}$ Im $(\Delta^*\frac{\partial\Delta}{\partial Z})$ and, noting that Im $(\Delta^*\Delta') = m_{12}$ Im $(\Delta^*\frac{\partial\Delta}{\partial Z})$

$$J = \frac{2e\hbar}{m}\,\frac{1}{m_{12}}\,|\Delta||\Delta'|\,\sin\,(\theta' - \theta) \tag{5.104}$$

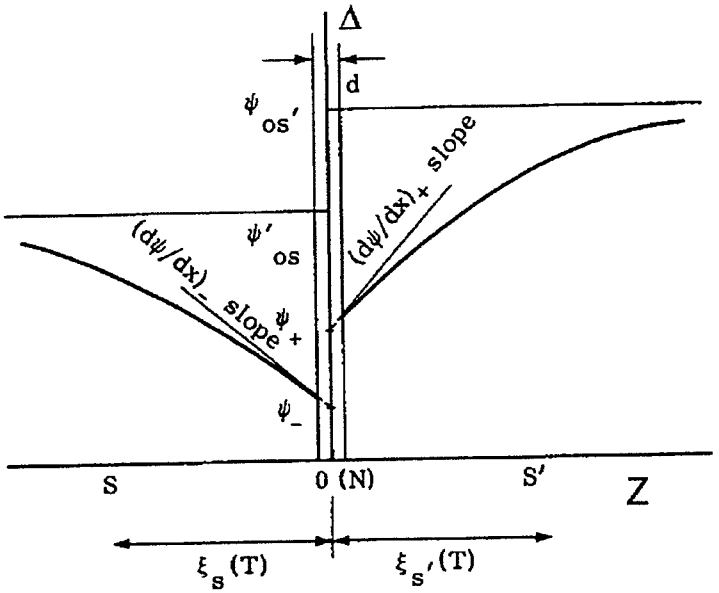

Figure 5.53: See text.

Note that from $J = J'$, i.e. Im $(\Delta^*\frac{\partial\Delta}{\partial Z}) =$ Im $(\Delta'^*\frac{\partial\Delta'}{\partial Z})$ one obtains

$$m_{11}m_{22} - m_{12}m_{21} = 1 \tag{5.105}$$

Relation 5.104 expresses the fact that a current

$$J = J_0 \sin\,(\theta' - \theta) \tag{5.106}$$

with

$$J_0 = \frac{2e\hbar}{m}\,\frac{1}{m_{12}}\,|\Delta||\Delta'| \tag{5.107}$$

flows through the barrier without voltage across it, i.e. the barrier behaves as being superconducting.

The phase change across the barrier is a well defined quantity, depending solely on the barrier properties. It locks the phase on one side with respect to that on the other side. If T is the transmission coefficient across the barrier $\frac{1}{m_{12}}$ is of the order of T/ξ for S = S'.

When A deviates from zero, the same conclusion is reached by using (Eq. 5.24). Note that the gauge invariant quantity introduced in (Eq. 5.52), $\mathcal{I} = \hbar \bigtriangledown \theta - \frac{2e}{c}A$ obeys the relation

$$J = \frac{2e}{m}\,\mathrm{Re}\left(\Delta^*[\hbar\frac{\bigtriangledown}{i} - \frac{2e}{c}A]\Delta\right) = \frac{2e}{m}|\Delta|^2\,\mathcal{I} \tag{5.108}$$

In both (5.106) and (5.108) it is the change of the phase of Δ which governs the presence of currents. When A deviates from zero $\bigtriangledown\theta$ must be replaced by $\bigtriangledown\theta - \frac{2e}{\hbar c}A$ and relation (5.105) is accordingly modified.

Taking $A = (0,\ 0, -xH_0)$ inside the barrier gives a magnetic field $H = \bigtriangledown_\wedge A = (0,\ H_0,\ 0)$ inside the barrier. Then $\theta' - \theta$ needs to be replaced by $\int(\bigtriangledown\theta - \frac{2e}{\hbar c}\,A)\cdot d\ell$ across the barrier $= \theta' - \theta + \frac{2eH_0}{\hbar c}\,x\Delta z$ where Δz is the average depth over which to integrate, $\Delta z \approx \lambda + \lambda'$ (neglecting the barrier thickness). Hence

$$J = J_0 \sin\left(\theta' - \theta + \frac{2e(\lambda+\lambda')H_0}{\hbar c}x\right) \tag{5.109}$$

Such modulations are indeed observed (Figs. 5.54 and 5.55) in various configurations. In particular geometries with two junctions allow for the observation of quantum interference effects over large distances (SQUID).

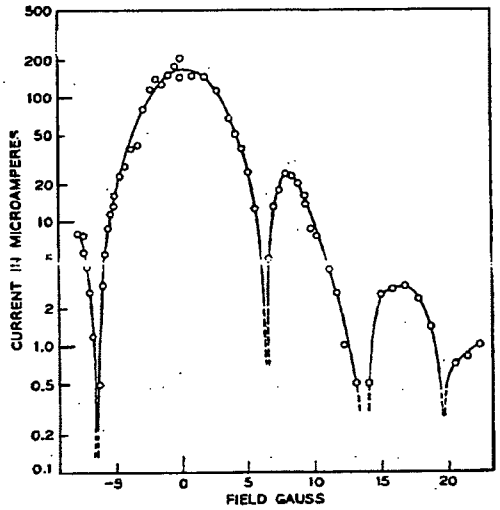

Figure 5.54: A single junction.

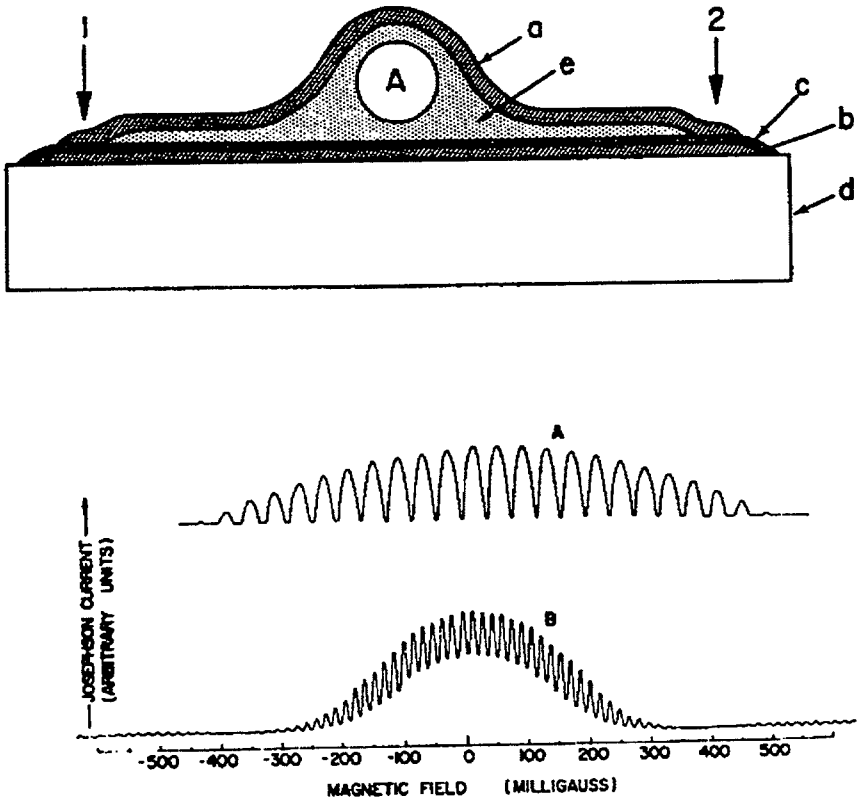

Figure 5.55: Interference with two junctions (1 and 2) and magnetic field in A.

Consider now a SIS' junction across which a voltage V is applied, $V = \int E dz$. Writing $J = J_0 \sin\phi$ with $\phi = \int [\nabla\theta - (2e/\hbar c)\ A]\ dz$ we have $d\phi/dt = -(2e/\hbar c) \int dA/dt\ dz = +2e/\hbar \int E dz$. For a constant V, ϕ is a linear function of time,

$$\phi = \theta' - \theta + \frac{2e}{\hbar} Vt \tag{5.110}$$

This implies the superposition of an ac current on the Josephson dc current, of frequency ω given by

$$\omega = \frac{2eV}{\hbar} = 484 \text{ MHz for } V - 1\mu V \tag{5.111}$$

This has allowed for a very accurate measurement of $\frac{2e}{\hbar}$ and, indirectly, of the fine structure constant [38].

APPENDIX

SUPERCONDUCTING MATERIALS

Known superconductors (see tables below for selected examples) include:

- Some elements (in particular transition elements with an incomplete d-shell).
- Some elements under pressure (Si, Ge, ...).
- Fullerides (alkali doped C_{60} compounds).
- Binary alloys and compounds.
- Intermetallic compounds (mostly A-15).
- Chevrel phases.
- Organic $(TMTSF)_2$ X and $(BEDT\text{-}TTF)_2$ X with low dimensionality.
- High T_c oxides. They are characterized by a very strong anisotropy (layered structures) a low coherence length and a large H_{c2} (in addition to their large T_c!). At room temperature they are insulators which have become metallic by doping. They are not described by a free electron gas model. The Coulomb interaction is important. d-wave pairing is likely to play an important rôle.

Elements	T_c	B_c
Al	1.18 K	0.105 kG
Ti	0.39	0.100
V	5.38	1.42
Zn	0.875	0.053
Ga	1.091	0.051
Zr	0.546	0.047
Nb	9.20	1.98
Mo	0.92	0.095
Tc	7.77	1.41
Ru	0.51	0.070
Cd	0.56	0.030
In	3.404	0.293
Sn	3.722	0.309
La	6.00	1.10
Ta	4.483	0.830
W	0.012	0.00107
Re	1.698	0.198
Os	0.655	0.065
Ir	0.14	0.019
Hg	4.153	0.412
Tl	2.39	0.171
Pb	7.193	0.803
Th	1.368	0.00162
Pa	1.4	–
U	0.68	–

Oxides	Tc
NbO	1
TiO	2
$SrTiO_{3-x}$	0.7
K_xWO_3	6
K_xMoO_3	4
K_x Re O_3	4
Li Ti204	13
Ba $PbBiO_3$	13

Binary alloys	Tc	Bc
Nb-Ti	9	140

A-15 Compounds	Tc	Bc
V_3 Al	9.6	–
V_3 Ga	15.4	230
V_3 Si	17.1	230
V_3 Ge	7	–
V_3 Sn	4.3	–
Nb_3 Al	18.9	330
Nb_3 Ga	20.3	340
Nb_3 Si	18.0	–
Nb_3 Ge	23	380
Nb_3 Sn	18.3	240

High Tc cuprates	Tc
$La_{2-x}M_xCuO_{4-y}$	38
M = Ba,Sr,Ca	
$x \sim 0.15$, y small	
$Nd_{2-x}Ce_xCuO_{4-y}$ (electron doped)	30
$Ba_{1-x}K_xBiO_3$ (isotropic, cubic)	30
$Pb_2Sr_2Y_{1-x}Ca_xCu_3O_8$	70
$R_1Ba_2Cu_{2+m}O_{6+m}$	
R:Y,La, Nd, Sm, Eu, Ho, Er, Tm, Lu	
$m = 1$ ('123')	92
$m = 1.5$ ('247')	95
$m = 2$ ('124')	82
$Bi_2Sr_2Ca_{n-1}Cu_nO_{2n+4}$	
$n = 1$ ('2201')	~ 10
$n = 2$ ('2212')	85
$n = 3$ ('2223')	110
$Tl_2Ba_2Ca_{n-1}Cu_nO_{2n+4}$	
$n = 1$ ('2201')	85
$n = 2$ ('2212')	105
$n = 3$ ('2223')	125

Chevrel phases	Tc	Bc
Sn Mo6 S8	12	340
Pb Mo6 S8	15	600
La Mo6 S8	7	450
Sn Mo6 Se8	4.8	–
Pb Mo6 Se8	3.6	38
La Mo6 Se8	11	50

Fullerides	Tc
$RbCs_2$ C_{60}	33
K_3 C_{60}	18
Rb_3 C_{60}	30

References

[1] Classic textbooks are:
R.P. Feynman, Statistical Mechanics, Frontiers in Physics;
P.G. de Gennes, Superconductivity of Metal and Alloys, Advanced Book Classics, Addison-Wesley;
M. Tinkham, Superconductivity, Documents on Modern Physics, Gordon and Breach and Introduction to superconductivity McGraw Hill, 1975.

[2] Examples of historical surveys are:
G.J. Gorter, Rev. Mod. Phys. 36 (1964) 3;
K. Mendelssohn, Rev. Mod. Phys. 36 (1964) 7 and Quest for Absolute Zero, McGraw Hill;
F. London, Superfluids, Vol. I, Wiley (1950);
M.R. Beasley, Adv. in Supercond., Kitizawa and Ishigura (eds.), Nagoya 1988, Springer;
S. Ortoli and J. Klein, Histoire et Légendes de la Superconduction, Calmann-Lévy.

[3] H. Kamerlingh Onnes, Comm. Phys. Lab. Univ. Leiden, no. 119, 120, 122 (1911) and Akad van Wetenschappen (Amsterdam) 14 (1911) 113, 818.

[4] W. Meissner and R. Oschsenfeld, Naturwiss. 21 (1933) 787.

[5] J. Bardeen, L.N. Cooper and J.R. Schrieffer, Phys. Rev. 106 (1957) 162 and 108 (1957) 1175.

[6] H. London and F. London, Proc. Roy. Soc. A149 (1935) 71 and Physica 2 (1935) 341;
F. London, Proc. Roy. Soc. A152 (1935) 24 and Phys. Rev. 74 (1948) 562.

[7] G.J. Gorter and H.B.G. Casimir, Physik. Z. 35 (1934) 963;
Z. techn. Physik 15 (1934) 539.

[8] A.B. Pippard, Proc. Roy. Soc. A216 (1953) 547.

[9] V.L. Ginzburg, L.D. Landau JETP (USSR) 20 (1950) 1064;
V.L. Ginzburg, Nuovo Cim. 11 (1955) 1234.

[10] B.D. Josephson, Phys. Lett. 1 (1962) 251 and Adv. in Phys. 14 (1965) 419.

[11] A.B. Pippard, Rev. Mod. Phys. 36 (1964) 328.

[12] J.G. Bednorz and K.A. Müller, Z. Phys. B64 (1986) 189.

[13] A.B. Pippard, The dynamics of conduction electrons, Documents on modern Physics, Gordon and Breach.

[14] L.N. Cooper, Phys. Rev. 104 (1956) 1189.

[15] H. Fröhlich, Phys. Rev. 79 (1950) 845 and Proc. Roy. Soc. A215 (1952) 291.

[16] E. Maxwell, Phys. Rev.78 (1950) 477;
C.A. Reynolds et al., Phys. Rev. 78 (1950) 487.

[17] V.F. Weisskopf, CERN 79–12, 21 Dec. 1979.

[18] N.N. Bogolioubov, JETP (USSR) 34 (1958) 58 and JETP (Sov. Phys.) ibid p. 41.

[19] P.W. Anderson, J. Phys. Chem. Solids 11 (1959) 26.

[20] G.M. Eliashberg, JETP (USSR) 38 (1960) 986 and JETP (Sov. Phys.) 11 (1960) 689;
JETP (USSR) 39 (1961) 1437 and JETP (Sov. Phys.) 12 (1961) 1000.

[21] J.P. Carbotte Rev. Mod. Phys. 62 (1990) 1027 and references therein.

[22] A.A. Abrikosov, L.P. Gor'kov and I.M. Khalatnikov JETP (USSR) 35 (1958) 265 and JETP (Sov. Phys.) 35 (1959) 182;
D.C. Mattis and J. Bardeen, Phys. Rev. 111 (1958) 412;
J. Halbritter, Z. Phys. 266 (1974) 209.

[23] G.E.H. Reuter and E.H. Sondheimer, Proc. Roy. Soc. A195 (1948) 336.

[24] N.N. Bogolioubov JETP (USSR) 34 (1958) 73 and JETP (Sov. Phys.) ibid. p. 51.
[25] L.P. Gor'kov JETP (USSR) 36 (1959) 1918 and JETP (Sov. Phys.) ibid p. 1364;
JETP (USSR) 37 (1959) 1407 and JETP (Sov. Phys.) 37 (1960) 998.
[26] B.S. Deaver Jr. and W.M. Fairbank, Phys. Rev. Lett. 7 (1961) 43;
R. Doll and M. Näbauer, Phys. Rev. Lett. 7 (1961) 51.
[27] L.V. Schubnikov et al., Physik Z. Sowjet Union, Suppl. (1936) p. 39.
[28] A.A. Abrikosov JETP (USSR) 32 (1957) 1442 and JETP (Sov. Phys.) 5 (1957) 1174.
[29] K. Maki, Physics 1 (1964) 21 and 127;
K. Maki and T. Tsuzuki, Phys. Rev. A139 (1964) 868;
J.L. Harden and V. Harp, Cryogenics (1963) 105;
E. Helfand and N.R. Werthamer, Phys. Rev. Lett. 13 (1964) 686; Phys. Rev. 147 (1965) 288;
N.R. Werthamer, E. Helf and P.C. Hohenberg, Phys. Rev. 147 (1965) 295;
G. Eilenberger, Phys. Rev. 153 (1967) 584;
W. Pesch and L. Kramer, J. Low Temp. Phys. 15 (1974) 367;
L. Kramer et al., J. Low Temp. Phys. 14 (1974) 29.
[30] A.M. Campbell and J.E. Evetts, Adv. Phys. 21 (1972) 199;
E.H. Brandt, Rep. Prog. Phys. 58 (1995) 1465 and references therein.
[31] J. Bardeen and M.J. Stephen, Phys. Rev. 140A (1965) 1197 and Phys. Rev. Letters 14 (1965) 112;
J. Bardeen and R.D. Sherman, Phys. Rev. B12 (1975) 2634;
J. Bardeen, Phys. Rev. B17 (1978) 1472;
M. Tinkham, Phys. Rev. Letters 13 (1964) 804;
Y.B. Kim, C.F. Hempstead, and A.R. Strnad, Phys. Rev. 139A (1965) 1163.
[32] R. Labusch, Crystal Lattice Defects 1 (1969) 1.
[33] C.P. Bean, Phys. Rev. Lett. 8 (1962) 250 and Rev. Mod. Phys. 36 (1964) 31;
H. London, Phys. Lett. 6 (1963) 162.
[34] J.I. Gittleman and B. Rosenblum; J. Appl. Phys. 39 (1968) 2617 and references therein.
[35] I. Giaever, Phys. Rev. Lett. 5 (1960) 147 and 464;
J. Nicol et al., Phys. Rev. Lett. 5 (1960) 461;
I. Giaever and K. Megerle, Phys. Rev. 122 (1961) 1101.
[36] I. Giaever et al., Phys. Rev. 126 (1962) 941;
J.M. Rowell et al., Phys. Rev. Lett. 9 (1962) 59;
J.M. Rowell et al., Phys. Rev. Lett. 10 (1963) 334;
W.L. McMillan and J.M. Rowell, Phys. Rev. Lett. 14 (1965) 108.
[37] P.W. Anderson and J.M. Rowell, Phys. Rev. Lett. 10 (1963) 230;
S. Shapiro, Phys. Rev. Lett. 11 (1963) 80;
J.M. Rowell, Phys. Rev. Lett. 11 (1963) 200;
R.C. Jacklevic et al., Phys. Rev. Lett. 12 (1964) 159 and 274;
R.E. Eck et al., Phys. Rev. Lett. 13 (1964) 15;
D.D. Coon and M.D. Fiske, Phys. Rev. 138A (1965) 744;
R.C. Jaklevic et al., Phys. Rev. 140A (1965) 1628.
[38] W.H. Parker et al., Phys. Rev. Lett. 18 (1967) 287;
J. Clarke, Am. J. of Phys. 38 (1970) 1071.